Geomechanical Aspects of Drilling in the Vienna Basin

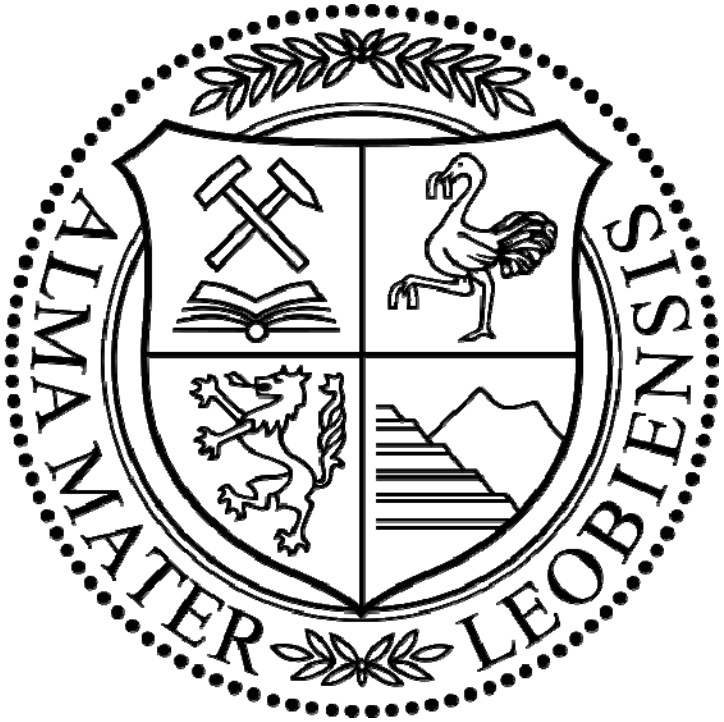

Department Mineral Resources and Petroleum Engineering

Montanuniversität Leoben, Austria

Alexander Heger

Leoben, June 2010

Affidavit

I declare in lieu of oath, that I wrote this thesis myself, using only literature cited in this volume.

Ich erkläre hiermit an Eides statt, dass ich die vorliegende Arbeit eigenhändig angefertigt habe, lediglich unter Verwendung der zitierten Literatur.

Leoben, June 10 2010,

Alexander Heger

Acknowledgement

First of all I want to thank DI Markus Doschek for advising my Master thesis and for giving me the opportunity to include all my thoughts and ideas in this work. I really enjoyed working with you Markus and I am very thankful for all the support you gave me.

Further on I want to thank DI Hermann F. Spörker for offering me the chance to write a thesis about geomechanics, for always being interested in my work and for his continuous support.

Gratitude is also dedicated to the University of Leoben and especially to my advisor Univ.-Prof. Dipl.-Ing. Dr.mont. Gerhard Thonhauser.

Special thanks go to Dr. Jennifer Miskimins, Dr. Tony Batchelor and Dr. Katja C. Schulze as well as to all the colleagues of OMV which supported me throughout my thesis.

Last but not least I want to thank my family and friends who have always lend me a hand and encouraged me during my whole academic studies.

Abstract (English)

The reason for this Master thesis was a disagreement between predicted mud weight window from a geomechanical study and actual field experience. The focus was on finding a way to challenge the outcome of geomechanical studies in general and further on gaining deeper insight into the procedure of data processing and mud weight window calculation of the company which has performed the geomechanical study.

The thesis describes the development of a geomechanical earth model which provides the input values for stress and mud weight window calculation. The three different stress regimes are explained as well as the development of a stress polygon. Determination and gradient computation of the three principle stresses, of pore pressure and of rock mechanical properties are discussed and supplemented with geomechanical theory.

A program for stress calculation and mud weight window prediction was developed to provide the ability of verifying the results of the study. The structure and the development steps of the program are explained and the diagrams included in the program are used to continuously exemplify geomechanical theory.

It was able to verify the results of the study from a calculation standpoint only, so further investigation is required to find the reason for the discrepancy. The company which has performed the study made the statement that underestimated rock strength could be an explanation for the inconsistency.

In addition, a sensitivity analysis was performed according to the input parameters which showed that pore pressure and maximum horizontal stress are the most important factors.

Additional findings have been made throughout the thesis work which explain the reason for break-outs at high mud weights in S_{Hmax} direction, the change of most

preferable horizontal drilling direction in a normal faulting stress regime with change in break out width allowance and the reason for S_{hmin} being the most preferable horizontal drilling direction in a normal faulting stress regime.

Abstract (German)

Der Grund für diese Diplomarbeit war eine Unstimmigkeit in Bezug auf das Spülungsgewicht, das in einer Geomechanik-Studie vorhergesagt wurde und der tatsächlichen Bohrerfahrung. Das Hauptaugenmerk wurde auf die Suche nach einer Methode gelegt, die es ermöglichen soll, das Ergebnis einer solchen Geomechanik-Studie zu überprüfen. Weiters wollte man einen tieferen Einblick in die Datenverarbeitung und die Berechnung des Spülungsgewichts der Firma bekommen, die die genannte Studie durchgeführt hatte.

Die Arbeit beschreibt, wie ein geomechanisches Model erstellt wird, welches in weiterer Folge die Eingabeparameter für die Spannungs- und Spülungsgewichtsberechnung vorgibt. Die drei unterschiedlichen Spannungsregime werden erklärt, wie auch der Aufbau eines Spannungspolygons. Die Berechnung der Spannungsgradienten der drei Hauptnormalspannungen, des Porendrucks und der Gesteinsparameter wird diskutiert und mit Theorie aus der Geomechanik ergänzt.

Ein Programm für die Spannungs- und Spülungsgewichtsberechnung wurde entwickelt um die Resultate von Studien überprüfen zu können. Der Aufbau dieses Programms wird schrittweise erklärt und die im Programm inkludierten Diagramme werden dazu herangezogen, um die Theorie im Hintergrund zu erklären.

Mit Hilfe des entwickelten Programms war es möglich, die Resultate der Studie zu verifizieren, was bedeutet, dass weitere Nachforschungen von Nöten sind, um den Grund für die Unstimmigkeit zu finden. Die Firma, die ursprünglich die Studie durchgeführt hatte, wurde um eine Stellungnahme gebeten und es wird vermutet, dass eine zu gering angenommene Gesteinsfestigkeit eine Erklärung sein könnte.

Zusätzlich wurde eine Sensitivitätsanalyse durchgeführt um die wichtigsten Eingabeparameter zu bestimmen, mit dem Resultat, dass der Porendruck wie auch die maximale, horizontale Spannung sich als dominant erwiesen.

Während der Arbeit wurden zusätzliche Erkenntnisse gewonnen, die eine Erklärung für das Versagen der Formation bei hohen Spülungsgewichten liefert, wie auch eine Begründung für den Wechsel der bevorzugten, horizontalen Bohrrichtung in einem Normal-Faulting Spannungsregime bei Änderung des zulässigen Winkels für Formationsbruch und die rechnerische Bestätigung für S_{hmin} als bevorzugte, horizontale Spannungsrichtung in einem Normal-Faulting Spannungsregime.

Contents

1. Introduction

1.1. Discrepancy of Predicted Mud Weight and Actual Field Experience

The starting point for this thesis was a discrepancy between predicted mud weight window from a geomechanical study performed by an internationally known service company, which is well accepted in the industry and actual field experience. Due to the fact that this project is subject to confidentiality within OMV no values, depths, areas, well or company names will be stated in this Master thesis. The geomechanical study of interest will further on be named “Study X” and the company which has performed the study will be called “Company X”.

The objective was to verify the calculation of the mud weight window as well as to deepen the understanding of the whole process of geomechanic earth model development and stress calculation. These achievements will add value to the company as in-depth knowledge in geomachanics will be created within OMV and so the ability is provided to challenge the outcome of geomechancial studies especially from a drilling standpoint, which is a great step forward to improve the whole process of reasonable and sustainable data gathering, processing and forecasting of drilling conditions.

To understand the development of a geomechanical earth model and to get a deeper insight of the data processing and mud weight window calculation of Study X a close interaction with Company X was realized.

For verifying the calculation of Study X a program was developed to recalculate the mud weight window. The program was designed in a way that the stress distribution around a well bore and its influence on well bore stability can be investigated in various ways.

1.2. Deepening the Process Understanding

OMV had the problem of insufficient insight and in-depth understanding of the work performed by the service company. This means that data from logs, FITs, LOTs and

core analysis were sent to Company X which processed the data and preformed calculations. OMV got back a report in the form of a power point presentation including the results. The problem here is the data processing and the calculations of Company X because OMV did not have sufficient insight and understanding to follow the process step by step and to see thereby possible pitfalls. Due to that issue it was also not possible to completely analyze and challenge the outcome of Study X from a drilling standpoint.

This problem of process understanding is present for a variety of different situations which means in general for cases where one or more processes within a sequence of processes steps are insufficiently understood. The author sees this circumstance as well fulfilled when software is used which is not understood in its principle mechanisms irrespective if this software is operated externally or internally. The result can be a loss of information, which is generally connected to a less accurate planning as well as the oversight of possible dangers.

2. Process of Geomechanical Earth Model Development

2.1. Stress Regimes

There exist three different stress regimes depending on the relationship of the three principle stresses (vertical stress (S_V), maximum horizontal stress (S_{Hmax}), and minimum horizontal stress (S_{hmin})).

2.1.1 Normal Faulting

The most likely encountered regime in upper hole sections is a normal faulting regime where the overburden stress is highest in magnitude followed by S_{Hmax} and S_{hmin}. Gravity is the main driving force for normal faulting and if faulting occurs the hanging wall will move downward relative to the footwall[1].

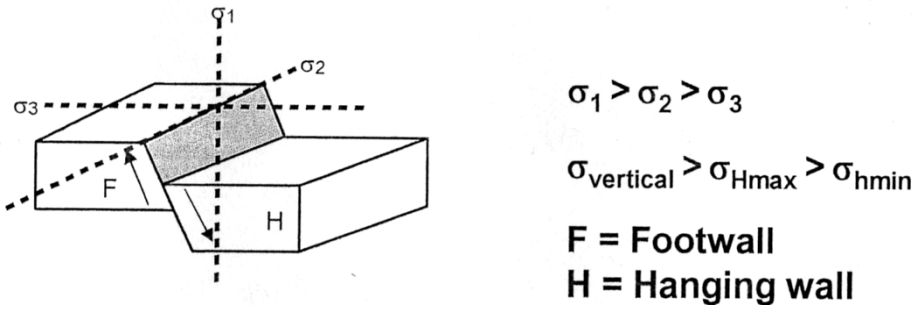

Figure 1, normal faulting[1]

2.1.2 Strike-Slip Faulting

The next possible arrangement is the strike-slip regime. The S_{Hmax} value has exceeded the vertical stress value but S_{hmin} remains below S_v. The reason for a horizontal stress to become larger in magnitude than the vertical stress is always some sort of additional horizontal stress input which is most likely due to tectonic movement but it is also possible that moving salt introduces an additional horizontal force. If a fault is formed blocks will tend to slide laterally.

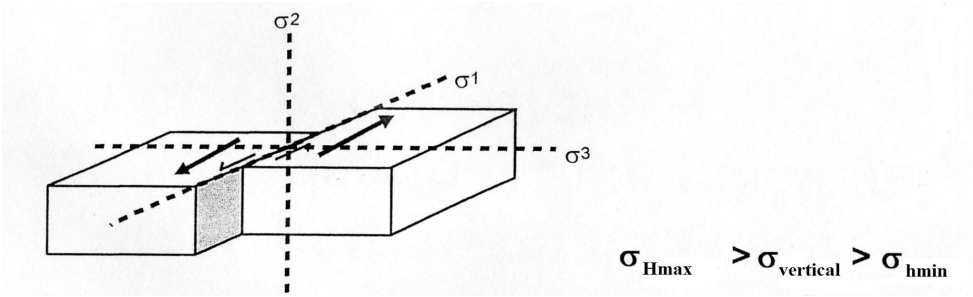

Figure 2, strike-slip faulting[1]

2.1.3 Reverse Faulting

If horizontal stress input increases the S_{hmin} value beyond S_v a reverse faulting regime is present with S_v as least principle stress. The main driving mechanism for this regime is compression and conditions are provided for horizontal fractures as S_v is the least stress.

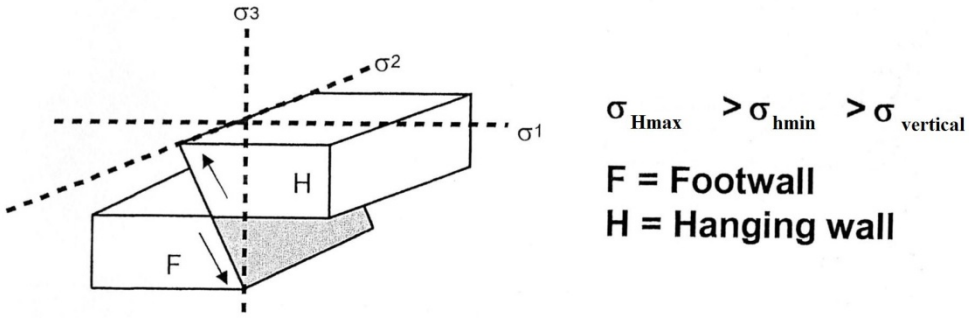

Figure 3, reverse faulting[1]

2.1.4 Stress Polygon

There exists a convenient way to include all these regimes into one diagram which can be useful by analyzing stress magnitudes.

The stress polygon (Figure 4) consists of two axis with S_{Hmax} on the ordinate and S_{hmin} on the abscissa. A straight line with a constant slope limits the stress values to the upper left corner as beyond this line towards the right lower corner S_{Hmax} would no longer be larger in magnitude compared to S_{hmin}.

The diagram is also based on the consideration that pore pressure can not exceed any of the three principle stresses because under this condition the formation would be fractured. This already sets a lower stress boundary which can also be seen in Figure 5

where a higher pore pressure shrinks the area of possible stress magnitudes. The physical explanation for this effect of pore pressure is Amonton´s law

$$\tau/\sigma_n = \mu \qquad (2.1^2)$$

τ…shear stress

σ_n…effective normal stress

μ…friction factor

The effective normal stress is defined as the total normal stress minus pore pressure (after Terzaghi). So an increase in pore pressure will decrease the effective normal stress and as the friction factor remains the same less shear stress is required until fault slip occurs.

It has to be stated that the stresses used in the stress polygon are effective stresses (total stress = rock stress + pore pressure → total stress – pore pressure = rock stress (effective normal stress))

The vertical line which is tagged with 1 in Figure 4 represents a critical limit for normal faulting which is calculated by the use of the following equation:

$$\sigma_1/\sigma_3 = (S_v - P_p) / (S_{hmin} - P_p) <= [(\mu^2 + 1)^{1/2} + \mu]^2 \qquad (2.2^2)$$

Generally a friction factor (μ) of 0.6 is assumed to be applicable[2]. With the critical relationship of S_{hmin} and S_v the triangle for normal faulting within the stress polygon is sufficiently defined. Both horizontal stresses have to be smaller or equal to the vertical stress, S_{Hmax} can not be smaller than S_{hmin}, and S_{hmin} can not become smaller than a critical value in combination with the vertical stress otherwise a normal fault would be generated in the formation according to Mohr Coulomb (only σ_{min} and σ_{max} govern shear failure). If a fault would occur stresses would be relieved to a level below the critical limit. The critical stress relationship between S_{hmin} and S_v is graphically presented in diagram a (Figure 4) in the right lower corner. The slope of the Mohr Coulomb straight line of failure is 0.6.

For a strike-slip regime the critical relationship between S_{Hmax} and S_{hmin} is calculated by the following equation:

$$\sigma_1/\sigma_3 = (S_{Hmax} - P_p) / (S_{hmin} - P_p) <= [(\mu^2 + 1)^{1/2} + \mu]^2 \qquad (2.3^2)$$

With the knowledge of the critical stress relationship the triangle for strike-slip faulting within the stress polygon is defined. S_{Hmax} has to be at least equal to the vertical stress, S_{hmin} must not exceed S_v, and S_{Hmax} and S_{hmin} have to be within a critical proportion to avoid failure of the formation under forming a strike-slip fault. The Mohr Coulomb stress diagram for the critical condition is also shown in Figure 4.

The critical ratio between S_{Hmax} and S_v for reverse faulting can be calculated by:

$$\sigma_1/\sigma_3 = (S_{Hmax} - P_p) / (S_v - P_p) <= [(\mu^2 + 1)^{1/2} + \mu]^2 \qquad (2.4^2)$$

This again defines the boundaries for reverse faulting where the horizontal stresses must at least be equal to the vertical stress, and maximum horizontal stress and vertical stress have to be below the critical ratio to avoid the generation of a reverse fault. The Mohr Coulomb diagram for the critical limit can be seen in Figure 4.

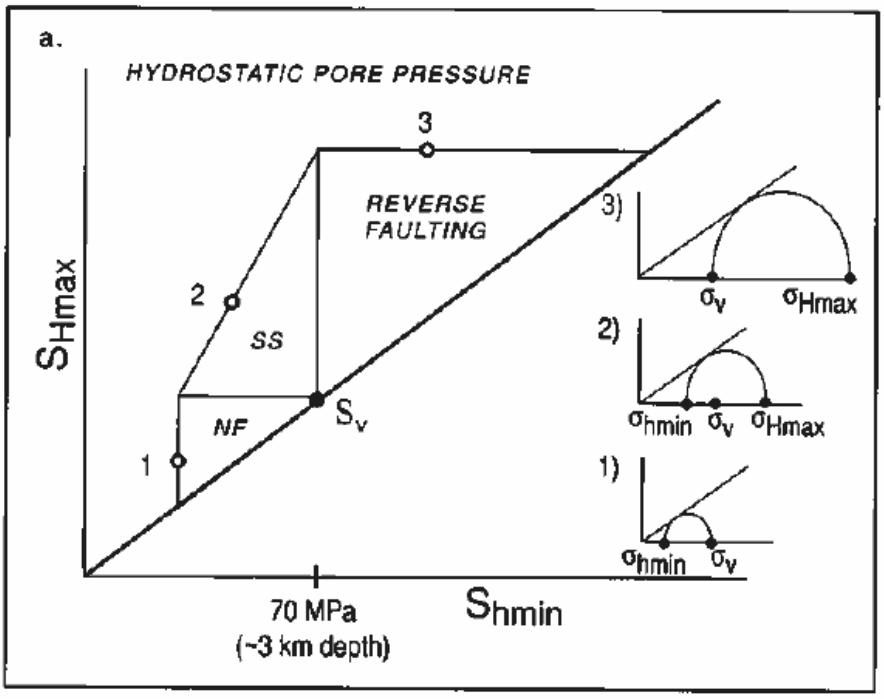

Figure 4, stress polygon 1[2]

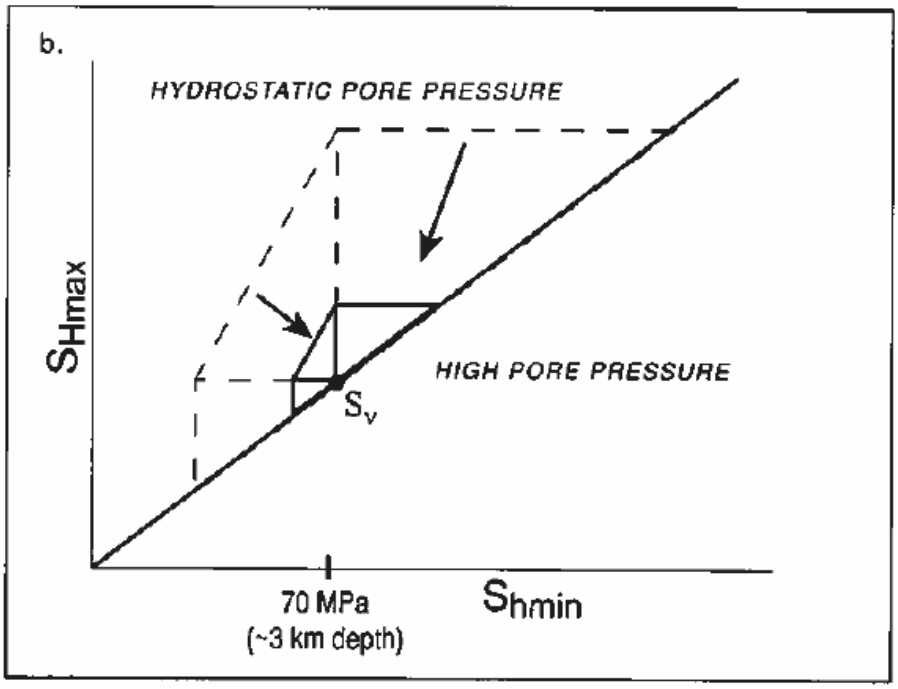

Figure 5, stress polygon 2[2]

The stress polygon is very useful for understanding as well as for calculation purposes of stress magnitudes as can be seen in the following chapters.

2.2. Input Parameters

In general the following data is required to build a geomechanical earth model:

- In-situ stress magnitudes
- In-situ stress orientations
- Pore pressure
- Rock mechanical properties

Throughout this chapter the important parameters, how they are gathered and their contribution to mud weight window calculation will be explained.

2.2.1 Vertical Stress, S_v

The vertical stress is basically the result of the overburden column and can be derived straight forward by integrating density times earth acceleration over depth.

$$S_v(z) = \int \rho(z) * g * dz \qquad (2.5^2)$$

The vertical stress can be calculated by integrating the bulk density log of the well under investigation. In case no density log is available a sonic log can be utilized to calculate a pseudo-density which is then used for integration. There are different correlations for calculating pseudo-density which are either based on lithology or compressive sonic velocity. Which one is chosen depends on best fit. If neither one of the two is applicable an exponential/polynomial extrapolation is used. An example for a lithology based correlation is the Belotti-correlation[2] as for compressive sonic velocity is the Gardener-correlation[2].

The outcome of investigation on vertical stress could look like the graph below which shows the overburden gradient over depth. In this case a pseudo-density was derived from a sonic log.

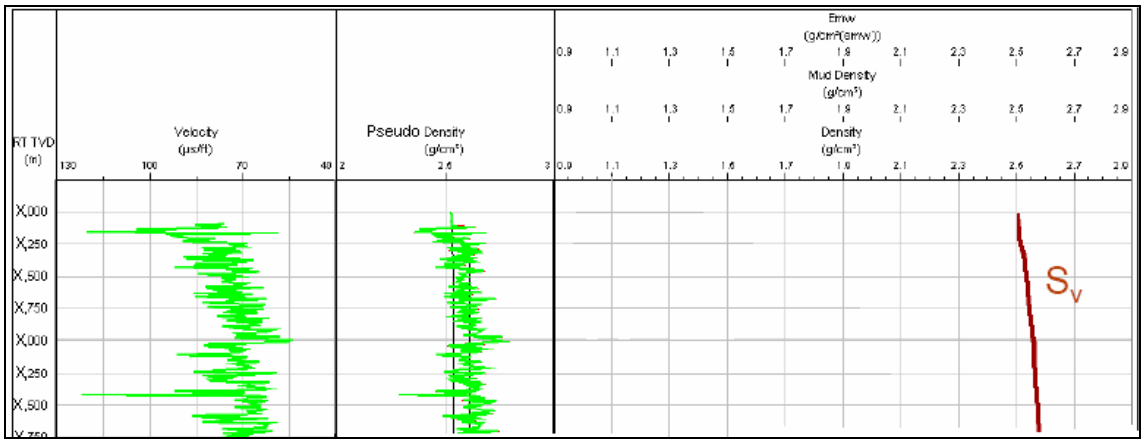

Figure 6, S_v[5]

2.2.2 Minimum Horizontal Stress, S_{hmin}

The minimum horizontal stress value is of great importance as it is governing the fracture gradient in normal and strike/slip faulting regimes. Methods to gain the value of S_{hmin} are leak-off tests (LOT) and extended leak-off tests (XLOT) whereas the later one is barely performed. Unfortunately, it is even common practice to do a formation integrity test (FIT) also known as limit test instead of a LOT which will give you actually no information about the minimum horizontal stress except a certain value (maximum pressure during FIT) beyond the S_{hmin} will be for sure. Formation integrity tests are executed for gathering information to prove the design limit of the next hole section but do not initiate a fracture at the wellbore wall.

Although LOTs have been performed for decades the process itself is poorly understood concerning the questions of fracture opening and physical reasons for the actual shape of the LOT curve. Even big oil companies have different attitudes towards these questions.

The point of interest during a LOT is the deviation from the straight line behavior of the pressure/volume curve. In the graph below (Figure7) which shows an XLOT this point is indentified as the fracture initiation pressure which is better known as the leak off pressure. As soon as the first data point clearly indicates a deviation pumping is stopped and the leak off pressure is taken as the minimum horizontal stress value. It is highly recommended to use volume on the x-axis instead of time as this is very beneficial from an operational standpoint due to the fact that a constant flow rate is hard to achieve.

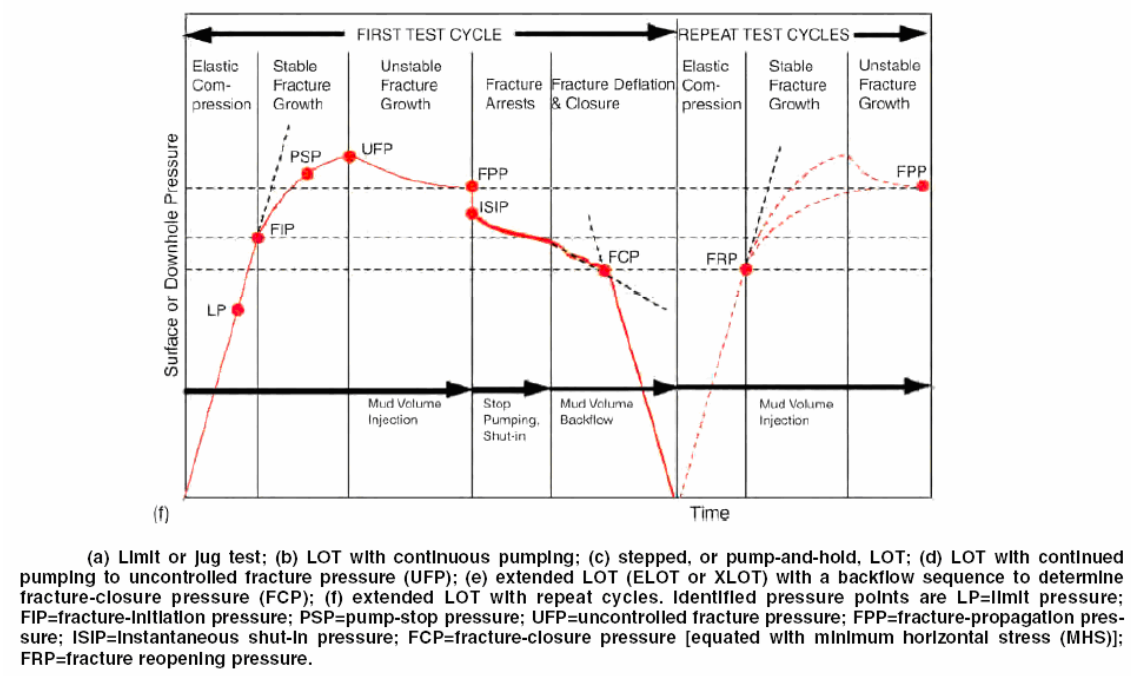

(a) Limit or jug test; (b) LOT with continuous pumping; (c) stepped, or pump-and-hold, LOT; (d) LOT with continued pumping to uncontrolled fracture pressure (UFP); (e) extended LOT (ELOT or XLOT) with a backflow sequence to determine fracture-closure pressure (FCP); (f) extended LOT with repeat cycles. Identified pressure points are LP=limit pressure; FIP=fracture-initiation pressure; PSP=pump-stop pressure; UFP=uncontrolled fracture pressure; FPP=fracture-propagation pressure; ISIP=instantaneous shut-in pressure; FCP=fracture-closure pressure [equated with minimum horizontal stress (MHS)]; FRP=fracture reopening pressure.

Figure 7, XLOT[3]

An XLOT will automatically damage the formation and could cause fluid loss problems during drilling the section. Still it would offer the opportunity to get a second value (FCP) for S_{hmin} to verify the leak off pressure. The fracture closure pressure (FCP) will generally be a little bit lower than the LOP due to a loss of tensile strength and breakdown of near-wellbore hoop stresses.

In case of an exploration well it is highly recommended to accurately perform a LOT to gain information of the current minimum stress value as it provides foundation of more accurate mud weight window predictions for future wells in the specific formation the casing is going to be set into.

In a brown field development the judgment on either performing a LOT or FIT is very dependent on the actual data available and should not be decided prior to a detailed investigation on the executed tests.

PWD offers the ability to estimate the minimum horizontal stress value. One advantage of the direct downhole pressure measurement is the improvement of accuracy of a LOT as there can be a significant difference between the calculated downhole pressure from surface readings and the actual downhole pressure measurement[2].

Another reliable valuation of S_{hmin} can be achieved by identifying a lost circulation incident in combination with a PWD in place. Lost circulation can just occur if a fracture has propagated into the far field away from the wellbore and thereby overcome the least principle stress which provides with a reasonable estimate of the minimum horizontal stress. The difficulty thereby is the exact identification of depth where losses appeared especially in a long open-hole section. It is important to find the right position as the S_{hmin} value is connected to a certain depth. To assume the loss too shallow would overestimate the minimum horizontal stress value whereas a too deep position would lead to an underestimation. Repeated resistivity logs might help to find the lost circulation zone[2].

Ballooning which is generally excepted to be the opening and closing of near wellbore fractures most likely occurs when drilling significantly beyond hydrostatic with an ECD close to S_{hmin} . Mud can be lost during dynamic conditions corresponding to an opening of the fracture and gained when pumping is stopped which means a closing of the fracture. This effect can as well be utilized to gain information about the minimum horizontal stress. In Appendix A the comparison of a conventional pressure record and a ballooning pressure record is shown. It can be seen that a curved pressure profile identifies ballooning which stands in contrast to the sharp pressure drop and build up

when pumps are turned off and on during normal operating conditions. ECD can be used as a lower boundary for S_{hmin} as lost circulation would have occurred if the least principle stress was lower[2].

To get a minimum horizontal stress gradient the available data points are commonly interpolated by the use of effective stress ratios varying from 0.4 to 0.6:

$$0.4 \text{ to } 0.6 = (S_{hmin} - PP)/(S_v - PP) \qquad (2.6^{2})$$

A graph for the S_{hmin} gradient could look like the one below.

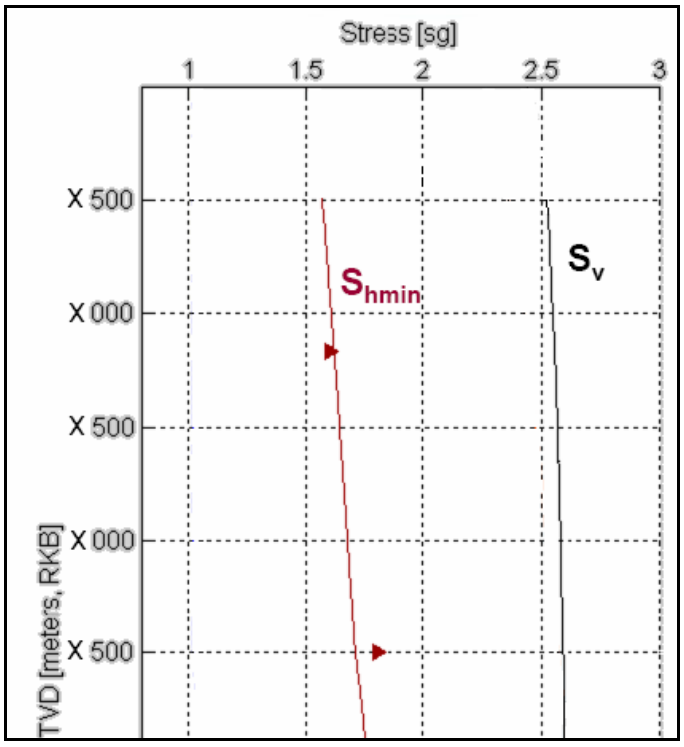

Figure 8, S_{hmin}[5]

2.2.3 Maximum Horizontal Stress, S_{Hmax}

Concerning the three principle stresses the maximum horizontal stress is the most difficult one to get as it can not be measured directly but needs to be calculated by modeling the wellbore failure. Break-outs will occur when the rock strength of the formation at the wellbore wall is overcome, which requires a certain relationship of the three principle stresses. Break-outs, subjected to a constant set of conditions, tend to deepen but not to grow in width[2]. Barton and Zoback[2] used the equilibrium state of

stress concentration and rock strength at the edge of the break out to derive the following equation for S_{Hmax} determination.

$$S_{Hmax} = ((C_0 + 2*P_p + \Delta P + \sigma^{\Delta T}) - S_{hmin}\,(1 + 2*\cos(2*\theta_b)))/(1 - 2*\cos(2*\theta_b)) \quad (2.7^2)$$

C_0 … unconfined compressive strength P_p … pore pressure

ΔP… wellbore pressure – pore pressure $\sigma^{\Delta T}$… stress due to thermal changes

$2*\theta_b$ … π – break out width (w_{bo})

The application of this equation demands an accurate determination of break out width which can be achieved by using ultrasonic borehole televiewers or electrical imaging devices both with the disadvantage of high cost.

The formula can also be used in combination with stress polygons like the one below.

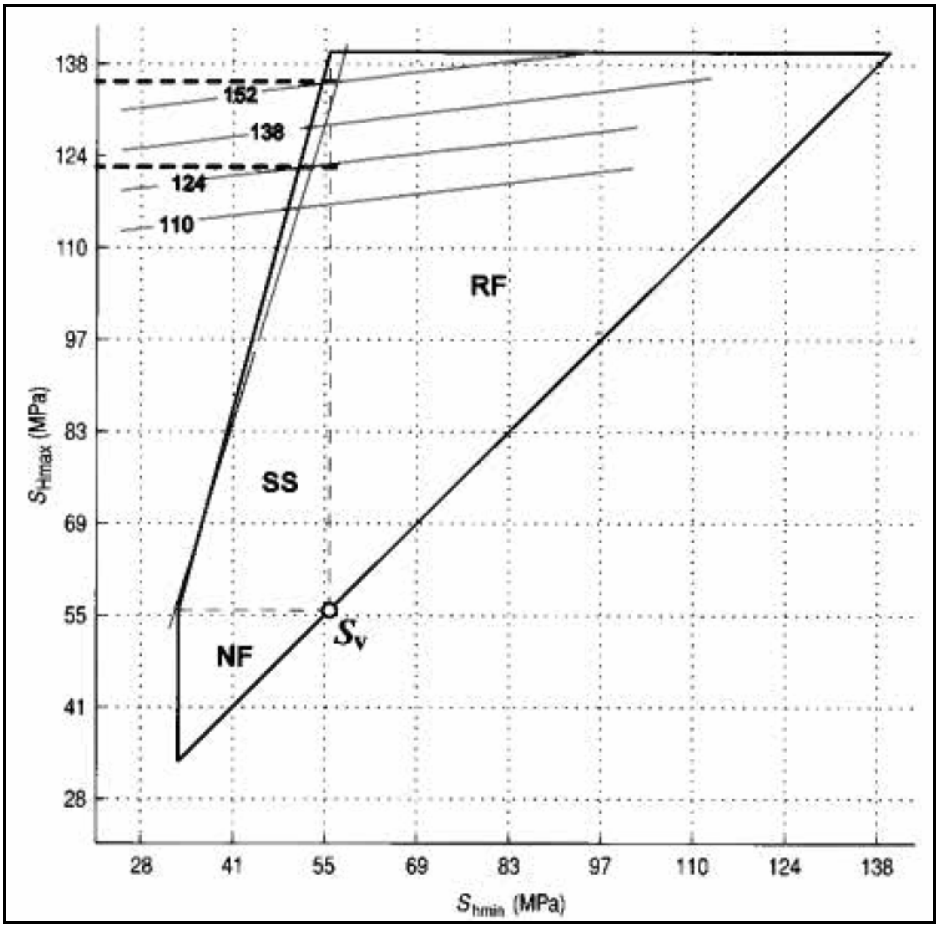

Figure 9, stress polygon[2]

The stress polygon represents a deep oil well in Australia[2] with an average break out width of 45°. Unconfined compressive strength was found to be 138 MPa with an uncertainty of +/- 14 MPa. The dark slightly tilted lines correspond to S_{Hmax} values required to produce 45° break-outs calculated by equation 2.7.

Drilling-induced tensile fractures have also been encountered in the well. The light diagonal line represents the required S_{Hmax} value to produce drilling-induced tensile fractures. As the minimum horizontal stress value has been found to be close to the vertical stress S_{Hmax} is approximately 130 MPa.

One should keep in mind that still knowledge of pore pressure, vertical stress, S_{hmin}, and a good estimate of rock strength is required. Figure 10 shows the sensitivity of S_{Hmax} according to rock strength and break out width. The black square shows the result for 45° BOW (break out width) and 138 MPa UCS (unconfined compressive strength or C_0)[2].

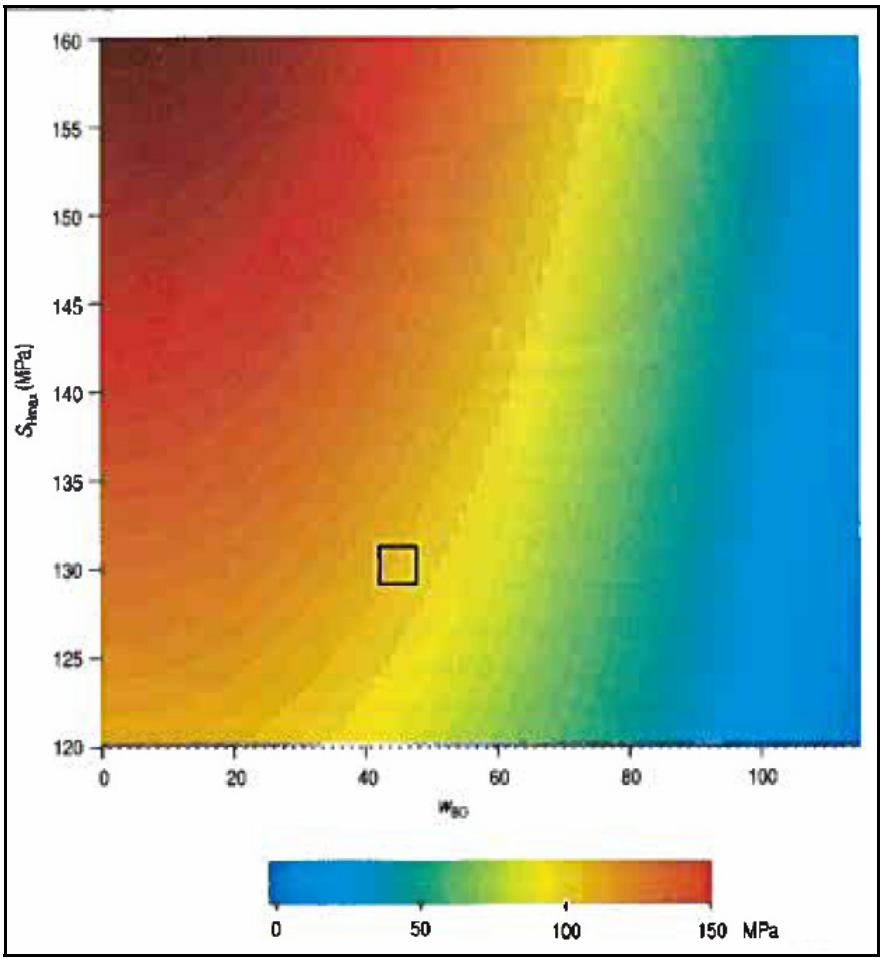

Figure 10, S_{Hmax} sensitivity[2]

It can be seen that also geological information according to stress regimes gives a helpful input for stress determination and demonstrates once more the importance of communication between the different disciplines.

Figure 11 shows a possible S_{Hmax} gradient diagram for normal faulting regime which becomes a strike-slip regime at the bottom..

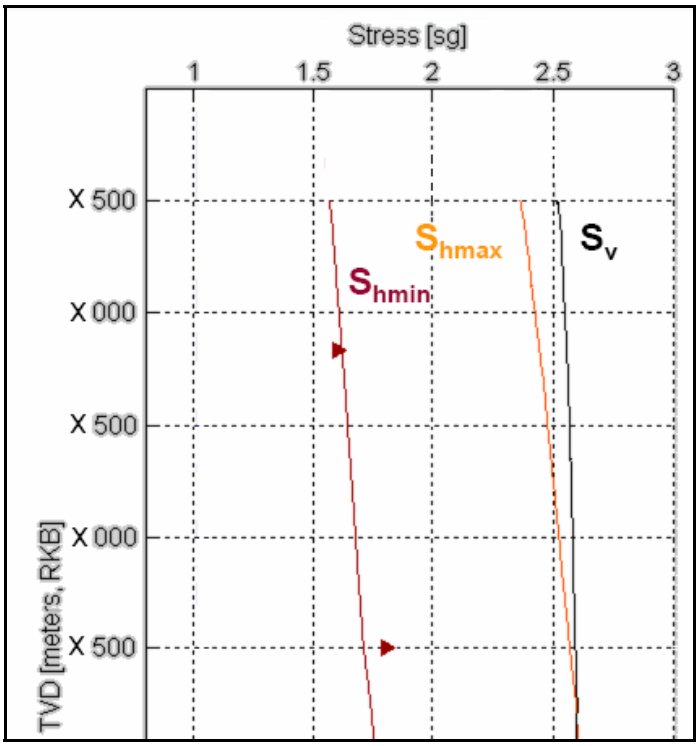

Figure 11, S_{Hmax}[5]

2.2.3.1 Use of Drilling-Induced Tensile Fractures for S_{Hmax} Estimation

Drilling-induced tensile fractures form when the difference between S_{Hmax} and S_{hmin} is significant and the minimum hoop stress (tangential stress) is under tension. This condition can be fulfilled in a strike-slip stress regime as the maximum and minimum horizontal stresses are σ_1 and σ_3. When looking at Kirsch equations for hoop stress calculation around a wellbore it becomes clear why the minima and maxima are achieved under a strike slip regime.

$$\sigma_{tanmax,\,eff} = 3*S_{Hmax} - S_{hmin} - P_{wellbore} - P_P \qquad (2.8^2)$$

$$\sigma_{tanmin,\,eff} = 3*S_{hmin} - S_{Hmax} - P_{wellbore} - P_P \qquad (2.9^2)$$

Figure 12 shows the effective stresses around the wellbore wall for a strike-slip regime under a hydrostatic condition (effective radial stress = 0). As soon as the mud weight is increased the minimum hoop stress will go under tension and drilling-induced tensile fractures will form (tensile strength of the formation (T_0) assumed to be 0).

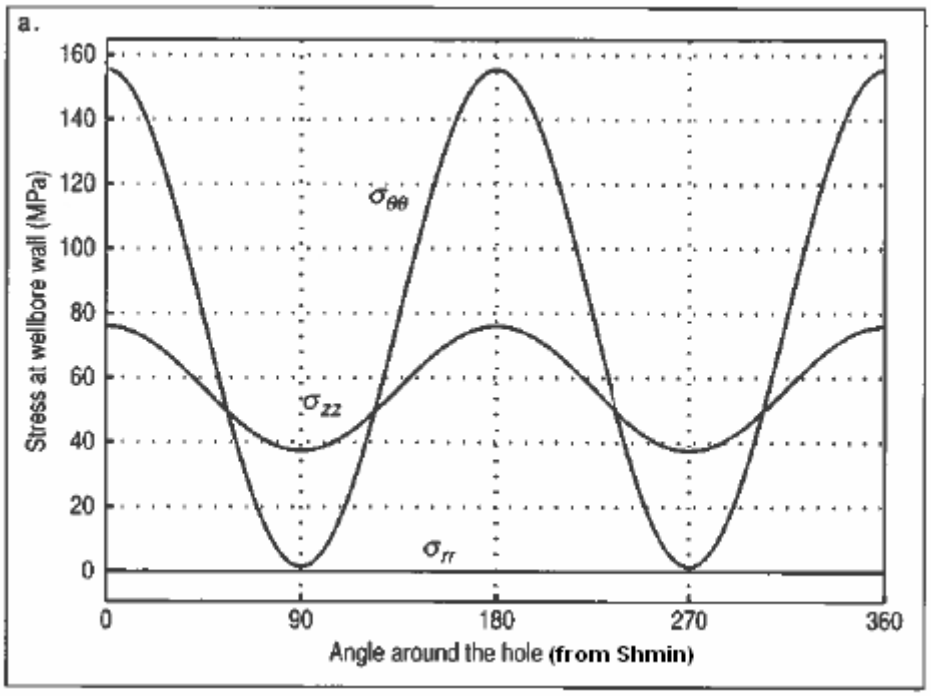

Figure 12, stresses in strike-slip regime[2]

Drilling-induced tensile fractures can be a useful way to estimate the magnitude of the maximum horizontal stress as the conditions for their occurrence in a vertical wellbore in absence of excessively high mud weights are basically identical to the values of S_{hmin} and S_{Hmax} according to a strike-slip regime in stable frictional condition[2]. The equation for the critical relationship between σ_1 and σ_3 for a strike-slip regime ($\mu = 0.6$) is

$$\sigma_1/\sigma_3 = (S_{Hmax} - P_p) / (S_{hmin} - P_p) = [(\mu^2 + 1)^{1/2} + \mu]^2 = 3.1 \qquad (2.10^2)$$

which can be simplified to

$$S_{Hmax} = 3.1*S_{hmin} - 2.1*P_p \qquad (2.11^2)$$

and rewritten as

$$S_{Hmax} = 3*S_{hmin} - 2*P_p + 0.1*(S_{hmin} - P_p) \qquad (2.12^2)$$

When rewriting the equation for the minimum hoop stress under strike-slip regime, which basically defines the onset of drilling-induced tensile fractures ($T_0 = 0$, ΔP is negligible) it will look like

$$\sigma_{\theta\theta min} = 3*S_{hmin} - S_{Hmax} - 2*P_P = 0 \qquad (2.13^2)$$

and when rearranging it to

$$S_{Hmax} = 3*S_{hmin} - 2*P_p \qquad (2.14^2)$$

it becomes obvious that the equations are almost equal because ($0.1*(S_{hmin} - P_p)$) is extremely small.

This effect can be noticed in Figure 9 where the light diagonal line contributing to the S_{Hmax}/S_{hmin} ratio for the appearance of drilling-induced tensile fractures has a very similar slope compared to the boundary line for strike-slip regime. If drilling-induced tensile fractures have been observed one can be very sure to be in a strike-slip regime with S_{hmin} below the value of the vertical stress.

The only way to detect drilling-induced tensile fractures is by the use of wellbore imaging logs (Figure 14, marked with thin black line) as these fractures will not propagate far-field as long as the mud weight is below the least principle stress. The minimum hoop stress increases with radius (Figure 13) and the fracture will propagate until the equilibrium of ΔP ($P_{wellbore} - P_p$) and the effective minimum hoop stress is found. Due to the little penetration of the fracture no noticeable influence on the drilling process will be observed.

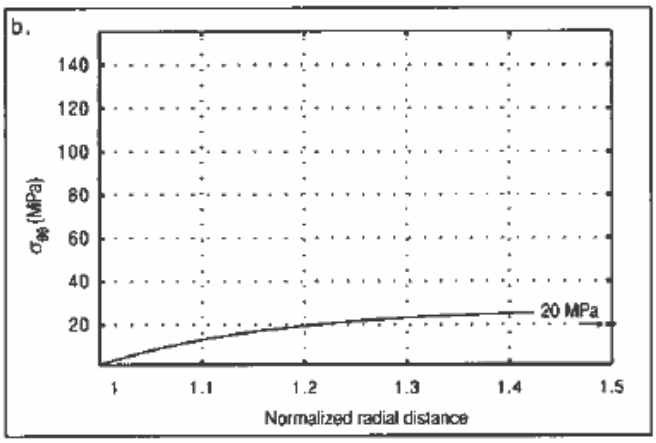

Figure 13, radial minimum hoop stress[2]

Figure 14, drilling induced tensile fractures[2]

2.2.4 In-situ Stress Orientation

The stress concentration around a vertical wellbore for the idealized case of a concentric borehole is generally calculated by the use of Kirsch equations (1898). Stress trajectories have to be either normal or parallel to the borehole wall as a free surface can not sustain any shear stress (Figure 15).

There exists a high stress concentration in S_{hmin} direction as the S_{Hmax} stress trajectories have to bend around the wellbore which leads to the maximum hoop stresses in minimum horizontal stress direction.

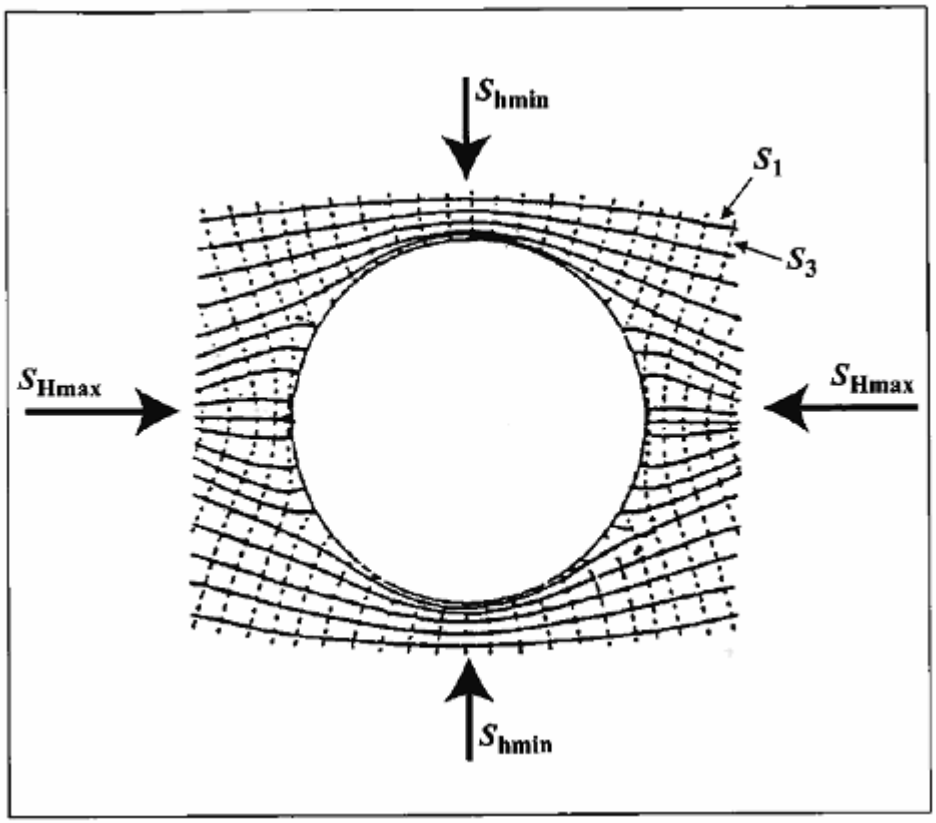

Figure 15, stress concentration around concentric borehole[2]

The opposite is true for the S_{Hmax} direction where the S_{Hmax} trajectories are separating further from each other which generates the minimum hoop stresses in maximum horizontal stress direction. Still both stresses are not independent from each other as can be seen from Kirsch equations for maximum and minimum effective hoop stress.

$$\sigma_{tanmax,\,eff} = 3*S_{Hmax} - S_{hmin} - P_{wellbore} - P_P \qquad (2.8^2)$$

$$\sigma_{tanmin,\,eff} = 3*S_{hmin} - S_{Hmax} - P_{wellbore} - P_P \qquad (2.9^2)$$

To find the orientation of the horizontal stresses it is logical consequence to seek for break-outs which will occur in S_{hmin} direction if no excessive mud weights are present. The horizontal stresses are generally assumed to be perpendicular to each other.

Common practice for break out detection is the utilization of magnetically oriented multi-arm caliper logs. The difficulty is to avoid a misinterpretation of key seats or washouts as break-outs.

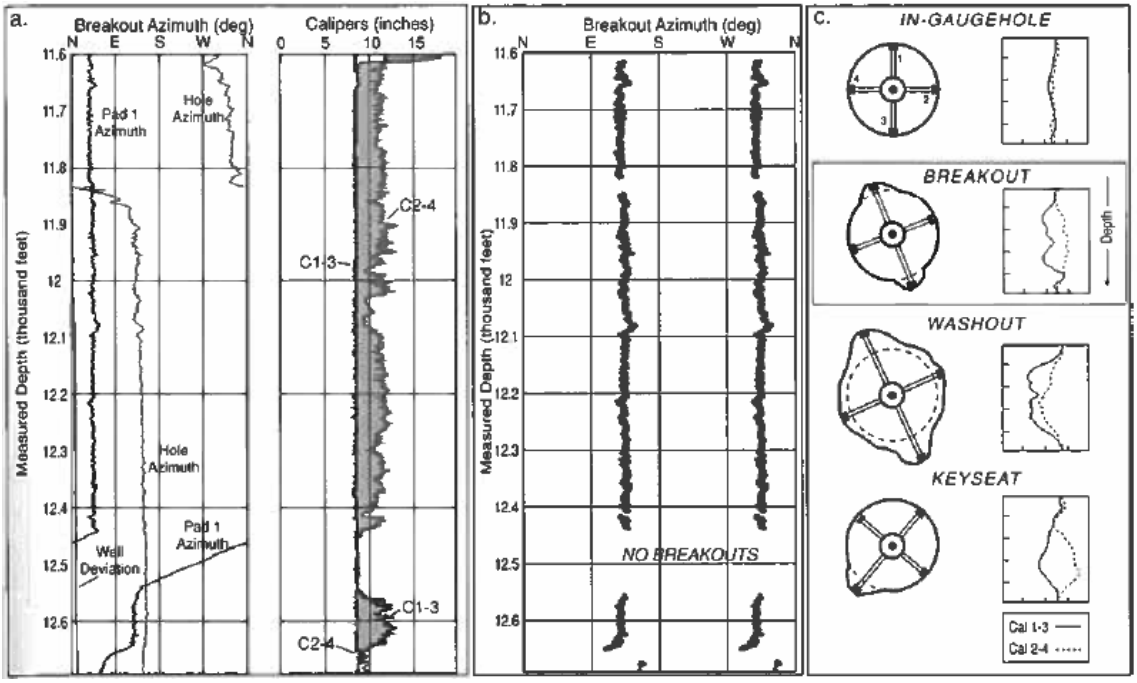

Figure 16, 4-arm caliper log[2]

Figure 16 shows on the very left side data derived from a dipmeter log providing surveys for hole azimuth, azimuth of a reference arm determined from a magnetometer (pad 1 azimuth) and the hole diameters from the 1-3 and 2-4 caliper arm pairs[2]. By strictly applying the criteria on the very right of Figure 16 break out azimuth can be found as shown in the mid diagram of Figure 16.

At 12,500 ft both caliper arm diameters are equal to bit size (8.5 in) giving confidence that neither break-outs nor key seats are present. If break-outs exist one pair of arms measures bit size and the other pair indicates an enlarged wellbore diameter. Under this condition if the principle horizontal stress orientation remains the same rotation of the tool is generally hindered as one pair is stuck in the enlarged part of the hole[2].

At the bottom of the hole section the caliper arm pairs have changed position as at shallower depth C 2-4 measured the enlarged hole diameter and C 1-3 did at the lower most part of the log[2]. As the indication of break-outs is not commonly as good as in this example it is usual to provide a quality ranking of the data to give an idea on reliability.

If borehole image logs are available it is generally possible to utilize drilling-induced tensile fractures which will form in S_{Hmax} direction to determine principle horizontal

stress directions. But one should not forget that the reasonable interpretation of image logs requires highly sophisticated skills.

For inclined wells break-outs have to be modeled to find out the horizontal principle stress directions.

2.2.5 Pore Pressure

Pore pressure is generally defined as a scalar hydraulic potential, the absolute upper boundary for the pore pressure is the overburden stress and it can not exceed the present effective minimum principle stress otherwise the formation would be fractured.

The pore pressure can be gathered directly by commonly applied downhole pressure measurement techniques. A fist idea of the pore pressure can also be gained from seismic data which is very convenient as the information can be generated prior to drilling. Pore pressure is often hard to evaluate in shales even after drilling due to very low permeability.

Indirect measurements by the use of sonic, density and resistivity logs generally utilize the correlation between Sv and porosity with the expectation of a decrease in porosity as Sv increases.

2.2.5.1 Reasons for Overpressure

(a) Disequilibrium Compaction

Disequilibrium compaction also called undercompaction is one possible and physically well understood mechanism resulting in overpressure. The overburden stress increases due to continuous sedimentation and causes compaction and a decline in porosity. If the hydraulic system is open and sufficient permeability is available in the formation that a hydraulic connection to the earth surface is provided then the loss of porosity will be compensated by fluid flow and no excessive pressure increase will happen[2].

Thus, overpressure will appear in formations with low permeability (shale), trapped sands which are not interconnected to other sands or in regions of rapid sedimentation where the fluid can not escape with the rate compaction increases[2].

An example for very high sedimentation rates and compaction induced pore pressure elevations is the Golf of Mexico where the Mississippi River deposited a large amount of sediments over the last million years[2].

(b) Tectonic Compression

Tectonic compression follows the same principle of pore pressure development as disequilibrium compaction. Thereby large-scale tectonic stress changes take place over a short geologic time period. In zones of tectonic compression reservoirs will have the strong tendency to high pore pressures and in comparison those located in extensional areas will commonly have lower pressure values. The costal area of California is an example for a tectonic compression zone[2].

(c) Hydrocarbon Column Heights

The lower density of hydrocarbons can be a reason for overpressure at the top of a reservoir especially if buoyant gas is present (Figure 17). The commonly known reason is the pressure equilibrium of the reservoir pressure and the hydrostatic formation pressure at the lower most part of the reservoir and a significantly steeper pressure gradient within the reservoir especially for gas.

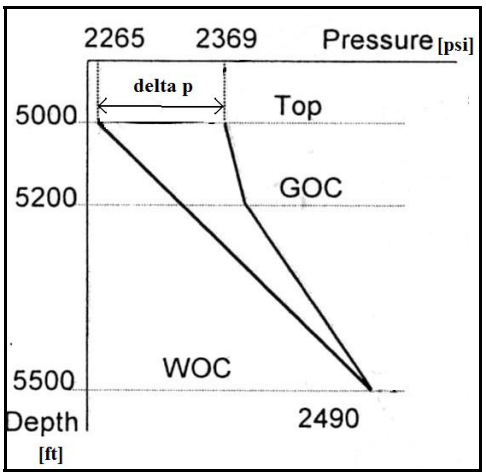

Figure 17, hydrocarbon column heights[4]

(d) Centroid Effect

High pore pressures can be encountered when drilling into the top of a tilted sand body enclosed in shale. The theory tells that sand was deposited, encased in shale and tilted afterwards. It is assumed that there is no pressure communication between sand and shale. Thus the top of the sand body has an elevated pressure and the bottom a lower pressure value compared to the surrounding shale. The depth at which the pressure in sand and shale are equal is called the centroid (Figure 18)[2].

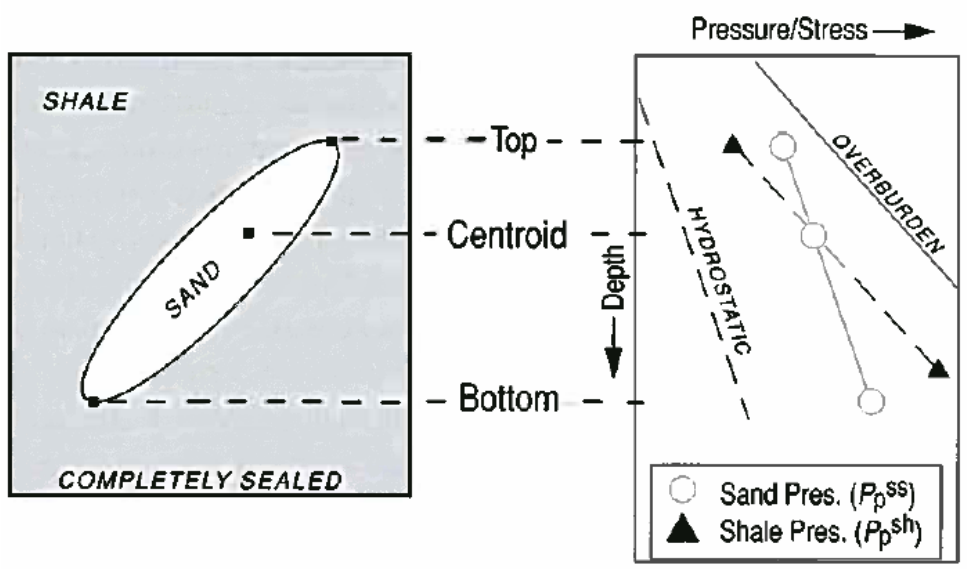

Figure 18, centroid effect[2]

(e) Dehydration Reactions

During the diagenesis of minerals it is possible that overpressure is generated. Smectite dehydration can lead to a volume increase of rock matrix and pore water. One part of this dehydration includes the transition from montmorillonite to illite which releases water from the crystalline structure of the montmorillonite at about[2] 100 °C.

A similar process of dehydration is the transition of anhydrite to gypsum which leads also to overpressure but occurs in shallower depth and at about 50 °C.

It has to be stated that these dehydration processes are very complex and not fully understood.

(f) Hydrocarbon Generation

The maturation of kerogen in the source rock leads to a significant increase in volume and can increase the pore pressure[2]. This effect is true for oil but even more for gas.

2.2.6 Rock Mechanical Properties

Estimating rock properties from geophysical well logs is based on the fact that many of the same factors affecting rock strength also influence elastic moduli among other parameters. A great majority of the formulas used to correlate the previous mentioned relationship utilize:

- P-wave velocity (Vp) as well expressed as travel time (slowness) of compressional waves along the wellbore wall (Δt, $\Delta t = Vp^{-1}$) with unit µs/ft,
- Young´s Modulus (E) which is usually derived from Vp and density data as well as
- Porosity (ϕ) (or density) data[2].

In general it can be stated that rock strength increases with Vp and E and decreases with higher porosity. It is important to notice that log derived properties strongly require calibration with core data as logs are dynamic measurements which average the properties and can not recognise little fractures or flaws leading to an overestimation of rock strength.

2.2.6.1 UCS (Unconfined Compressive Strength)

UCS is one of the most important parameters concerning rock mechanical properties. It can be derived from core tests (static) and log correlations (dynamic).

The most common rock mechanical tests are the uniaxial compressive test which means axial compression of a core sample without confining stress until failure occurs (Figure 19) and the triaxial compressive test where the core sample is subjected to axial and radial stress until the rock breaks (Figure 19).

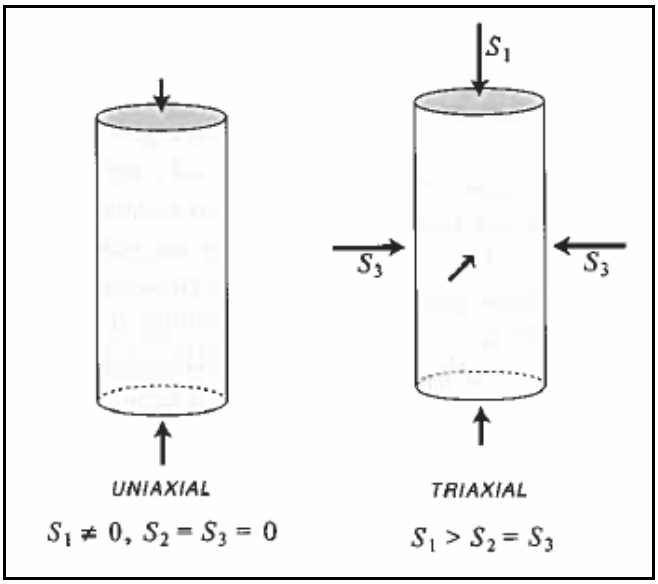

Figure 19, uniaxial and triaxial test[2]

The uniaxial test provides a value for UCS which is the stress at failure. A number of triaxial tests allow the establishment of a Mohr Coulomb failure envelope (Figure 20) which can be reasonably approximated by a straight line (Figure 21).

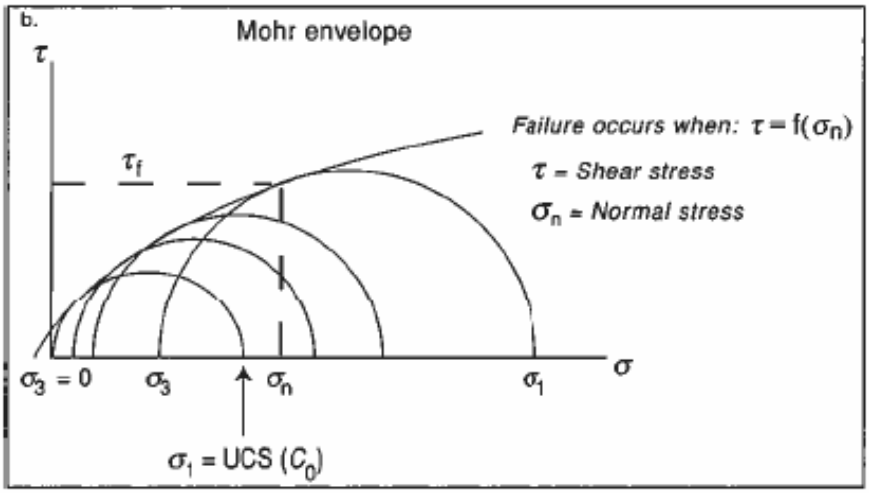

Figure 20, Mohr Coulomb failure envelope[2]

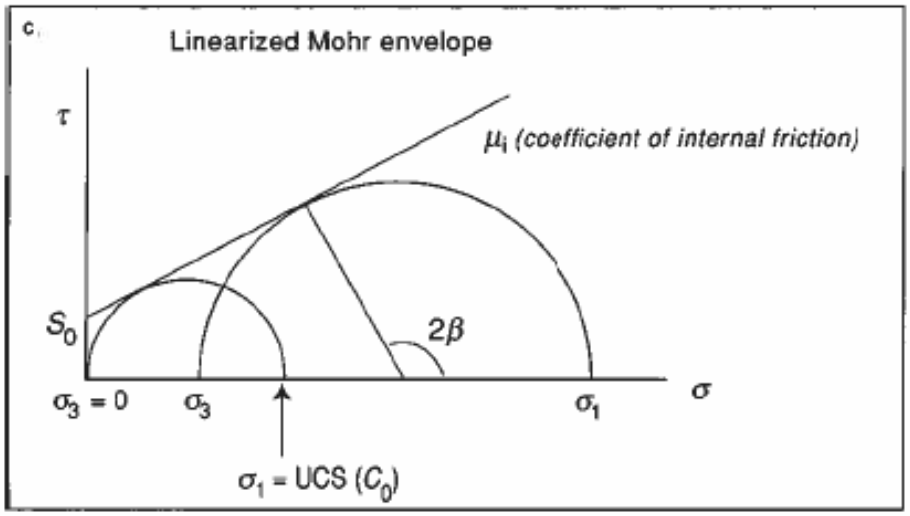

Figure 21, Mohr Coulomb failure straight[2]

The equation for the linearized Mohr failure line is

$$\tau = S_0 + \sigma_n * \mu_i \qquad (2.15^2)$$

S_0…cohesion

μ_i…coefficient of internal friction (slope of linearized Mohr envelope)

$\phi = \tan(\mu_i)$

$\beta = \tan(45+\phi/2)^2$

The UCS value gathered by core analysis should be used to calibrate the dynamic log correlation. Appendix B lists empirical relationships between UCS and other physical properties for sandstone, shale and limestone.

2.2.6.2 Angle of Internal Friction

The angle of internal friction (ϕ) can be gained from core tests (Figure 21, $\phi = \tan(\mu_i)$). It is important not to confuse the coefficient of internal friction (μ_i) with the friction coefficient (μ). Even if both have identical equations for zero cohesion

friction coefficient: $\tau/\sigma_n = \mu$ (2.1^2)

coefficient of internal friction: $\tau = S_0 + \sigma_n * \mu_i$ (2.15^2)

$S_0 = 0$

it has to be remembered that μ describes slip on a pre-existing fault whereas μ_i represents the increase in strength of intact rock with pressure (slope of Mohr Coulomb straight of failure).

There are very few relationships for the angle of internal friction and geophysical measurements because even weak rocks have relatively high values of ϕ and the link between the internal friction angle and micro-mechanical features of rock is very complex[2]. Experiments have still proven that shale with a high Young´s modulus generally tends to have a high ϕ. Table 4 provides two relationships for ϕ and rock properties in shale and shaly sedimentary rocks.

	Φ degree	General comments	Reference
27	$\sin^{-1}((V_p-1000)/(V_p+1000))$	Applicable to shale	(Lal 1999)
28	$70-0.417GR$	Applicable to shaly sedimentary rocks with $60 < GR < 120$	Unpublished
Units used: V_p (m/s), GR (API)			

Table 1, empirical relationship for angle of internal friction in shale and shaly sedimentary rocks[2]

The angle of internal friction is of significant less importance for calculations compared to UCS.

2.2.6.3 Survey of Rock Mechanical Properties

Figure 22 shows a possible survey of UCS, Poisson´s ratio and internal friction coefficient. Poisson´s ratio can also be derived from sonic logs by use of the equation

$$\nu = (V_p^2 - 2*V_s^2)/(2*(V_p^2 - V_s^2)) \qquad (2.16^2)$$

Young´s modulus is calculated by

$$E = \rho * V_s^2*(3*V_p^2 - 4*V_s^2)/(V_p^2 - V_s^2) \qquad (2.17^2)$$

V_p…velocity of compressional waves

V_s…velocity of shear waves

Appendix B gives additional equations for calculating rock mechanical properties like Poisson´s ratio (ν), Young´s modulus (E), Bulk modulus (K), Shear modulus (G), Lame´s

coefficient (λ) and relative rock stiffness (M). If two parameters are known the other 4 can be calculated.

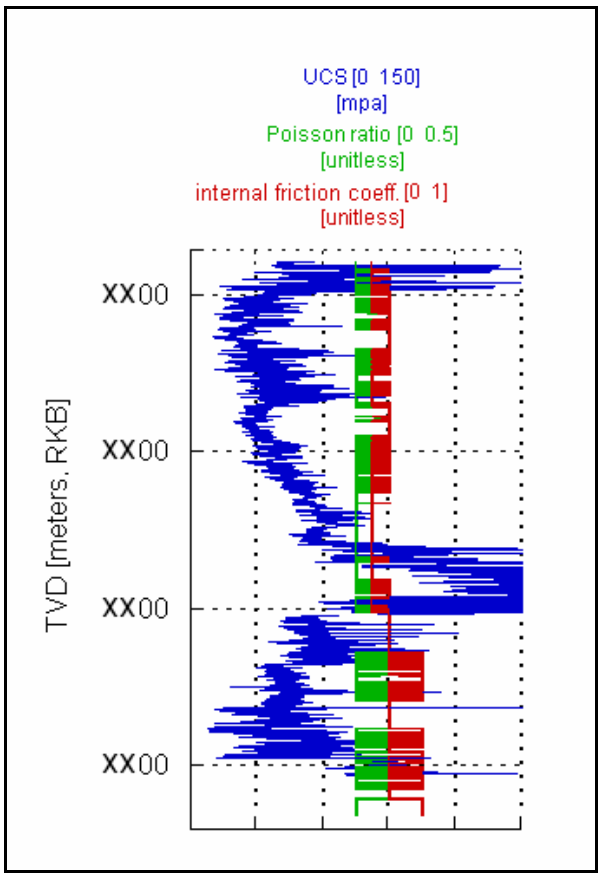

Figure 22, survey of rock mechanical properties[5]

2.2.7 Calculation of Mud Weight Window

The input parameters S_v, S_{Hmax}, S_{hmin}, the orientation of these stresses, P_P, UCS, angle of internal friction and Poisson´s ratio represent the geomechanical earth model. Their values are used to calculate the lower mud weight at which shear failure would appear (lower boundary of the mud weight window) as well as the least principle stress is used to get a value for the fracture pressure (upper boundary of the mud weight window). How these limits are calculated will be explained in detail throughout the next chapter.

The result of these calculations could look like Figure 23. The red survey is the collapse pressure curve in unit of equivalent mud weight. As one can see depending on depth either the pore pressure governs the lower mud weight boundary or the collapse pressure. Whenever the collapse pressure curve has a higher value than the pore pressure an overhydrostatic condition is required to avoid wellbore stability problems.

The lower green column represents one hole section. The mud weight window for this section is calculated at the two most critical points.

If the highest peak of the collapse pressure curve is larger in magnitude than the highest value of pore pressure in a section then the calculation for the lower mud weight window boundary is performed at the depth of this specific collapse pressure peak because at this point the highest mud weight for the lower boundary is required.

In case of pore pressure being larger in magnitude the point of highest value within the section would be the depth of investigation. Definition of bottom depth of a section is not necessarily connected to the highest collapse pressure peak or pore pressure.

The lowest value of minimum principle stress within a section is the most critical point for the upper mud weight window boundary. Most of the times this is encountered at the upper most part of a section as the fracture gradient (minimum principle stress) is usually lower at shallower depth.

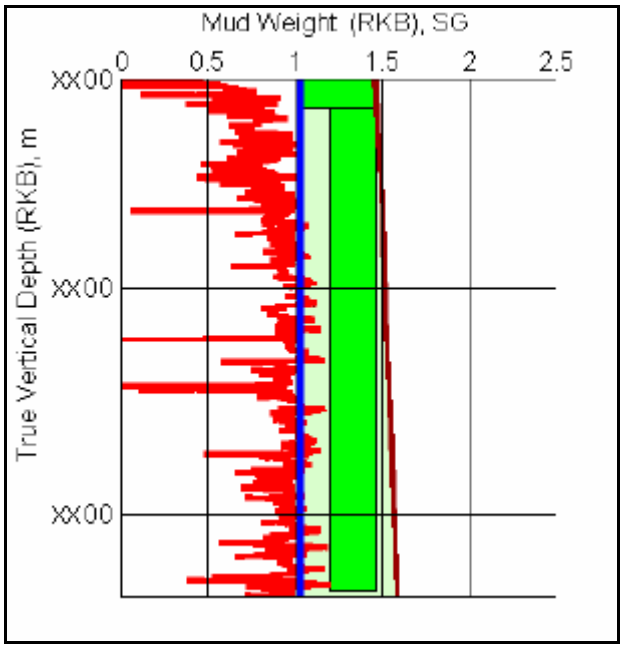

Figure 23, mud weight window diagram[5]

This procedure is done for every section in the well which provides with helpful information about mud weight windows for proper project planning.

3. Development of Calculation Program ("Fastcheck")

One objective of this Master´s thesis was to challenge the outcome of Study X in terms of mud weight window prediction. As focus was put on calculation it was necessary to find a way of verifying the results of Company X. It was decided to recalculate the critical points of the study as explained in the previous chapter. For that purpose and to gain a deep insight in the calculation process a program was developed for stress and mud weight window calculation named "Fastcheck". The program is Excel-based and this chapter is meant to explain its development step by step.

3.1. Stress Calculation

3.1.1 Kirsch Equations

The starting point in the development of such a program is the calculation of the three different types of normal stresses acting around a wellbore which are tangential (hoop), axial and radial stresses. The commonly used equations have been derived by Kirsch in 1898.

$$\sigma_{tan,abs} = 0{,}5*(\sigma_{Hmax} + \sigma_{hmin})*(1+ r_w^2/r^2) - 0{,}5*(\sigma_{Hmax} - \sigma_{hmin})*$$

$$(1+3* r_w^4/r^4)*\cos(2*\theta) - p_w * r_w^2/r^2 \qquad (2.18^2)$$

$$\sigma_{axial,abs} = \sigma_v - 0{,}5*(\sigma_{Hmax} - \sigma_{hmin})*\nu*(4*r_w^2/r^2)*\cos(2*\theta) \qquad (2.19^2)$$

$$\sigma_{radial,abs} = 0{,}5*(\sigma_{Hmax} + \sigma_{hmin})*(1- r_w^2/r^2) + 0{,}5*(\sigma_{Hmax} - \sigma_{hmin})*$$

$$(1+3* r_w^4/r^4 - 4* r_w^2/r^2)*\cos(2*\theta) + p_w * r_w^2/r^2 \qquad (2.20^2)$$

r_w…wellbore radius

r…radius of calculated point

θ…azimuth from S_{Hmax} direction

ν…Poisson´s ratio

The above equations calculate absolute stresses. Thus, to get effective stresses pore pressure has to be subtracted.

When looking at the formulas it can be seen that one can calculate the stress for any azimuth and radius around the wellbore. This means that a complete stress distribution around the wellbore for each of the three stresses can be computed. The cos(2*θ) term produces maxima and minima every 90 degrees which seems to be logic according to Figure 15.

The axial stress equation will become the far field stress (σ_v) all around the wellbore if the horizontal stresses are equal ((σ_{Hmax} - σ_{hmin}) = 0). The reason for this is that the horizontal stresses are originally generated by the vertical stress by translation via Poisson´s ratio. This would conclude that the horizontal stresses have to be equal. The reason for the horizontal stresses to be unequal as discussed in chapter 2 is an additional horizontal stress input due to e.g. tectonic movements. This means that now this additional horizontal stress is translated via Poisson´s ratio into vertical stress which is the reason why the axial stress is azimuthally fluctuating around the far field vertical stress value with maxima in S_{hmin} direction and minima in S_{Hmax} direction.

An even more exact answer would be that due to the maxima and minima of tangential stresses produced by the horizontal stress difference the axial stress will have maxima and minima at the same locations.

It is also important to notice that the axial stress has no mud weight included in the formula which makes the axial stress only dependent on far field stresses, Poisson´s ratio, radius of calculated point and azimuth. The physical explanation is simply the absence of a surface on which the pressure could act on. This fact means also that axial stresses will not change with different mud weights but remain constant for a given set of far field stresses and rock properties.

According to the radial stress it can be seen that the term (1+3* r_w^4/r^4 - 4* r_w^4/r^4)*cos(2*θ) becomes 0 for r = r_w so at the wellbore wall. This is reasonable as the pressure generated by the mud weight is uniformly acting on the wellbore wall. Why the radial stress is dependent on azimuth as the radius of investigated point is increased will become clear during the discussion on Figure 26 and 27.

3.1.2 Excel Sheets for Stress Calculation and According Diagrams

Figure 24 shows the first excel sheet with the input parameters at the upper left corner and the calculated values in the lower row. Vertical, maximum and minimum horizontal stresses as well as pore pressure and mud weight are used to calculate the effective tangential, axial and radial stresses utilizing Kirsch equations. The excel sheet specifically computes the stress values for r = r_w. As one can see in the right lower corner the effective radial stress is calculated which is equal along the azimuth and effective tangential stress is evaluated in 5° steps around the wellbore wall. The same is done for the effective axial stress in the same row further to the right (not visible on Figure 24). In this sheet tangential and axial stresses are calculated for 360° in 5° steps but as it is a symmetrical problem it is just necessary to calculate 90° as these values will be repeated.

				θ [°]	θ [°]	r [in]	rw [in]	
σv [ppg]	19,3	β [°]	60	0,00	50,00	4,50	4,50	
σHmax [ppg]	18			5,00	55,00			
σhmin [ppg]	16			10,00	60,00			
pore pressure [ppg]	8,4			15,00	65,00			
UCS = C_0 [psi]	3000			20,00	70,00			
Φ [°]	30			25,00	75,00			
T_0 [psi]	1500			30,00	80,00			
mud weight density [ppg]	13,5			35,00	85,00			
poisson´s ratio	0,25			40,00	90,00			
				45,00				
						θ [°]	0	5
depth (ft)	σv	σHmax	σhmin	pore p	pw	σr eff	σt eff 0	σt eff 5
10000,00	10036,00	9360,00	8320,00	4368,00	7020,00	2652,00	4212,00	4243,60

Figure 24, excel sheet stress calculation

This sheet has been reproduced for 19 increasing radii until the influence of the wellbore on stresses almost disappeared. With the gained data out of the various excel sheets stress distributions for all three stresses around the wellbore are already available. A wellbore radius of 4.5 inch was chosen which is not of importance as the stress magnitudes are independent from the radius due to the fact that a wellbore area is insignificantly small compared to the expansion of a formation.

A personal objective according to the program was a high level of transparency. For the achievement of this requirement a reasonable amount of diagrams was added to visualize the calculated data and to help understand and analyze the influence on changing parameters.

With the calculated stresses from the excel sheet presented in Figure 24 it was already possible to produce the diagram from Figure 25. Most important are the effective tangential stress curve in blue, the pink curve representing the effective axial stress and the yellow line for effective radial stress. 0 degree azimuth means S_{Hmax} direction where the minima of axial and tangential stress are present. At 90° the maxima can be observed. The other lines will be explained later in this chapter.

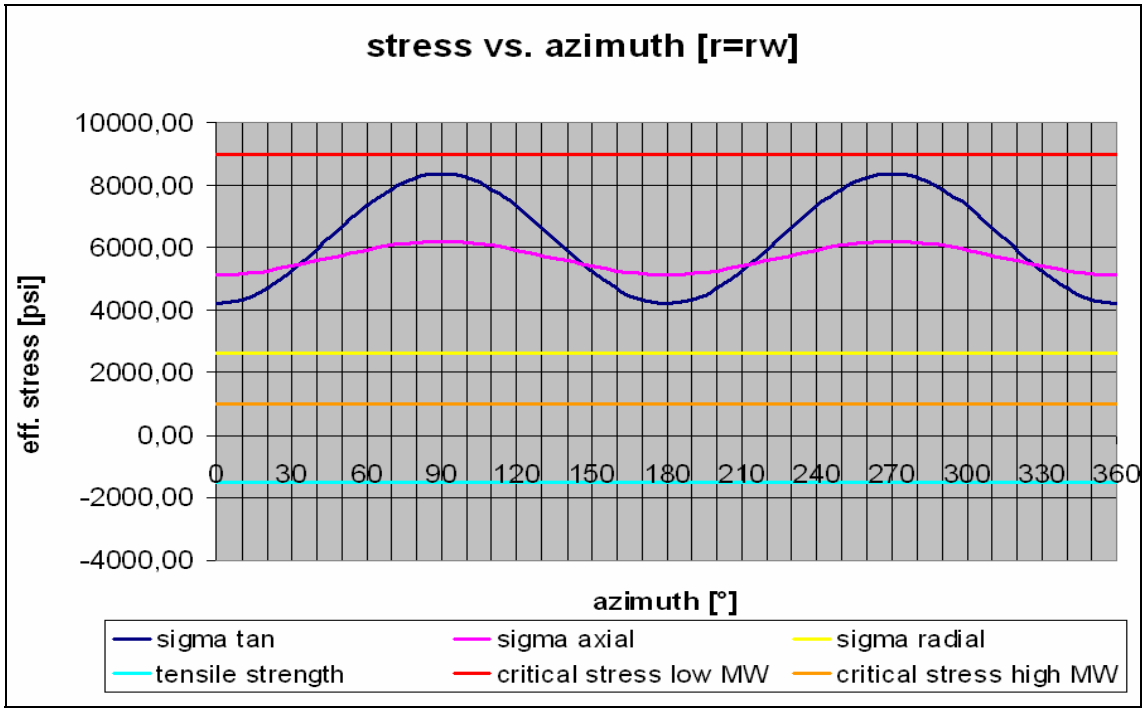

Figure 25, stress vs. azimuth

The additional data gathered by increasing the radius enabled the creation of radial diagrams (Figure 26, Figure 27). Due to the complex interaction of the maximum and minimum horizontal stresses the tangential stress in Figure 26 increases a little bit with increasing radius for the given set of input parameters (Figure 24) before it declines to S_{hmin}. The far field tangential stress (no more influence by the wellbore) for a diagram in direction of S_{Hmax} will be at the S_{hmin} value. For a better understanding it is recommended to study Figure 15 in further detail.

The axial stress is at its minimum in S_{Hmax} direction and will rapidly reach the vertical stress value as the radius is increased.

The radial stress is equal at the wellbore wall for both diagrams as discussed previously. In S_{Hmax} direction the radial stress will increase in the far field to S_{Hmax}. It is again recommended to study Figure 15 in further detail.

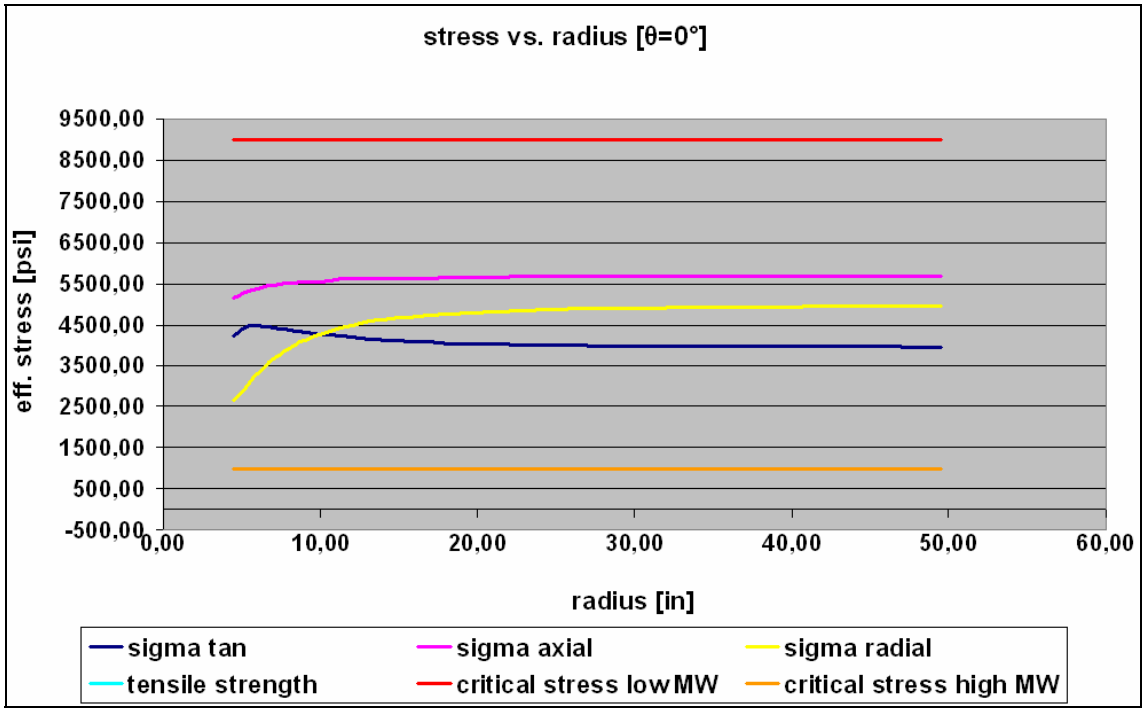

Figure 26, stress vs. radius θ= 0°

In the diagram for S_{hmin} direction (Figure 27) the maximum values for tangential and radial stress will be reached. The tangential stress will decrease to S_{hmax} with increasing radius.

The axial stress reaches its maximum as the tangential stress is at its maximum and will decrease to the vertical stress with increasing radius.

The radial stress at the wellbore wall is the value of the pressure difference between pore pressure and wellbore pressure due to the fact that effective stresses are presented in all shown diagrams. Radial stress will finally increase to S_{hmin} as going deeper into the formation.

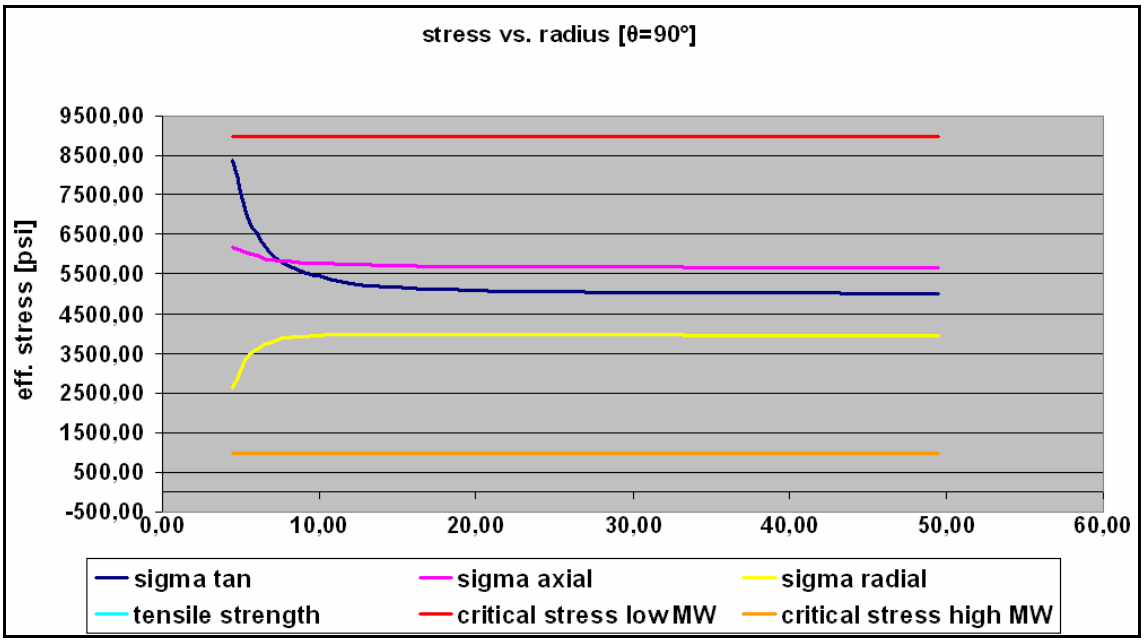

Figure 27, stress vs. radius θ = 90°

As mentioned earlier in this chapter due to the availability of all the data around the wellbore for the three normal stresses it is possible to generate a stress distribution.

Figure 28 shows a 3D diagram of the tangential stress distribution around the wellbore in an unfolded manner. Basically it is the combination of the three presented 2D stress diagrams. It is a convenient way to look at the same issue from a different perspective and it is very helpful for understanding purposes. Additional 3D diagrams for axial and radial stress distribution can be found in Appendix C. The whole program is designed in a continuously up dating way so if any parameter is changed all the diagrams will immediately change as well which gives the ability to quickly observe and analyze input variations.

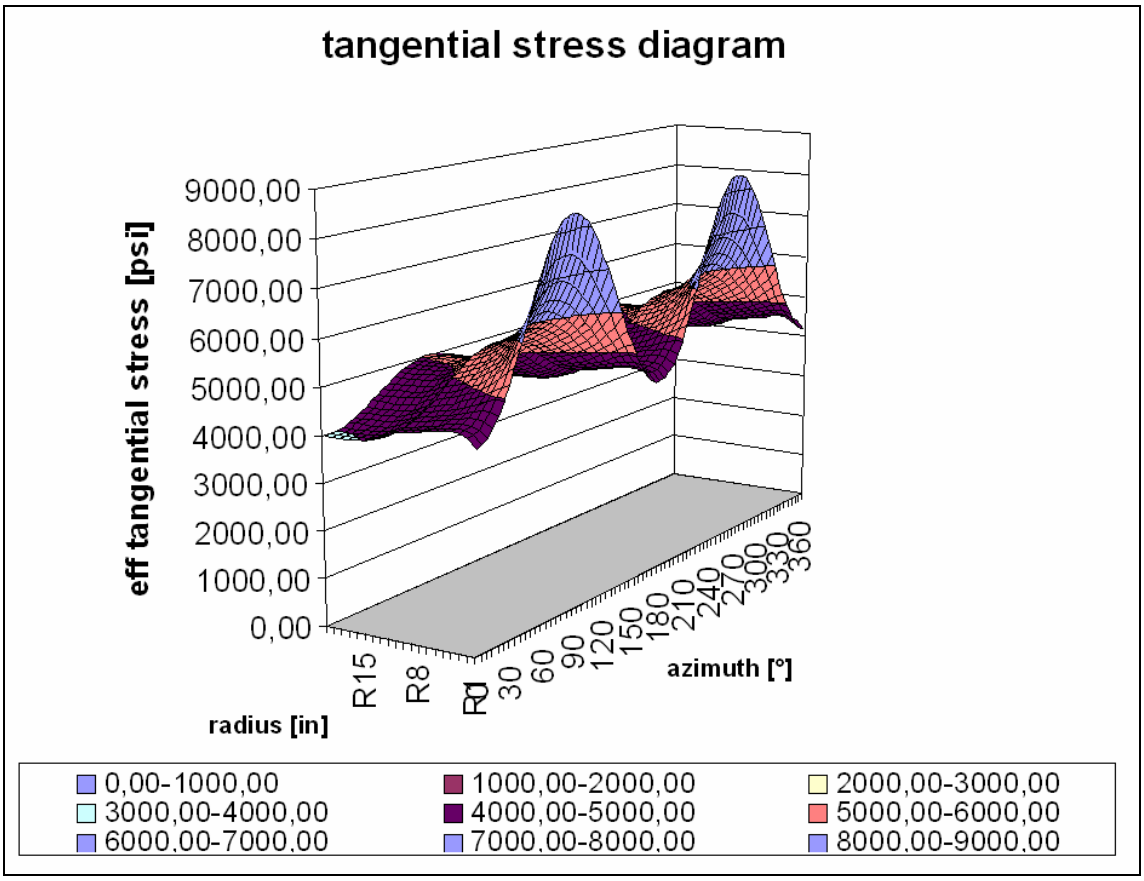

Figure 28, 3D tangential stress diagram

3.2. Mohr Coulomb Stress Diagram

The Mohr Coulomb stress diagram is commonly used in the industry to represent stress relationships and failure conditions. With the integration of this very useful tool into the program I was able to even further analyze different parameter sets.

Figure 29 shows a Mohr Coulomb stress diagram for S_{Hmax} and S_{hmin} direction at the wellbore wall. One should keep in mind that the brown and blue circle are independent as they are 90° shifted but for the purpose of good overview both have been combined into one diagram. In a vertical wellbore failure will initiate at one of these two directions.

The Mohr Coulomb failure criterion utilizes only the minimum and maximum stress for failure calculation. The diagram shows exactly this approach which is the reason why the minima and maxima for each direction always define the stress circle. This type of presentation is actually a three dimensional Mohr Coulomb stress diagram as all three

stresses are included (tangential, axial and radial). The program realizes which two out of the three stresses are at highest and lowest value and draws the circles accordingly.

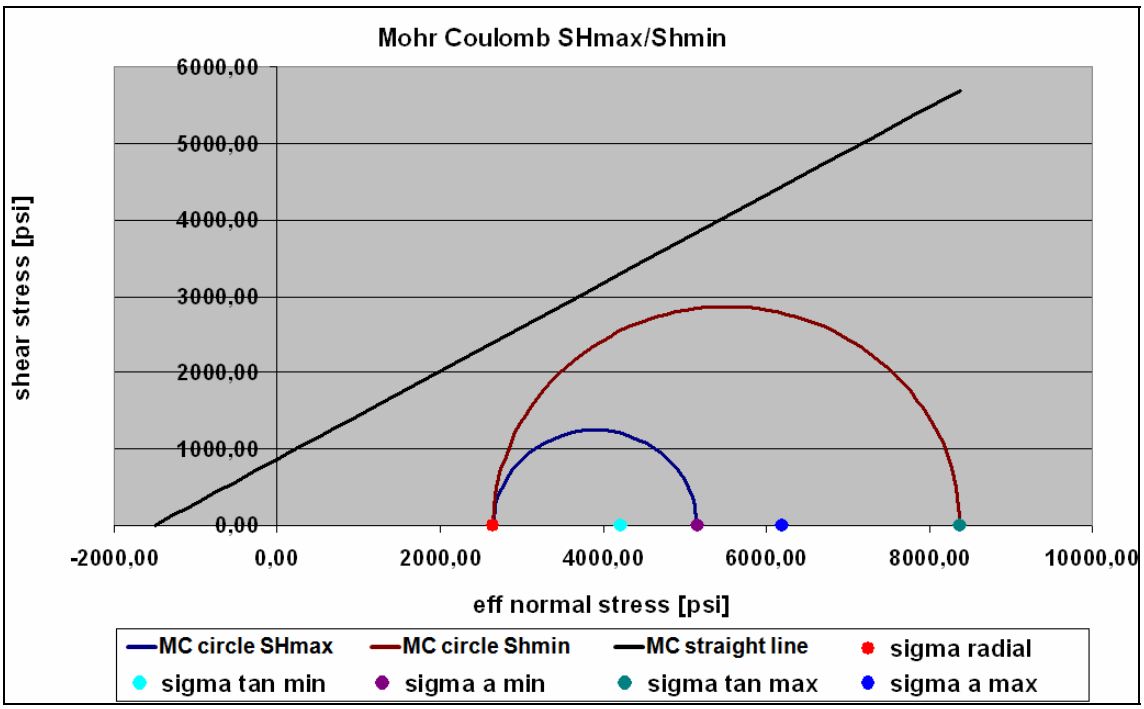

Figure 29, Mohr Coulomb stress diagram

3.2.1 Mohr Coulomb Failure Criterion and Mud Weight Calculation

The Mohr Coulomb stress diagram provides the great opportunity to change the mud weight and to see at which value failure will occur. Based on this fact a failure criterion was developed simply on the indication if a circle is touching the straight line of failure or not. More precisely an indicator was programmed if the shear stress value at the possible point of contact (Figure 21) of the stress circle is equal or larger than the shear stress value of the straight line of failure (Figure 30).

If the criterion is fulfilled failure occurs which gives a boundary for the mud weight window in terms of rock strength. It has to be kept in mind that the lower mud weight boundary must not go below the pore pressure for conventional overbalanced drilling as well as the upper mud weight boundary is set by the least principle stress.

The linearized Mohr Coulomb failure criterion is generally written as

$$\sigma_1 = C_0 + \beta * \sigma_3 \qquad (2.21^2)$$

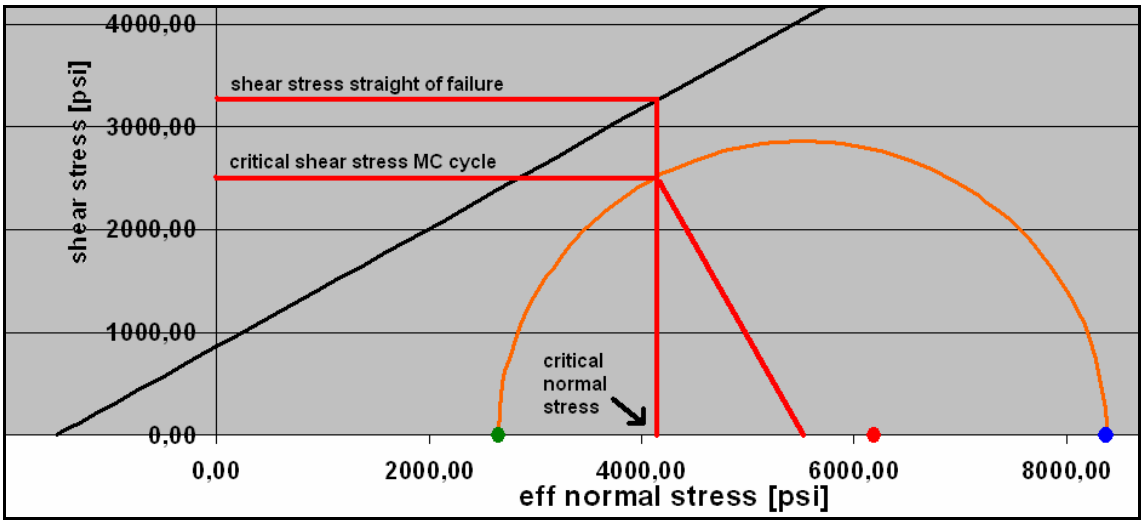

Figure 30, explanation of shear stress indicator

mud weight density [ppg]	max	min	sigma critical	shear critical	failure yes
0,00	11232,00	-4368,00	-468,00	6755,00	1
0,10	11180,00	-4316,00	-442,00	6709,96	1
0,20	11128,00	-4264,00	-416,00	6664,93	1
0,30	11076,00	-4212,00	-390,00	6619,90	1
0,40	11024,00	-4160,00	-364,00	6574,86	1
0,50	10972,00	-4108,00	-338,00	6529,83	1

Figure 31, mud weight window calculation

No macros were included for the reason of transparency and so the mud weight was varied from 0 to 25 ppg in 0.1 ppg steps to find the mud weight window. Figure 31 shows a cutout of the excel sheet. At 0 ppg the rock will fail and as the mud weight is increased the point where the critical shear stress of the Mohr Coulomb stress circle will become smaller than the shear stress of the straight line of failure will be reached. The program realizes the change from failure to stable condition and sets the boundary for the lower mud weight window. The opposite happens for the upper limit. As soon as conditions change from stable to unstable the boundary is set.

In terms of stresses the radial stress is the lowest for low mud weights (effective radial stress is zero at hydrostatic condition, Figure 32). For hydrostatic condition it is obvious that for the given set of input parameters the formation would fail. A further increase of mud weight elevates the value of $\sigma_{radial,\ eff}$ which is the reason for the shrinkage of the Mohr Coulomb stress circles. Figure 33 shows the MC diagram for a mud weight of 13 ppg (input as presented in Figure 24). The stable condition has already been

achieved. Still it can be observed that a decrease in MW would cause the formation to fail initially in S_{hmin} direction (brown circle).

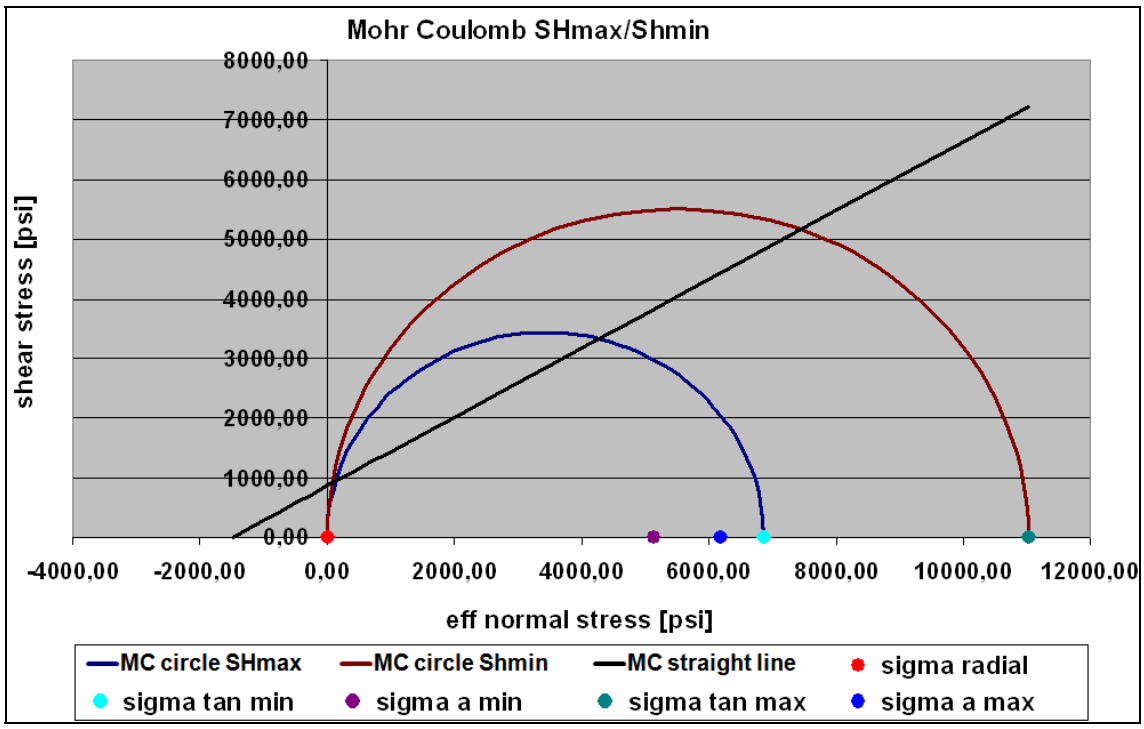

Figure 32, MC for hydrostatic condition

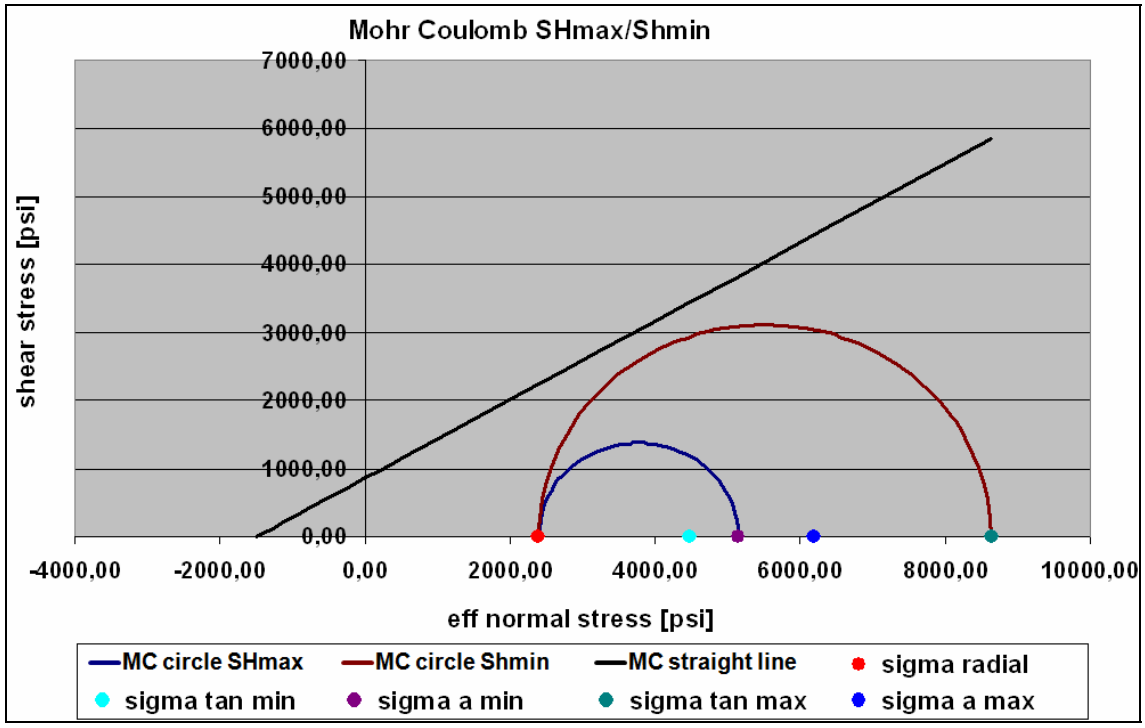

Figure 33, MC at 13 ppg

A further means that the minimum effective tangential stress becomes the least stress. At a mud weight of 19.7 ppg the failure criterion is fulfilled again (Figure 34) but in direction of S_{Hmax}.

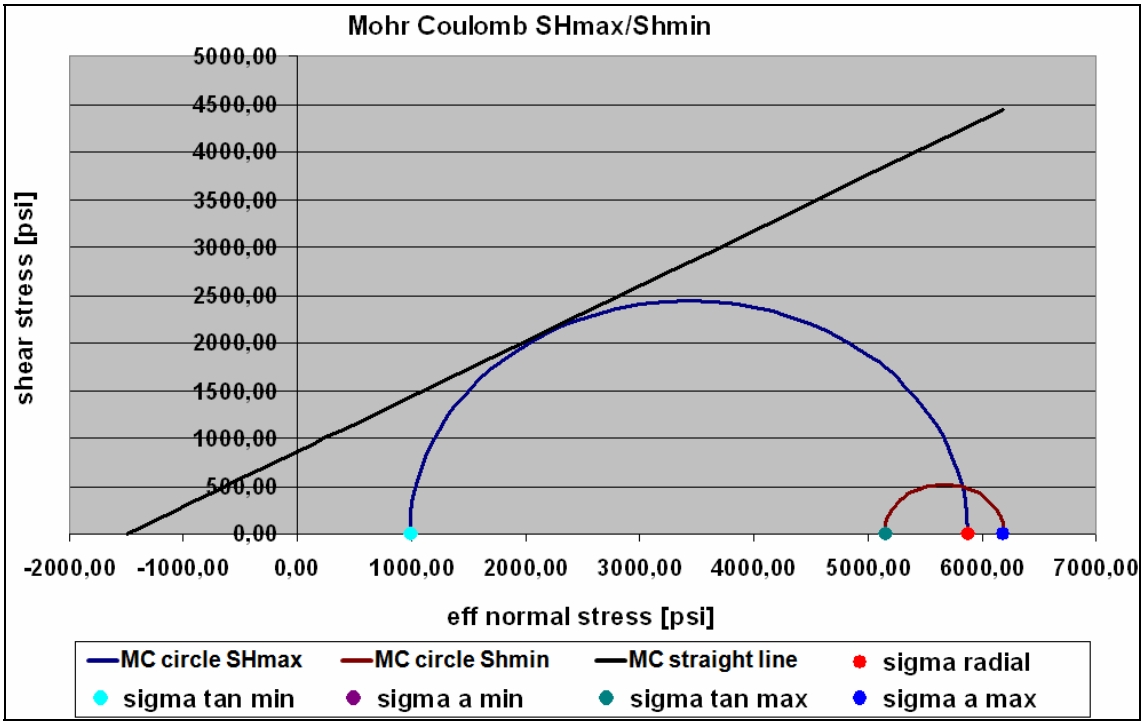

Figure 34, MC at 19.7 ppg

This condition would never be achieved in reality for this set of data as the least principle stress has an equivalent mud weight of 16 ppg. So the upper limit of the MWW would be 16 ppg. Still it is possible that shear failure appears in S_{Hmax} direction prior to fracture pressure.

3.2.1.1 Tensile Failure

There are basically two types of failure which are shear and tensile failure. Tensile failure will appear if the tensile strength (T_0) of the rock is overcome. This limit is displayed as turquoise line in the azimuthal stress diagram (Figure 25).

Usually rock has very little tensile strength and thus it is often assumed to be zero. In the Mohr Coulomb stress diagram tensile strength is the distance from the origin to the intersection of the straight line of failure and the x-axis. The linearized form of the Mohr envelope generally overestimates T_0. Due to that fact the program was designed to offer the possibility to use a reduced tensile strength. If a measure of tensile

strength is available one can use this value otherwise the system will utilize the calculated value from the intersection point. The tensile failure criterion is written as

$$\sigma_3 <= -T_0 \qquad (2.22^2)$$

The minus is included as tensile rock strength is usually written as a positive number although the convention states positive normal stress to be written as a positive value and a negative one with a minus. Tensile failure was included in the program using the above equation.

Tensile failure due to negative tangential stress will most likely appear in a strike slip regime as mentioned previously (drilling-induced tensile fractures). If the mud weight is reduced below the pore pressure tensile failure could also appear in a radial direction. Theoretically tensile failure could also happen in axial direction if the axial stress becomes sufficiently negative.

3.3. Break Out Width Allowance

Break out width is generally defined as the included angle between the edges of a break-out.

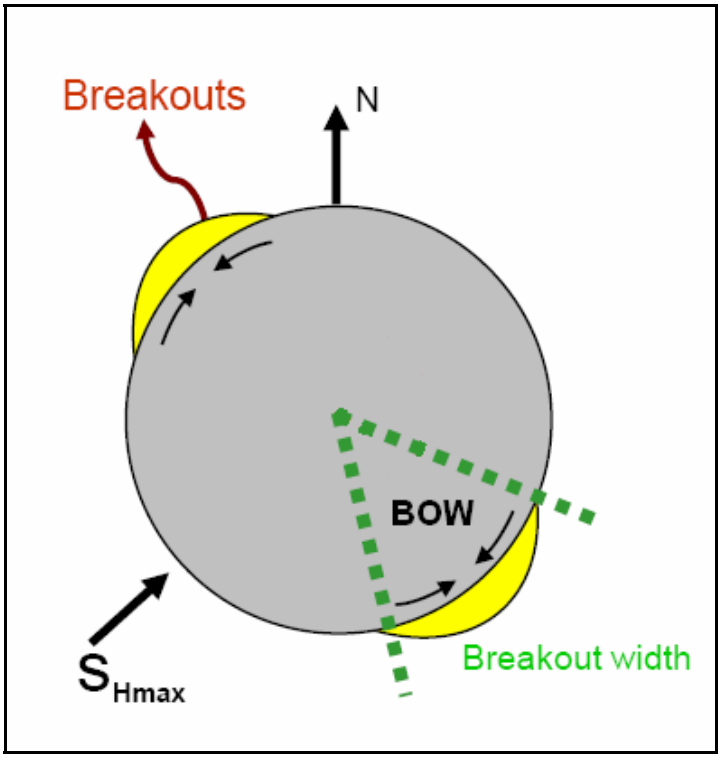

Figure 35, break out width

Company X calculated the MWW with 90° break out allowance for vertical wells as tests and experience showed that a borehole will remain stable as long as half of the circumference consists of intact rock[2]. This circumstance required the introduction of a break out width allowance in the program.

Break-outs will initiate if the three principle stresses are in a critical relationship as discussed in the previous chapter. The Mohr Coulomb failure criterion utilizes just the minimum and maximum principle stress. For a given set of parameters including a certain MW below the critical value for shear failure a specific break out width is present. Figure 36 shows an azimuthal stress diagram for 90° break-outs. The red line represents the critical stress relationship at which shear failure occurs. It has to be interpreted that if the maximum stress out of the three exceeds the stress value indicated by the red line all three stresses (for MC failure criterion the minimum and maximum stress) are in a relationship that shear failure will initiate.

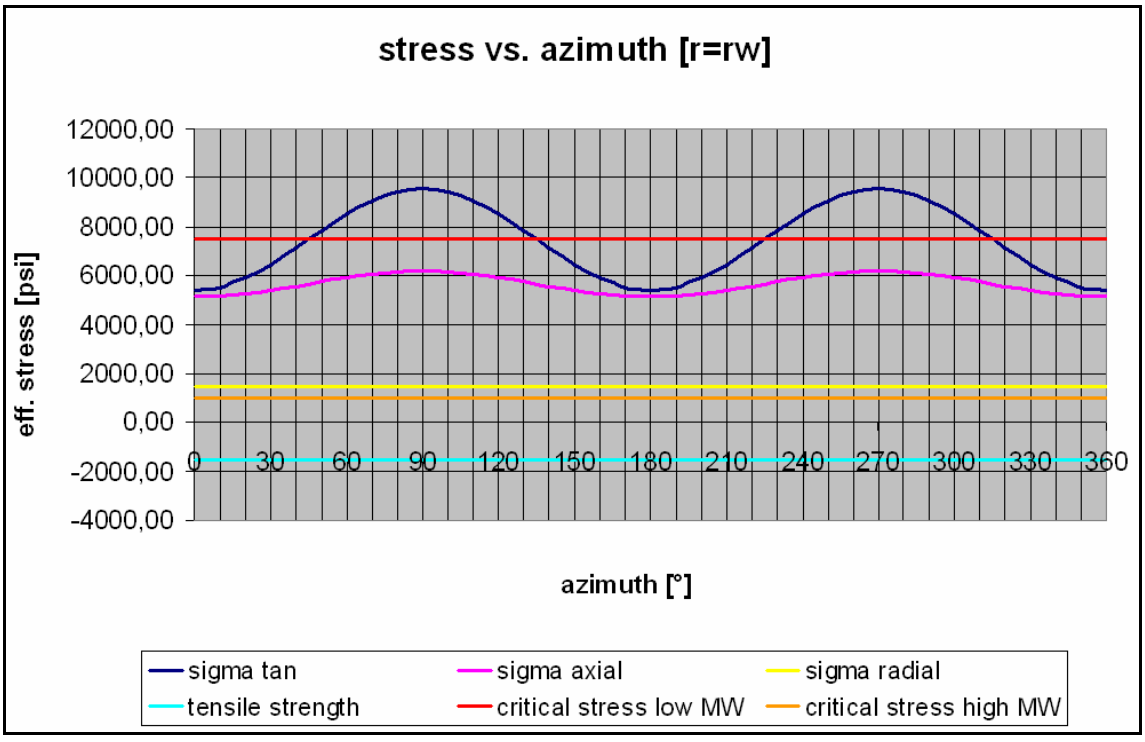

Figure 36, 90° bow

According to MC failure criterion the two stresses governing shear failure are tangential and radial stress for this particular situation. If we follow the dark blue curve from 0 to 90° one can see that up to 45° the relationship between tangential and radial

stress is not critical. As the dark blue curve intersects the red line shear failure initiates until both intersect again at 135° which includes 90° of break-outs.

The program decreases the mud weight in 0.1 ppg steps starting at the critical MW for shear failure initiation and calculates the critical stress value (red line) and the according break out width for each situation. If the required bow is in agreement with the calculated one the specific MW is set as the lower mud weight window boundary (Figure 37, FALSCH means no failure).

azimuth [°]	critical stress indi [psi]	max [psi]	min [psi]	mw indicator [ppg]
0	FALSCH	5408,00	1456,00	0,00
5	FALSCH	5439,60	1456,00	0,00
10	FALSCH	5533,44	1456,00	0,00
15	FALSCH	5686,67	1456,00	0,00
20	FALSCH	5894,63	1456,00	0,00
25	FALSCH	6151,00	1456,00	0,00
30	FALSCH	6448,00	1456,00	0,00
35	FALSCH	6776,60	1456,00	0,00
40	FALSCH	7126,81	1456,00	0,00
45	7488	7488,00	1456,00	11,20
50	7849	7849,19	1456,00	0,00
55	8199	8199,40	1456,00	0,00
60	8528	8528,00	1456,00	0,00
65	8825	8825,00	1456,00	0,00
70	9081	9081,37	1456,00	0,00
75	9289	9289,33	1456,00	0,00
80	9443	9442,56	1456,00	0,00
85	9536	9536,40	1456,00	0,00
90	9568	9568,00	1456,00	0,00

Figure 37, break out width calculation

It was already mentioned in the text that break-outs can also appear at high mud weights in S_{Hmax} direction below fracture pressure (Figure 38). This situation appears most likely if the least principle stress is very small compared to the intermediate and maximum stress which is the reason for the low minimum tangential stress in Figure 38.

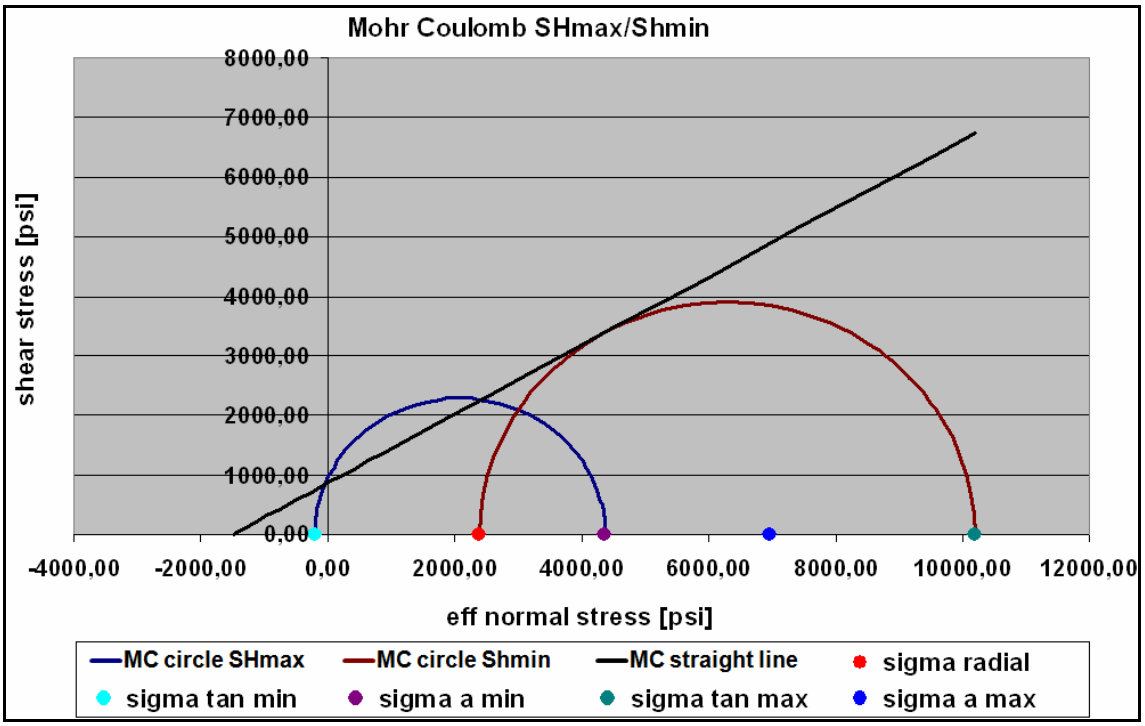

Figure 38, MC diagram break-outs high MW

Due to the fact that these break-outs might cause wellbore stability problems a critical stress value for high mud weights was introduced in the program. The same principle as for break out width at low MW was used with the difference that the program does not allow to set an acceptable break out width allowance for high mud weights but the actual break out width for a given mud weight is calculated and displayed for high mud weights.

In Figure 39 one can see that the tangential and axial stress govern the MC failure criterion (S_{Hmax} direction). The orange line indicates the critical stress value for the minimum principle stress at which the stress relationship of all three principle stresses causes the formation to fail.

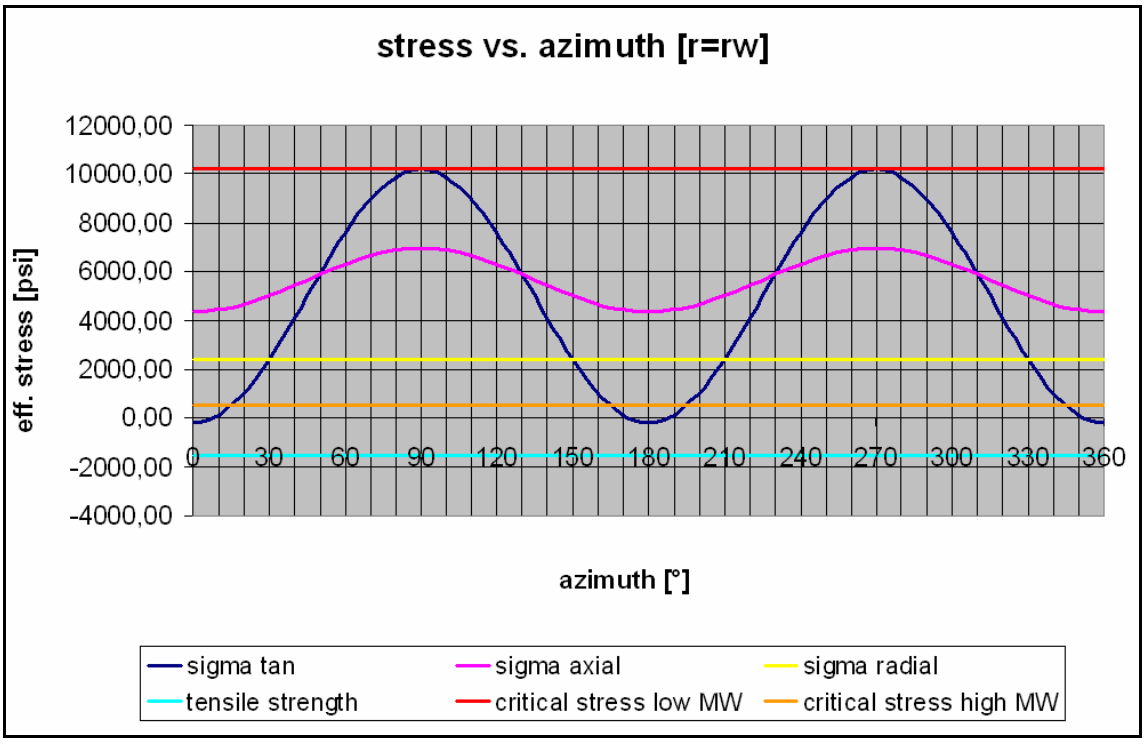

Figure 39, break-outs at high mud weight

3.4. Monte Carlo Simulation

The program is able to calculate mud weight windows for given parameters and certain break out allowances. To account for uncertainties distributions can be set for the values of the input parameters. This is common practice of Company X and it has to be stated that the value of uncertainty of each parameter is depended on the judgment of the particular editor according to a geomechanical study. It is also true that each study will be influenced to a certain degree by all the interpretations of the person in charge.

If the program user takes the same parameter values and distributions as the company which has performed the study “Fastcheck” will compute the same results within the variance of Monte Carlo simulation.

It is still possible to change every parameter if required. So if the program user is confident that e.g. the pore pressure is very uniform he/she can decrease the uncertainty by reducing the standard deviation of the distribution.

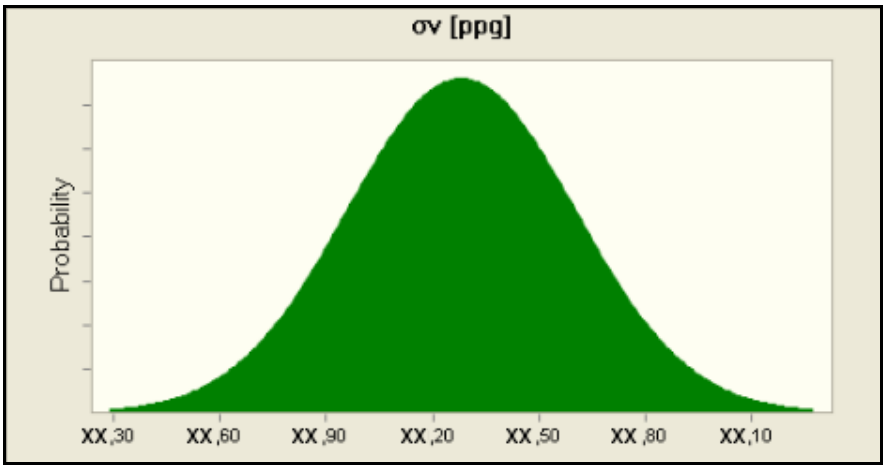

Figure 40, normal distribution for vertical stress

Figure 40 shows a normal distribution for vertical stress used for Study X. σ_v had an uncertainty of +/- 5% of the most likely value. Generally the vertical stress will have a smaller uncertainty as the minimum horizontal stress (+/- 7% for Study X) and the maximum horizontal stress (+/- 9% for Study X). These different uncertainties contribute to the accuracy of the measurement or calculation techniques of the three principle stresses. Throughout Study X normal distributions for vertical and horizontal stresses have been used.

Due to the fact that the three principle stresses do not show any tendency to other distributions the normal distribution is considered to be the most appropriate one.

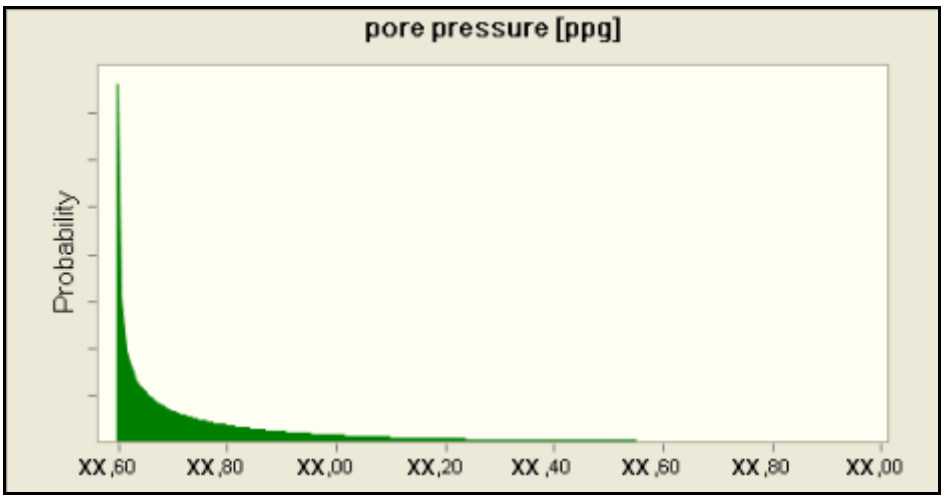

Figure 41, gamma distribution for pore pressure

Pore pressure was either varied +/- 10 % (normal distribution) or cut off by hydrostatic pressure on the low side (hydrostatic/+10 %, Figure 41) or by the least principle stress as maximum value (- 10 %/ least principle stress, Figure 42).

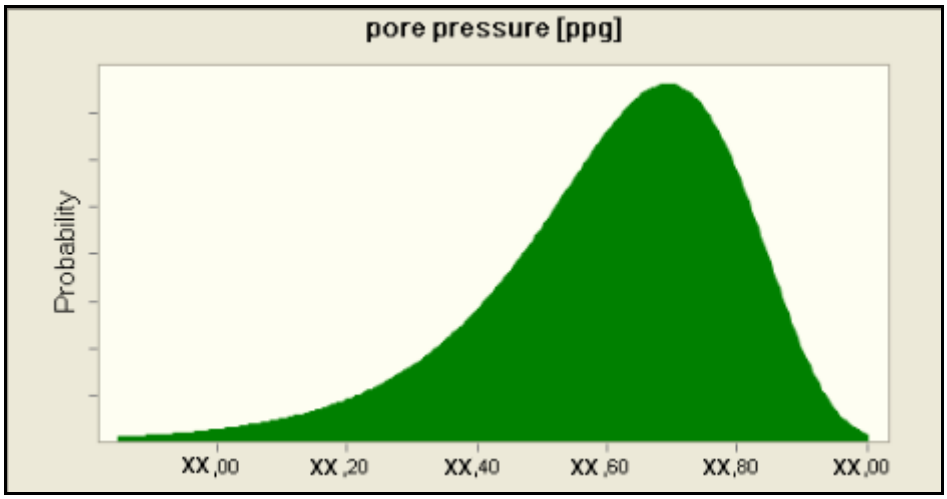

Figure 42, minimum extreme distribution for pore pressure

Gamma and minimum extreme distribution were used as these distributions most beneficially represented the given situation out of the distributions provided by Crystal Ball (used Monte Carlo simulation software). A normal distribution cut off at the most likely value to the upper or lower side would be even better but experience showed that a change in distribution e.g. from triangular to normal distribution does not have a significant impact on the result.

For UCS a normal distribution with +/- 20 % was utilized for Study X. Literature shows that for UCS distributions often a log-normal distribution is used[2]. This would have been applicable here as well but as Company X went for a normal distribution it was decided to prefer the same distribution.

Poisson´s ratio was used within a range of 0.25 to 0.3 so a uniform distribution was applicable (Figure 43).

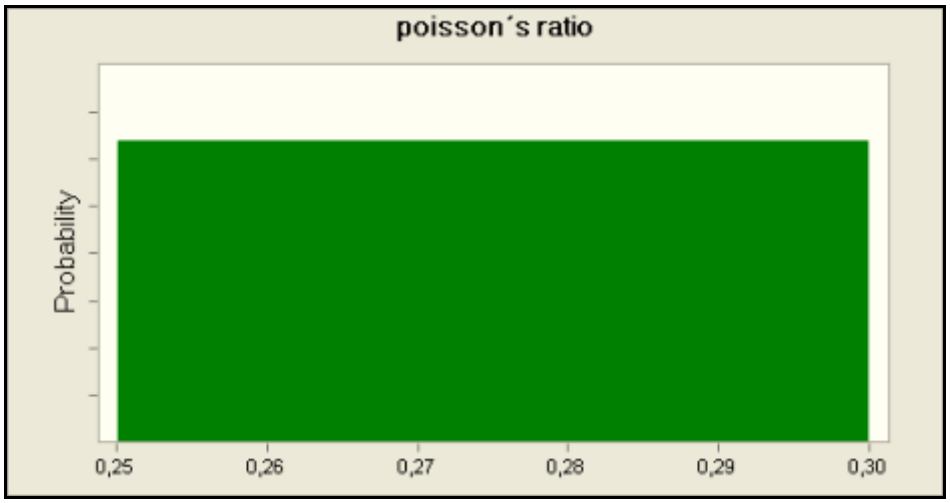

Figure 43, uniform distribution for Poisson´s ratio

Angle of internal friction was kept at a constant level for the calculation of a specific section.

Monte Carlo simulation was performed with 10,000 iterations by utilizing the software Crystal Ball.

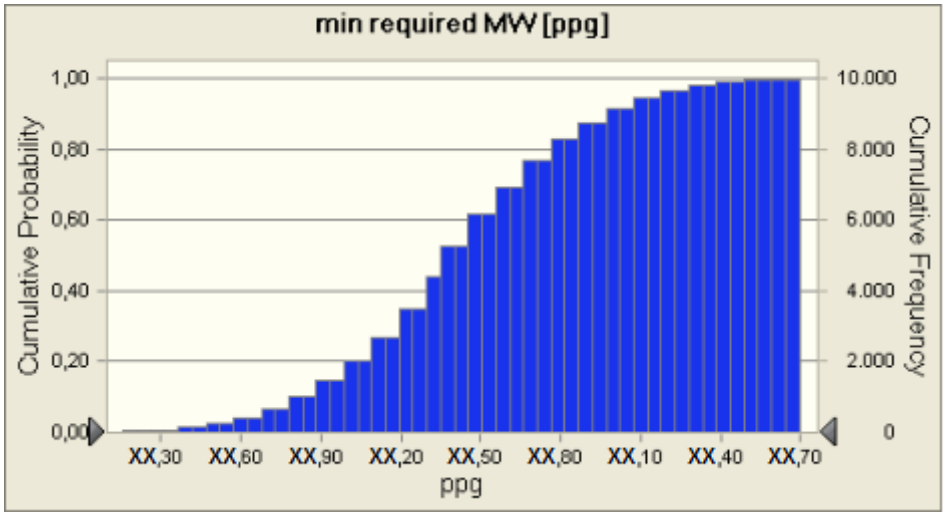

Figure 44, cumulative frequency min required MW

Figure 44 shows a possible outcome for the lower boundary of the mud weight window. It does not have the typical S-shape as the pore pressure was the dominant factor and the according distribution was cut off by hydrostatic pressure at the lower limit (Figure 41). The simulation for the lower boundary has been calculated at the most critical point in the according section.

Cumulative frequency for the upper mud weight boundary could look like Figure 45. The reason for the S-shape is the normal distribution of S_{hmin} which was the only governing parameter for the upper mud weight limit throughout all simulations performed. The distribution was calculated for the upper most part of the according section as the fracture pressure was lowest there which made it the most critical point for the upper MW boundary.

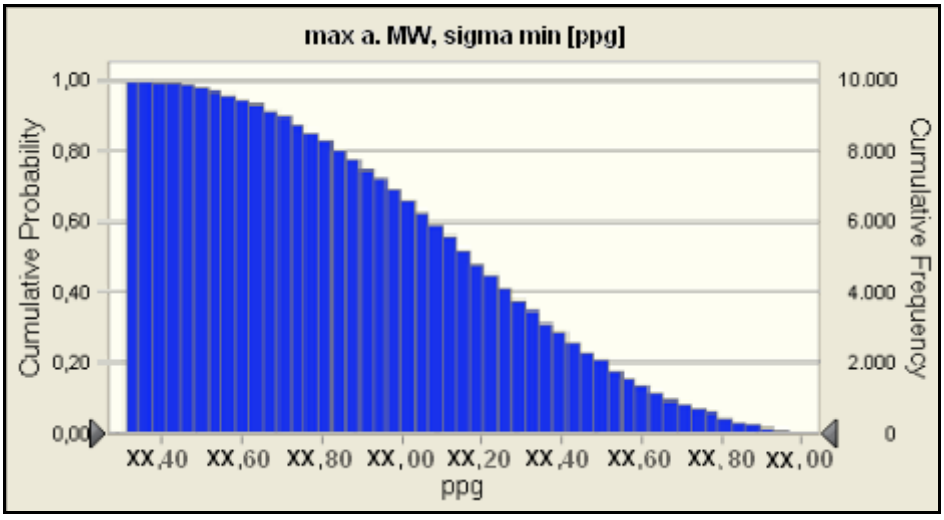

Figure 45, cumulative frequency maximum allowable MW

The P50 (most likely) and P90 (included safety) values from both distributions are used to set values for the mud weight window.

3.5. User Interface

Figure 46 shows the input frame of the user interface which consists of the three principle stresses, pore pressure, UCS, angle of internal friction, mud weight density, Poisson´s ratio, depth of investigation, break out width allowance, reduced tensile strength, and the calculated value if no reduced T_0 was used.

Input:	
vertical	
σv [ppg]	19,3
σHmax [ppg]	18
σhmin [ppg]	16
pore pressure [ppg]	8,4
UCS = C_0 [psi]	3000
Φ [°]	30
mud weight density [ppg]	13
poisson´s ratio	0,25
TVD [ft]	10000
Break out width [°]	90
T_0 [psi] input	0
if Tzero is not given, keep it zero in the "Tzero input" frame, it will be calculated automatically below	
T_0 [psi]	1500
Tzero is calculated by Czero and phi, don´t fill in a number	

Figure 46, user interface input

The first part of the output consists of minimum required MW which is always connected to the given break out allowance (failure at low mud weight), maximum allowable MW if the least principle stress is set as the upper most boundary, maximum allowable MW at which the formation would fail (failure at high mud weight), maximum and minimum of all effective principle stresses, and all values of effective principle stresses (Figure 47).

Output:	
Total	
min required MW [ppg]	11,20
max a. MWW, σmin [ppg]	16,00
max allowable MW [ppg]	19,70
sigma max [psi]	8632,00
sigma min [psi]	2392,00
sigma radial [psi]	2392,00
sigma tan max [psi]	8632,00
sigma tan min [psi]	4472,00
sigma axial max [psi]	6188,00
sigma axial min [psi]	5148,00

Figure 47, output

The user interface provides additional information about all critical MW values in terms of shear failure and tensile failure in minimum and maximum horizontal stress direction.

additional information:			
shear failure:			
SHmax direction		Shmin direction	
min required MW [ppg]	10,30	min required MW [ppg]	12,30
max allowable MW [ppg]	19,70	max allowable MW [ppg]	25,00
tensile failure:			
SHmax direction		Shmin direction	
min required MW [ppg]	5,50	min required MW [ppg]	5,50
max allowable MW [ppg]	24,50	max allowable MW [ppg]	25,00
for max a. MW, if the value is 25 ppg, the max range of MW is reached			
actual break out width for given MW (low MW) [°]	0,00		
actual break out width for given MW (high MW) [°]	0,00		
critical stress for given MW (low MW) [psi]	8996,00		
critical stress for given MW (high MW) [psi]	988,00		

Figure 48, additional output

It also presents the actual break out width for low and high mud weight for the given mud weight and the according critical stress values (Figure 48).

4. Results

Due to the development of the program “Fastcheck” for stress and mud weight window calculation, investigations in literature about geomechanics and the close interaction with Company X I was able to achieve all required objectives for this Master thesis.

4.1. MW Calculation

Fastcheck has been proven to work correctly by two independent internationally well known companies dealing with geomachnics.

I was able to verify the results for Study X from a calculation standpoint. Table 2 shows the computed values from Company X and “Fastcheck” in percentage beyond the expected mud weight value for the specific section where the discrepancy was found.

	Company X	Fastcheck
P90	+ 12.7%	+ 20.9%
P50	+ 10.0%	+ 17.2%

Table 2, percentage beyond expected value

The reason for the values of “Fastcheck” to be significantly higher compared to the results of Company X is the use of different failure criterions. Company X used the more precise modified Lade criterion whereas “Fastcheck” used linearized Mohr Coulomb failure criterion. MC criterion was used on purpose as it is the most conservative criterion which requires all other criterions to produce a larger MWW.

As the reason for the discrepancy was not found to be the calculation itself Company X was asked to make a statement on their interpretation. They assumed that an underestimation of rock strength is most likely the cause for the inconsistency as this was indicated by the UCS log (Figure 49, red and blue circle) and that this zone of weak rock elevated the mud weight to its high value. They stated to normally cut off such peaks as they are likely to be caused by bad log data but they failed to apply this procedure here.

If the rock strength would be averaged at this specific hole location of the significant peak (blue cycle Figure 49) the collapse pressure curve would decrease significantly to a value equal or even below the pore pressure. Still the author is concerned to apply this method with too much levity.

One problem is that a number of peaks are present in this hole section (Figure 51 shows the actual curve used for MWW prediction) which means that just the flattening of one peak will not significantly lower the mud weight as the next largest peak will keep the mud weight elevated. This means that all peaks would have to be averaged which brings in to question the scientific nature of this approach.

It requires years of geomechanical experience to judge if the flattening of the collapse pressure curve is reasonable and to what extend it is defensible. The author warns to apply this procedure too easily for the purpose of meeting expectations.

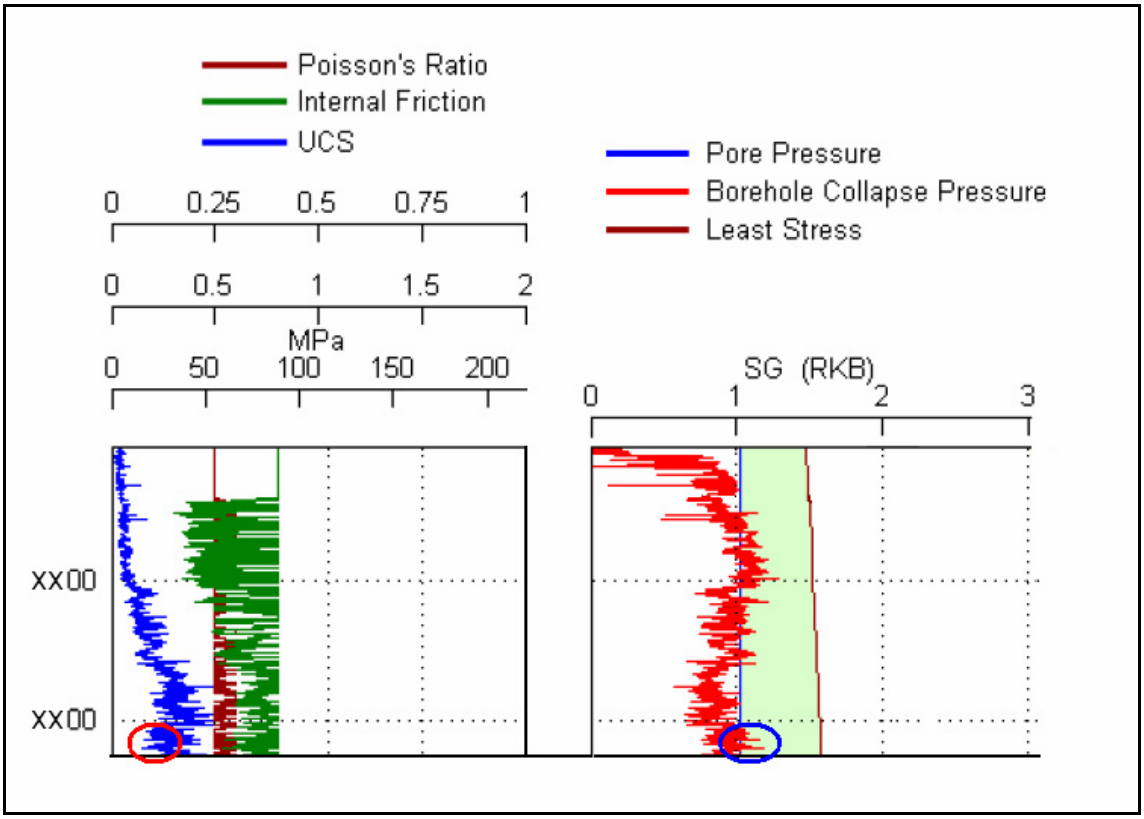

Figure 49, peak of collapse pressure curve[5]

Due to the fact that the results from Company X could be proven a very deep insight into the calculation process could be gained and “Fastcheck” provides the ability to

verify results from geomechanical studies by recalculating the most critical points of the different hole sections.

Further on it is recommended to require a confidence level in geomechanical studies according to the amount and quality of data available for different hole sections. This approach could conclude to use P50 values for sections with a high density of good quality data and P90 values (additional safety) where just little data is available.

4.2. Sensitivity Analysis

Another requirement arose during the work which was evaluation of sensitivity according to the different input parameters. Sensitivity analysis has been performed for all three stress regimes and different break out allowances by varying the input parameters by +/- 10%.

4.2.1 Normal Faulting Stress Regime

For a normal faulting regime with 0 degree break out allowance a tornado chart has been computed.

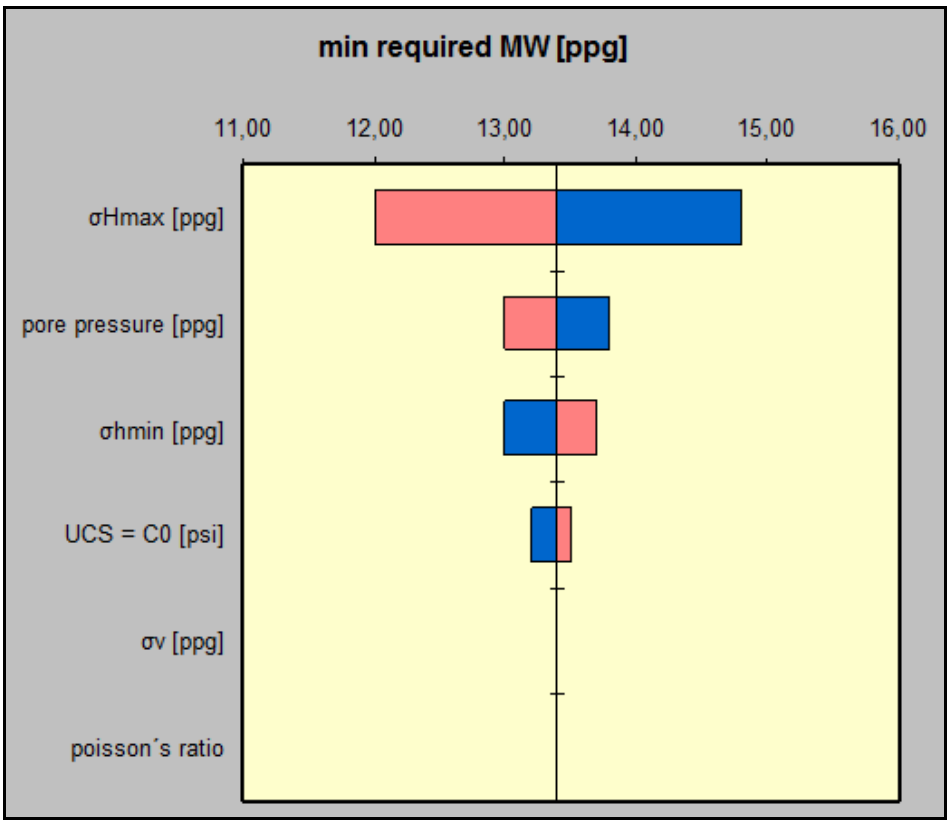

Figure 50, tornado chart normal faulting 0 degree BOW

According to Figure 50 the most important parameter is S_{Hmax} followed by pore pressure, S_{hmin}, and UCS. The result met the expectations as the maximum tangential stress is the governing factor for the lower mud weight boundary if the collapse pressure curve (for 90° BOW) is dominant which is true for this situation (Figure 51).

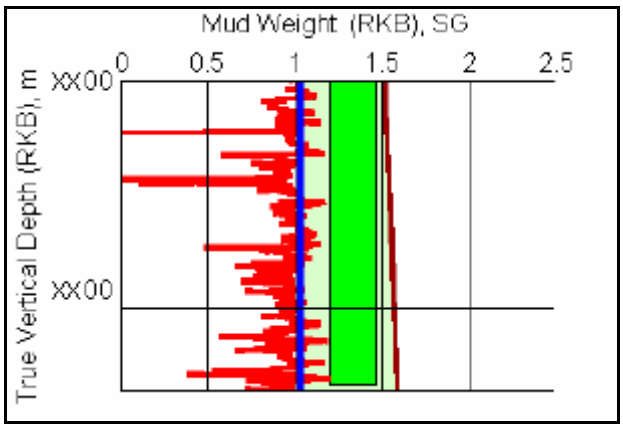

Figure 51, dominant collapse pressure curve[5]

The maximum horizontal stress contributes to the maximum tangential stress with a factor 3, pore pressure and S_{hmin} with factor 1. Pore pressure gives the minimum stress for the MC failure criterion as well which is the reason why it is ranked prior to S_{hmin}.

$$\sigma_{tanmax,\,eff} = 3*S_{Hmax} - S_{hmin} - P_P - P_w \qquad (2.8^2)$$

For a BOW of 30 (Figure 52) and 60 degrees (Figure 53) one can see the decrease of sensitivity according to S_{Hmax} and S_{hmin}. As still the tangential stress dominates the maximum value for the MC failure criterion (Figure 54) the reason for this behavior can be found in the equation for tangential stress. For a break out width of 30° ($\theta = 75$) the formula of tangential stress at the wellbore wall results

$$\sigma_{tan\theta 75,\,eff} = 2.73*S_{Hmax} - 0.73*S_{hmin} - P_P - P_w \qquad (2.23^2)$$

For BOW of 60° ($\theta = 60$) the equation yields

$$\sigma_{tan\theta 60,\,eff} = 2*S_{Hmax} - P_P - P_w \qquad (2.24^2)$$

The tornado chart for 90° BOW (Figure 55) as well as Figure 56 show that the axial stress becomes more important which is the interpretation for the increased value of S_v.

$$\sigma_{axial\theta 45} = \sigma_v \qquad (2.25^2)$$

The tangential stress still strongly contributes to sensitivity with the equation for 90° break out width (θ = 45) which results

$$\sigma_{tan\theta 45,\ eff} = S_{Hmax} + S_{hmin} - P_P - P_w \qquad (2.26^2)$$

It is important to notice that the algebraic sign of S_{hmin} changes from minus to plus with an increase in break out width allowance with zero sensitivity at 60° bow (θ = 60) which can also be seen in the change of the colors of the bars in the tornado chart contributing to S_{hmin}. Blue means an increase in parameter value and the direction of the bar means the influence on the outcome value. A blue bar to the right means an increase in parameter value will cause an increase in outcome value and a blue bar to the left means a decrease of the outcome by an increase in parameter value.

One can see that S_{Hmax} is the most important parameter as long as the collapse pressure curve is dominant compared to the pore pressure curve or in other words as the weakness of the rock will govern the lower mud weight limit and not the pore pressure. Unfortunately all the other parameters are required to calculate S_{Hmax} which means the more accurate all remaining parameters are gathered the more exact the prediction for S_{Hmax} will be.

Pore pressure is a very important parameter and should be measured precisely independent on situation. Taken into account that P_p has been the second most important parameter for dominance of collapse pressure curve and is the most important parameter if the pore pressure curve governs the lower mud weight limit pore pressure might even be the most important parameter.

The problem with a ranking of important parameters is generally that it is not known in advance if rock strength or pore pressure will govern the lower mud weight boundary. Still as mentioned above P_p will be important for both situations.

It should also be remembered that these sensitivities are true for MC failure criterion but change if any other failure criterion is used.

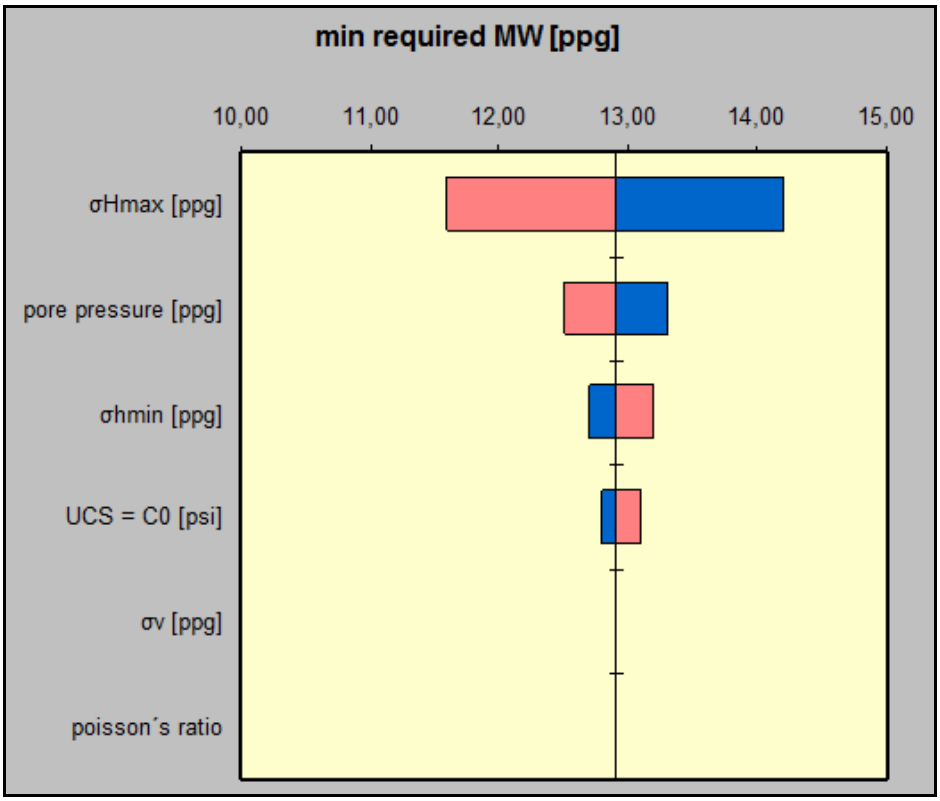

Figure 52, tornado chart normal faulting 30 degree BOW

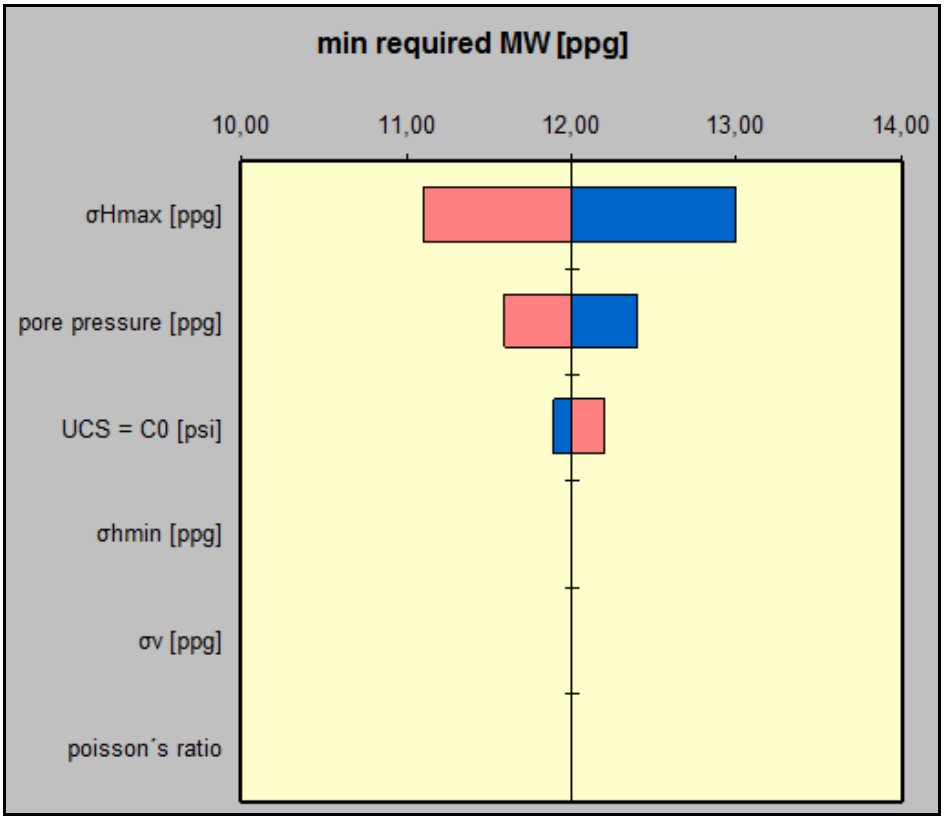

Figure 53, tornado chart normal faulting 60 degree BOW

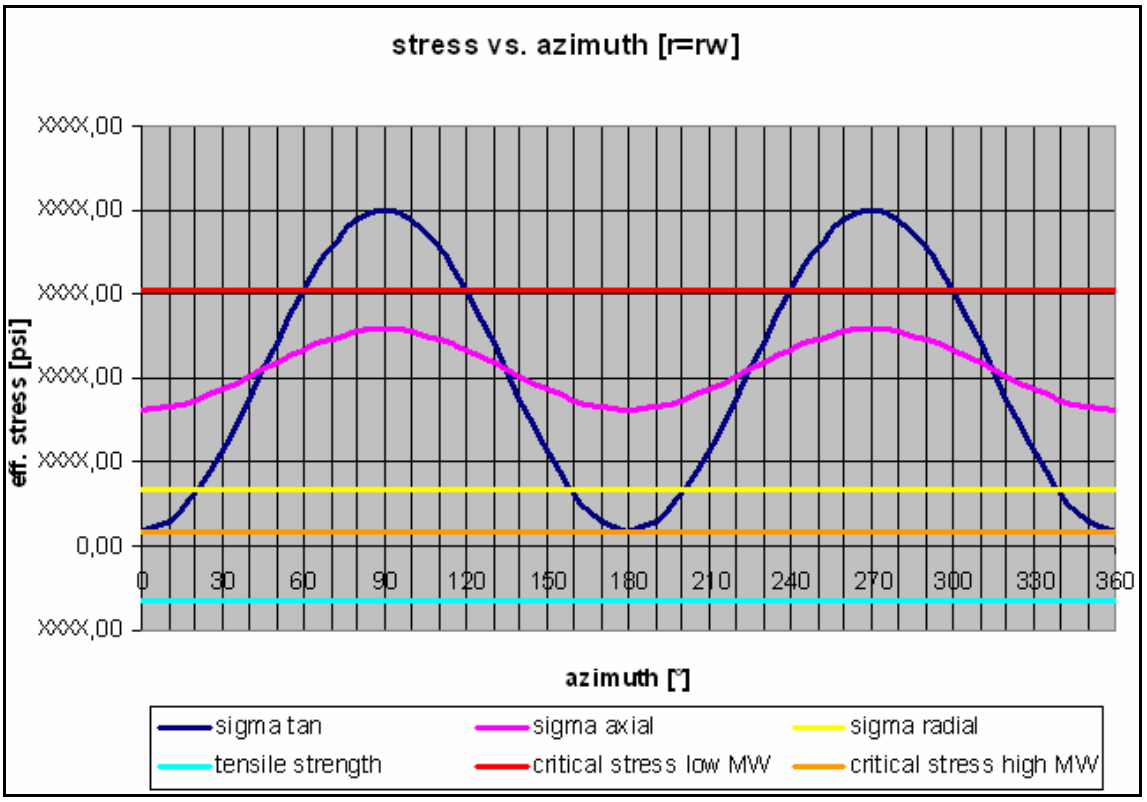

Figure 54, azimuthal stress diagram for 60 degree BOW NF regime

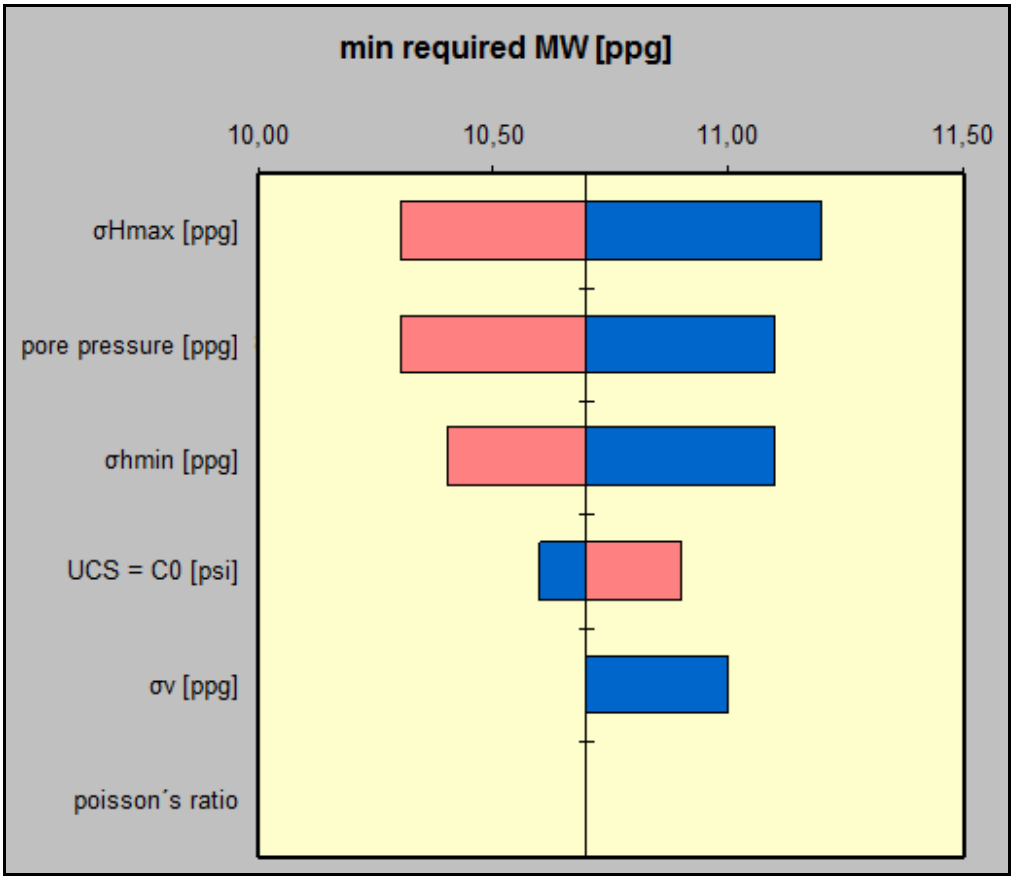

Figure 55, tornado chart normal faulting 90 degree BOW

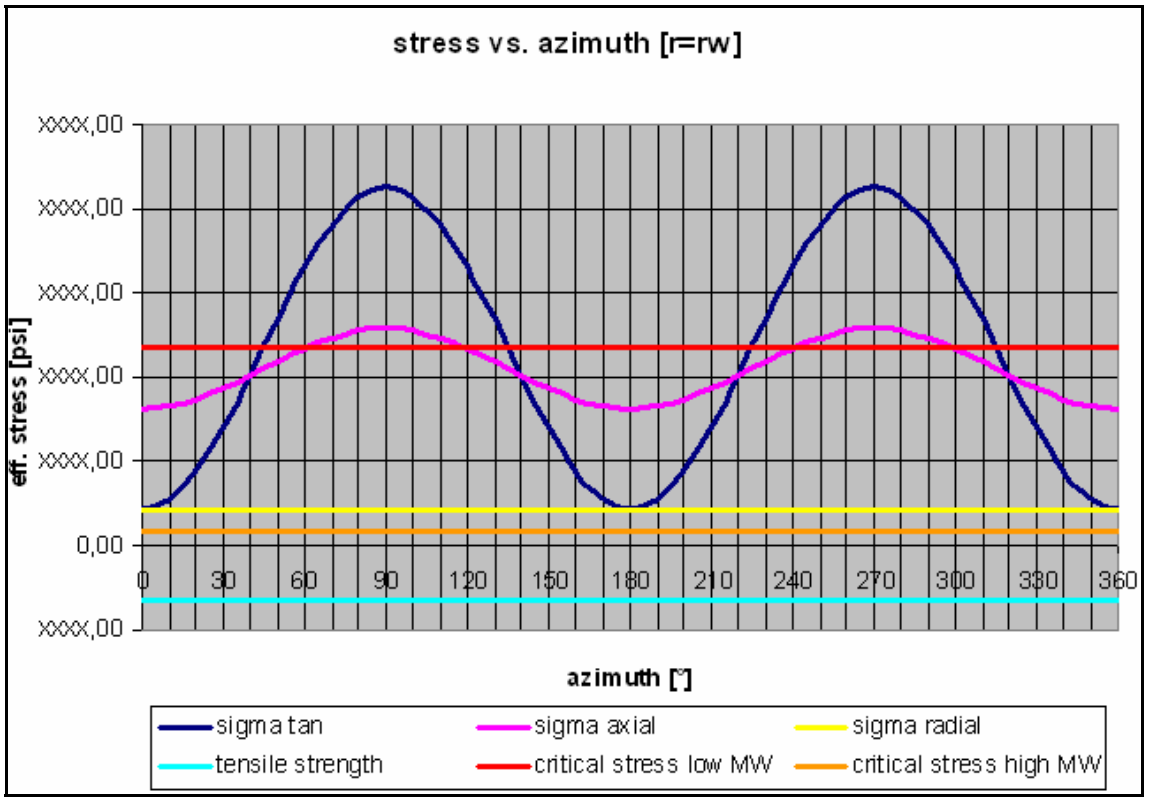

Figure 56, azimuthal stress diagram for 90 degree BOW NF regime

4.2.2 Strike-Slip Faulting Stress Regime

The same procedure was done for a strike-slip regime with the same observations like for normal faulting. The tornado chart for 0 degree BOW looks very similar compared to normal faulting except a higher sensitivity of pore pressure.

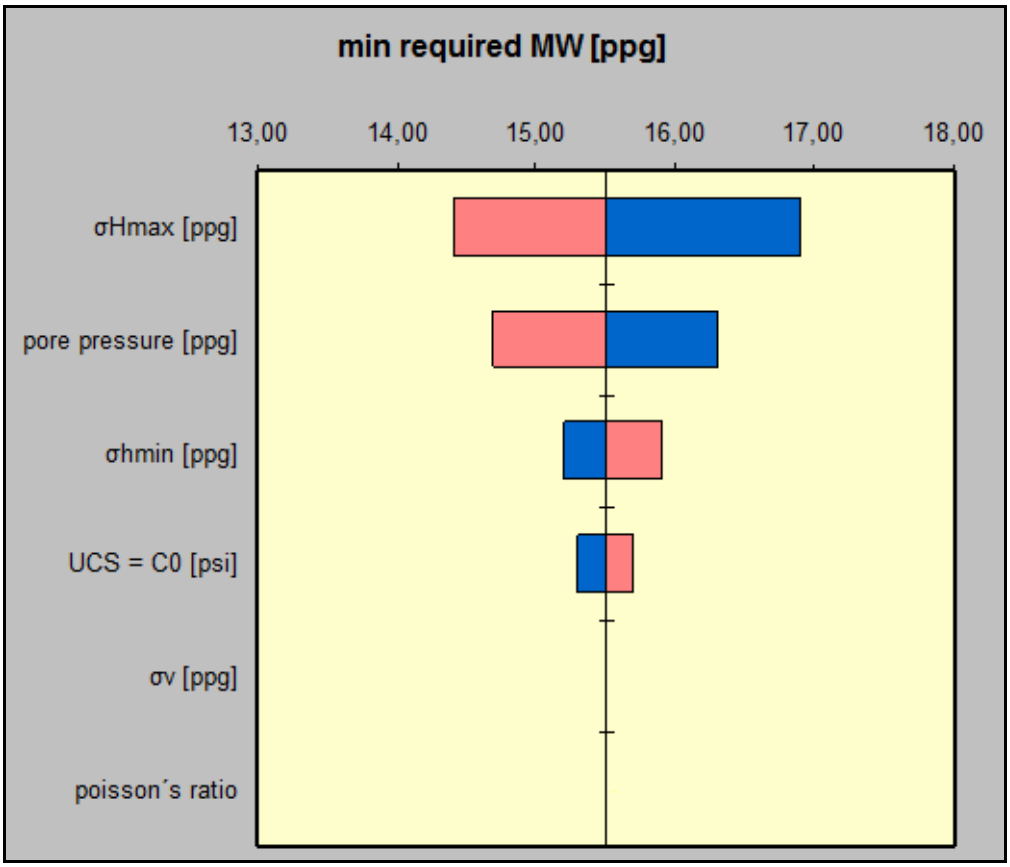

Figure 57, tornado chart strike-slip faulting 0 degree BOW

Figure 58 shows the most important difference to the previous example as now the collapse pressure curve is just slightly dominant. This gives the reason for the higher sensitivity of the pore pressure. Figure 57, 59, 60 and 61 clearly indicate the higher influence of P_p compared to the tornado charts of the previous example. Especially Figure 61 results that pore pressure is even the most important parameter.

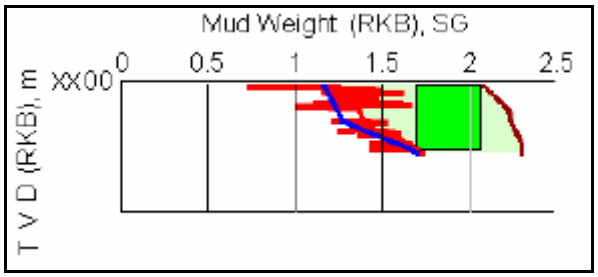

Figure 58, less dominant collapse pressure curve[5]

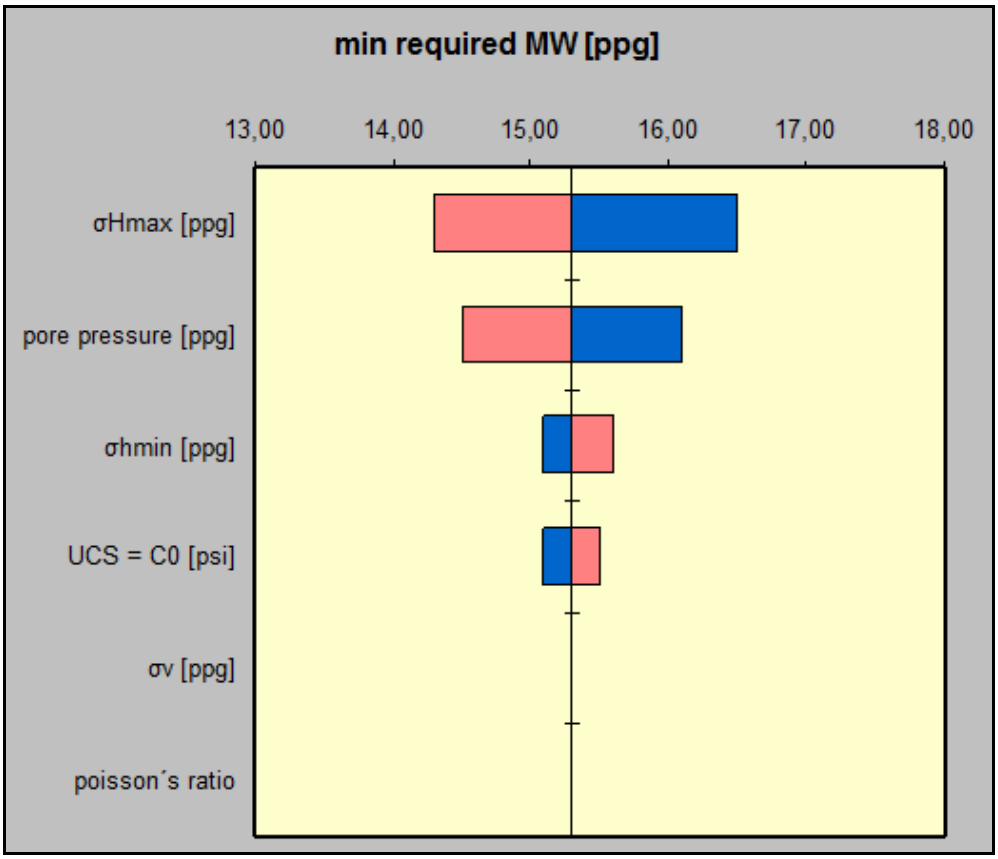

Figure 59, tornado chart strike-slip faulting 30 degree BOW

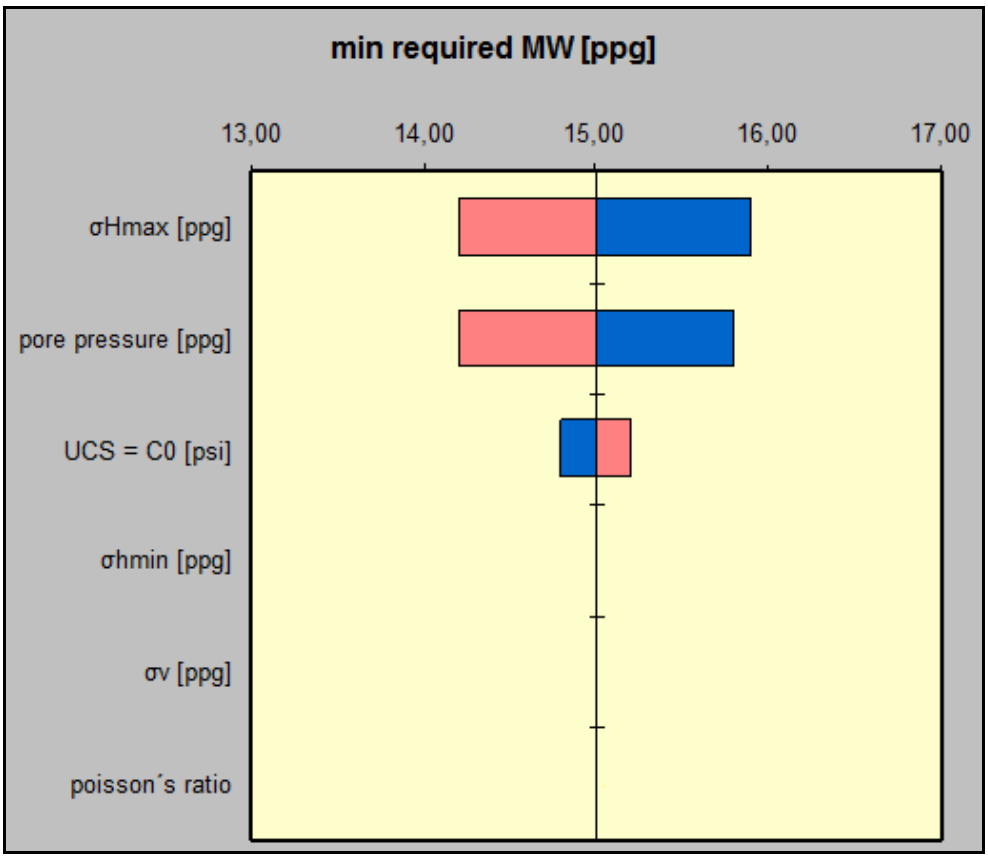

Figure 60, tornado chart strike-slip faulting 60 degree BOW

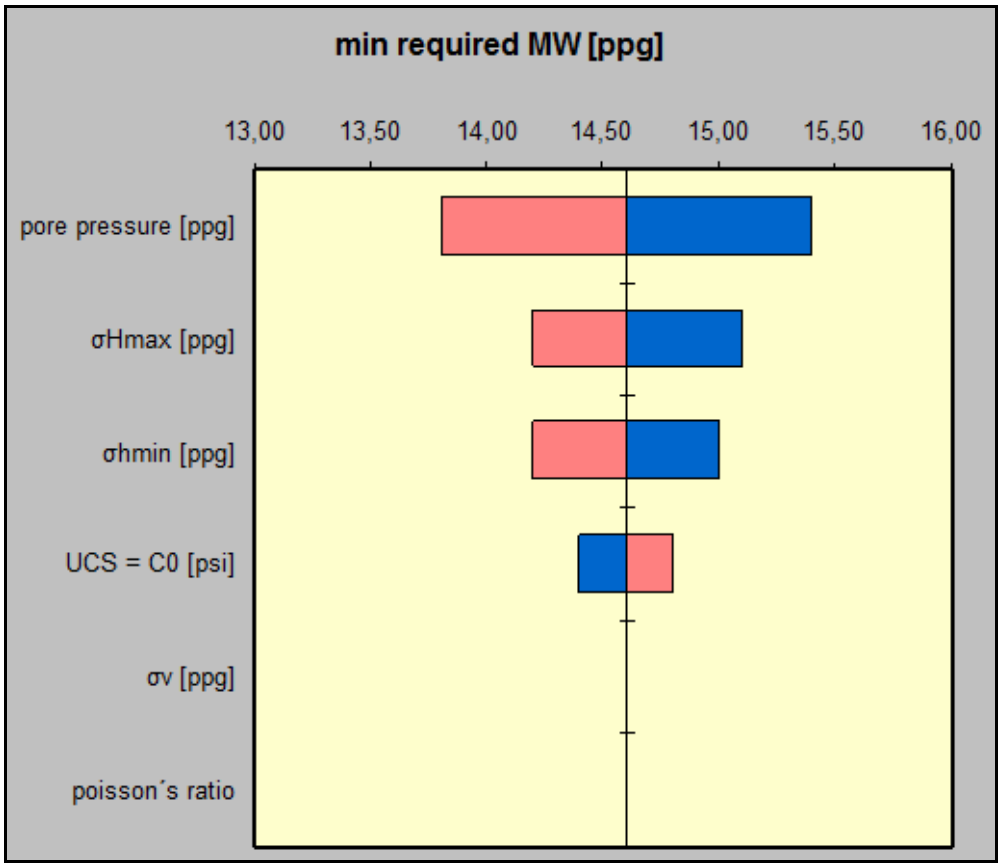

Figure 61, tornado chart strike-slip faulting 90 degree BOW

4.2.3 Reverse Faulting Stress Regime

Sensitivity analysis has also been performed for a reverse faulting stress regime with dominant pore pressure curve (Figure 62).

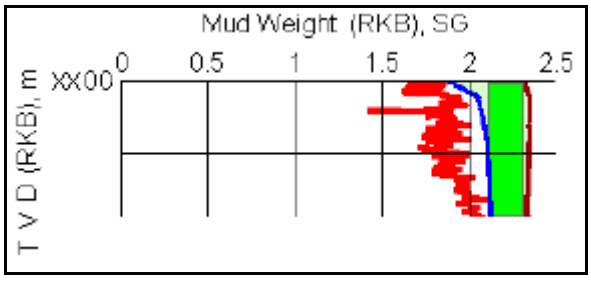

Figure 62, dominant pore pressure[5]

The expected outcome was a strong pore pressure sensitivity (Figure 63, Figure 64). Due to the fact that for 90° BOW the model is still sensitive to S_{Hmax} and S_{hmin} it can be concluded that during varying the parameters the collapse pressure curve still influenced the lower mud weight boundary.

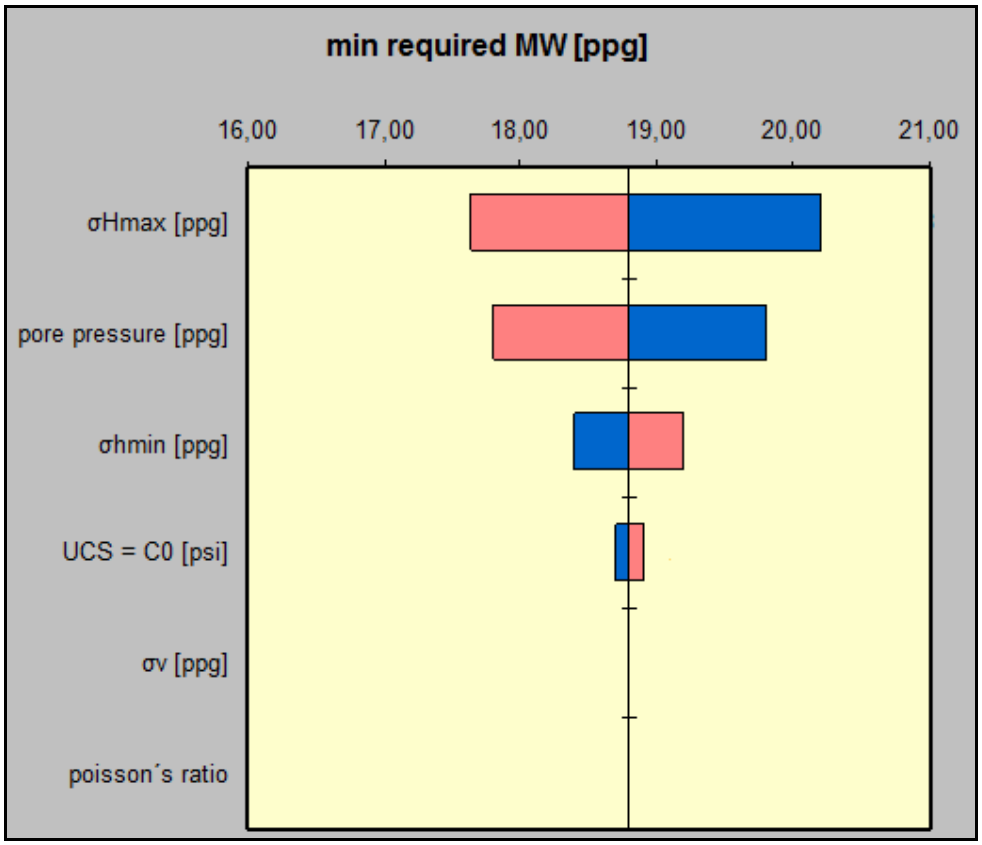

Figure 63, tornado chart reverse faulting 0 degree BOW

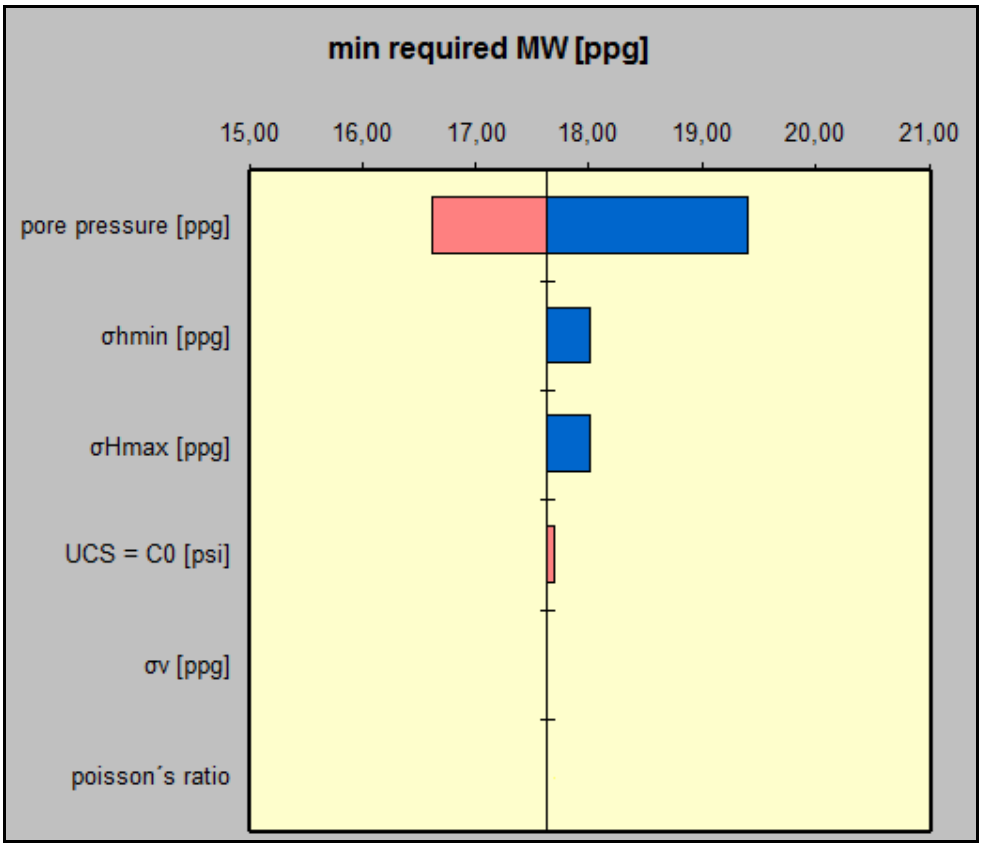

Figure 64, tornado chart reverse faulting 90 degree BOW

It can be stated that pore pressure and S_{Hmax} are the most important parameters for the presented examples. Different stress regimes showed no influence on the parameters but the specific stress relationship and accordingly either the dominance of the collapse pressure or pore pressure curve.

4.2.4 Sensitivity for horizontal stresses depending on S_v

Due to the fact that the horizontal stresses to a certain degree physically depend on S_v sensitivity analysis has been performed for all three stress regimes as well as 0° and 90° break out allowance. The outcome was as expected that the vertical stress is most dominant for almost all situations (Appendix D). It can be understood as the combination of the sensitivities for Sv, S_{Hmax}, and S_{hmin}.

When vertical stress is varied both horizontal stresses are varied accordingly. It is important to mention that for 0° and 30° BOW the two horizontal stresses have different algebraic signs resulting in a reduced sensitivity of the vertical stress.

It has to be stated that the approach of connecting the horizontal stresses to the vertical stress should be handled with care as first of all the measuring of S_{hmin} is completely independent from the vertical stress and S_{Hmax} is dependent on all parameters from a calculation standpoint. Secondly it is also difficult to distinguish for a horizontal stress between the vertical stress input and additional horizontal stress input produced by e.g. tectonic movements. The simple utilization of Poisson´s ratio is not considered to be a reliable procedure.

5. Additional Findings

The calculation program “Fastcheck” was designed in a way to allow the user to learn about stresses and the influence of different conditions on the mud weight. Due to that fact some additional findings have been achieved throughout the work for this Master thesis.

5.1. Break-outs at High Mud Weights

The general understanding for the condition of break-outs to appear is an insufficient mud weight which causes the rock to fail due to excessive stresses in S_{hmin} direction. This definition oversimplifies the situation as stress is a tensor which means that the failure of rock is basically dependent on the relationship of all three principle stresses. The formation will not fail if all three stresses are high but if the difference is large.

Input:	
vertical	
σv [ppg]	19,3
σHmax [ppg]	18
σhmin [ppg]	13,5
pore pressure [ppg]	8,4
UCS = C_0 [psi]	3000
Φ [°]	30
mud weight density [ppg]	12,9
poisson´s ratio	0,25
TVD [ft]	10000
Break out width [°]	0
Output:	
Total	
min required MW [ppg]	12,90
max a. MW , σmin [ppg]	13,50
max allowable MW [ppg]	13,10
sigma radial [psi]	2340,00
sigma tan max [psi]	9984,00
sigma tan min [psi]	624,00
sigma axial max [psi]	6838,00
sigma axial min [psi]	4498,00

Figure 65, set of parameters for break-outs at high MW normal faulting regime

Figure 65 shows a set of parameters, the MWW and the maximum and minimum stress values at which break-outs at high mud weights will appear prior to the fracture pressure.

The lower mud weight boundary is at 12.9 ppg, the upper boundary for rock failure at 13.1 ppg and the fracture pressure mud weight equivalent is 13.5 ppg.

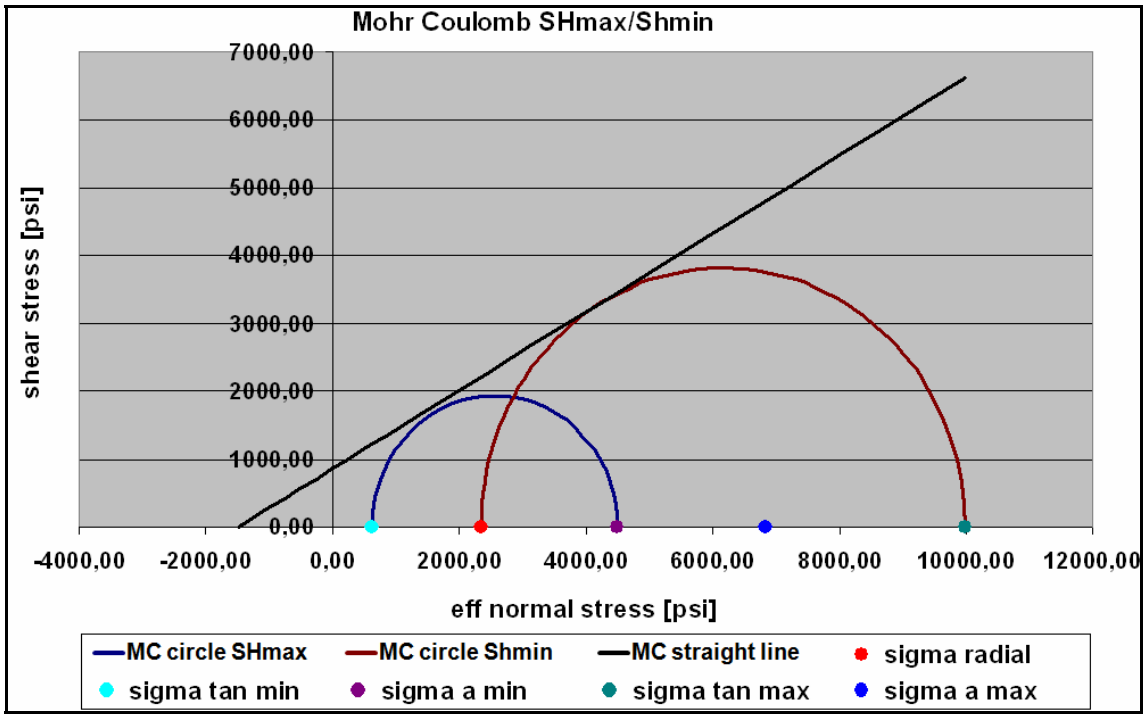

Figure 66, MC stress diagram for 12.9 ppg

The Mohr Coulomb stress diagram for a MW of 12.9 ppg (Figure 66) shows that the stress relationship in S_{hmin} direction where the maxima appear is at a critical condition (brown circle). In S_{Hmax} direction the critical state is not yet reached (blue circle). It is important to notice that the minimum stress for S_{hmin} direction is the radial stress as the tangential and axial stress are at their maximum and for S_{Hmax} direction the minimum stress is the tangential stress as in S_{hmin} direction the minimum stresses are encountered.

If the mud weight is increased to 13.1 ppg (Figure 67) the stress condition in S_{Hmax} direction is critical due to the fact that the minimum tangential stress has decreased from the initial value of 624 psi at 12.9 ppg to 520 psi at 13.1 ppg (comparison Figure 65 and 68). The minimum axial stress remained at its value as the axial stress is independent from mud weight. So the stress circle in S_{Hmax} direction became larger as

the stress circle in S_{hmin} direction became smaller due to the fact that the radial stress increased and the maximum tangential stress decreased from 9984 psi at 12.9 ppg to 9880 psi at 13.1 ppg (comparison of Figure 65 and 68).

This is also the reason why for the condition of wellbore stability problems during drilling the first attempt is usually to increase the mud weight as the reaction will be a smaller stress circle in S_{hmin} direction.

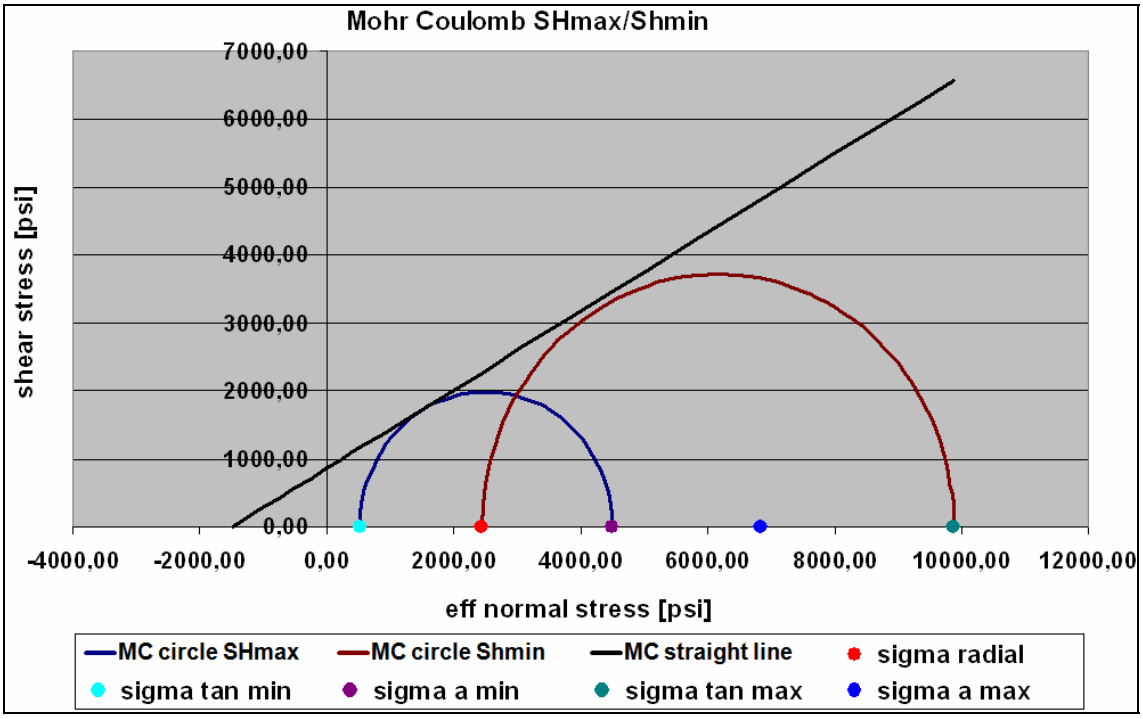

Figure 67, MC stress diagram for 13.1 ppg

sigma radial [psi]	2444,00
sigma tan max [psi]	9880,00
sigma tan min [psi]	520,00
sigma axial max [psi]	6838,00
sigma axial min [psi]	4498,00

Figure 68, minimum and maximum stress values for 13.1 ppg

If the mud weight is increased to the fracture pressure of 13.5 ppg (Figure 69) approximately 10° break-outs will occur in S_{Hmax} direction (Figure 70) for this particular set of parameters.

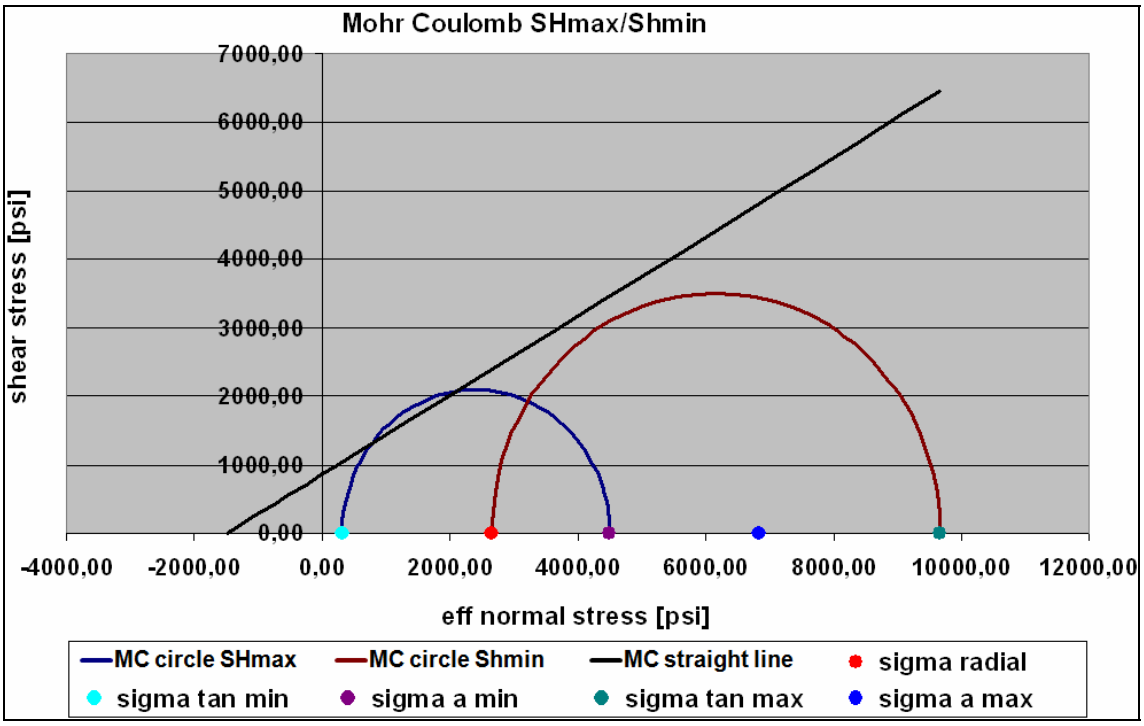

Figure 69, MC stress diagram for 13.5 ppg

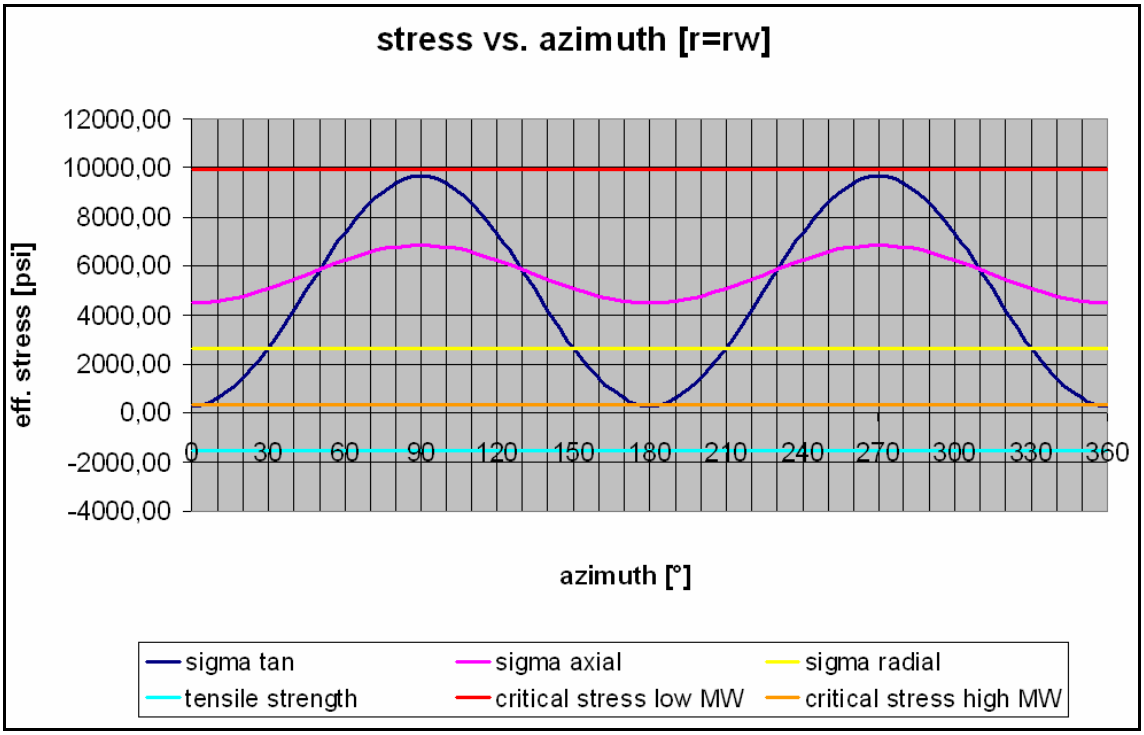

Figure 70, azimuthal stress diagram for 13.5 ppg

The presented example is very similar to actual field data. Conditions for break-outs in S_{Hmax} direction at high mud weights are achieved whenever the difference between the maximum and minimum horizontal stress becomes significantly large.

5.2. Most Preferable Horizontal Drilling Direction Changes with Break Out Width Allowance

During reading of Study X a phenomena was encountered which could not be explained straightaway by Company X. It was the change in most preferable horizontal drilling direction caused by a change of break out allowance from 0° to 90° in a normal faulting stress regime. “Fastcheck” was used to analyze the reason for this behavior.

“Fastcheck” was designed to analyze vertical wells primarily but by changing the stresses like they would act around a horizontal well I was able to explore the above mentioned behavior.

Figure 71 shows a set of parameters for a normal faulting regime with 0 degree break out width. These values are the starting point of the investigation and the vertical case will be included in the analysis for reason of completeness.

Input:	
vertical	
σv [ppg]	20
σHmax [ppg]	18
σhmin [ppg]	16
pore pressure [ppg]	8,5
UCS = C_0 [psi]	1800
Φ [°]	30
mud weight density [ppg]	11,8
poisson´s ratio	0,3
TVD [ft]	10000
Break out width [°]	0
Output:	
Total	
min required MW [ppg]	12,90
max a. MW, σmin [ppg]	16,00
max allowable MW [ppg]	19,10

Figure 71, set of parameters

If the break out width allowance is increase to 90° the mud weight window will change to 11.8 ppg for the lower boundary.

Input:	
vertical	
σv [ppg]	20
σHmax [ppg]	18
σhmin [ppg]	16
Break out width [°]	90
Output:	
Total	
min required MW [ppg]	11,80
max a. MW, σmin [ppg]	16,00
max allowable MW [ppg]	19,10

Figure 72, MWW for 90° BOW

For a well drilled in S_{Hmax} direction the vertical stress value has to be changed to the maximum horizontal stress in the input of "Fastcheck" as the vertical stress will act as the maximum tangential stress (Figure 73). Thus, the maximum horizontal stress has to become the axial stress and the minimum horizontal stress remains as it will still be the minimum tangential stress acting on the wellbore.

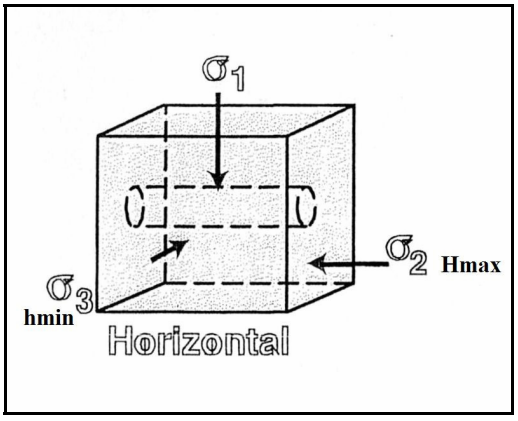

Figure 73, drilling in S_{Hmax} direction[1]

The well drilled in maximum horizontal direction will have a lower mud weight boundary of 14.4 ppg for 0° BOW (Figure 74). For a BOW of 90° the lower mud weight limit will decrease to 12.3 ppg (Figure 75).

Input:	
vertical	
σv [ppg]	18
σHmax [ppg]	20
σhmin [ppg]	16
Break out width [°]	0
Output:	
Total	
min required MW [ppg]	14,40
max a. MW, σmin [ppg]	16,00
max allowable MW [ppg]	17,60

Figure 74, well in S_{Hmax} direction for 0° BOW

Input:	
vertical	
σv [ppg]	18
σHmax [ppg]	20
σhmin [ppg]	16
Break out width [°]	90
Output:	
Total	
min required MW [ppg]	12,30
max a. MW, σmin [ppg]	16,00
max allowable MW [ppg]	17,60

Figure 75, well in S_{Hmax} direction for 90° BOW

When a well is drilled in S_{hmin} direction the vertical stress value in the input of "Fastcheck" has to be changed to the S_{hmin} value as the minimum horizontal stress will act as the axial stress. The vertical stress value has to be filled in the box of the maximum horizontal stress as S_v will act as the maximum tangential stress and the maximum horizontal stress value has to replace the value in the minimum horizontal stress box because the S_{Hmax} value will act as the minimum tangential stress (Figure 76). The lower mud weight boundary for 0° BOW is 13.9 ppg and for 90° BOW it is 12.8 ppg.

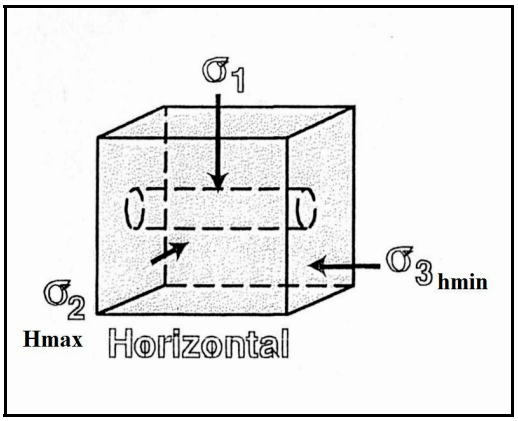

Figure 76, drilling in S_{hmin} direction[1]

Input:	
vertical	
σv [ppg]	16
σHmax [ppg]	20
σhmin [ppg]	18
Break out width [°]	0
Output:	
Total	
min required MW [ppg]	13,90
max a. MW, σmin [ppg]	16,00
max allowable MW [ppg]	22,10

Figure 77, well in S_{hmin} direction for 0° BOW

Input:	
vertical	
σv [ppg]	16
σHmax [ppg]	20
σhmin [ppg]	18
Break out width [°]	90
Output:	
Total	
min required MW [ppg]	12,80
max a. MW, σmin [ppg]	16,00
max allowable MW [ppg]	22,10

Figure 78, well in S_{hmin} direction for 90° BOW

	lower MW limit vertical well	lower MW limit horizontal well in SHmax direction	lower MW limit horizontal well in Shmin direction
0° bow	12.9	14.4	13.9
90° bow	11.8	12.3	12.8

Table 3, lower mud weight boundaries

The previously described phenomena can be seen in table 3 as the lower MW limit for a horizontal well drilled in S_{hmin} direction for 0 degree break out width (13.9 ppg) is lower compared to a well drilled in S_{Hmax} direction (14.4 ppg) which is compliant with the generally known theory (next chapter). So S_{hmin} is the best direction to drill horizontally from a wellbore stability standpoint. This is not true if 90° break out allowance is applied as the S_{hmin} value is 12.8 ppg which is higher than 12.3 ppg for S_{Hmax}. The upper limit of the mud weight window is always the least principle stress which is for a certain depth the same no matter which direction the well is drilled.

A vertical well in a normal faulting regime is the most preferable compared to horizontally drilled wells as the difference of the tangential stresses is less compared to a horizontal well.

The reason for the phenomena can be found in the according azimuthal stress diagrams. When comparing Figure 79 and 80 one can see that for drilling in the maximum horizontal stress direction first of all the maximum horizontal stress is significantly higher than for drilling in minimum horizontal stress direction which is the reason for S_{hmin} being the best direction to drill horizontally if 0 BOW is required (next chapter). Secondly the slope of the cosine curve for the tangential stress in S_{Hmax} direction is steeper compared to S_{hmin} direction which is already the reason for the change in most preferable drilling direction with increased BOW.

The explanation can be seen in Figure 81 and 82 because the steeper slope allows the critical stress and so the according MW to decrease further until 90°of included angle are reached.

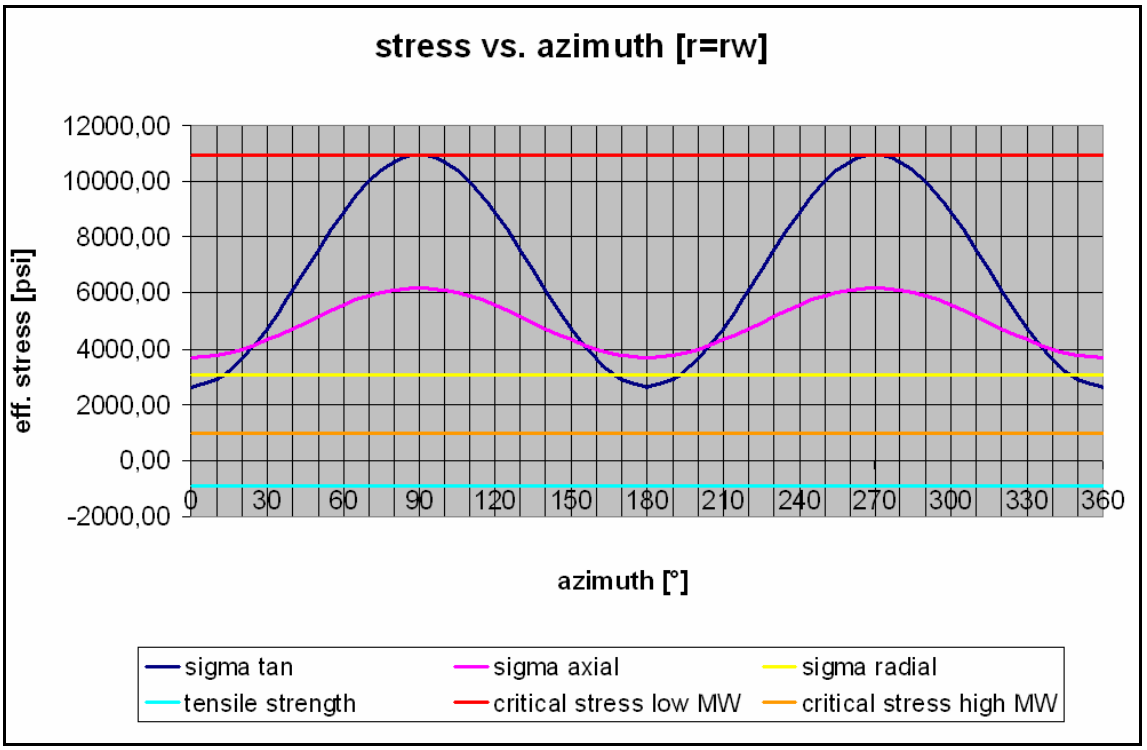

Figure 79, azimuthal stress diagram for S_{Hmax} drilling direction and 0° BOW

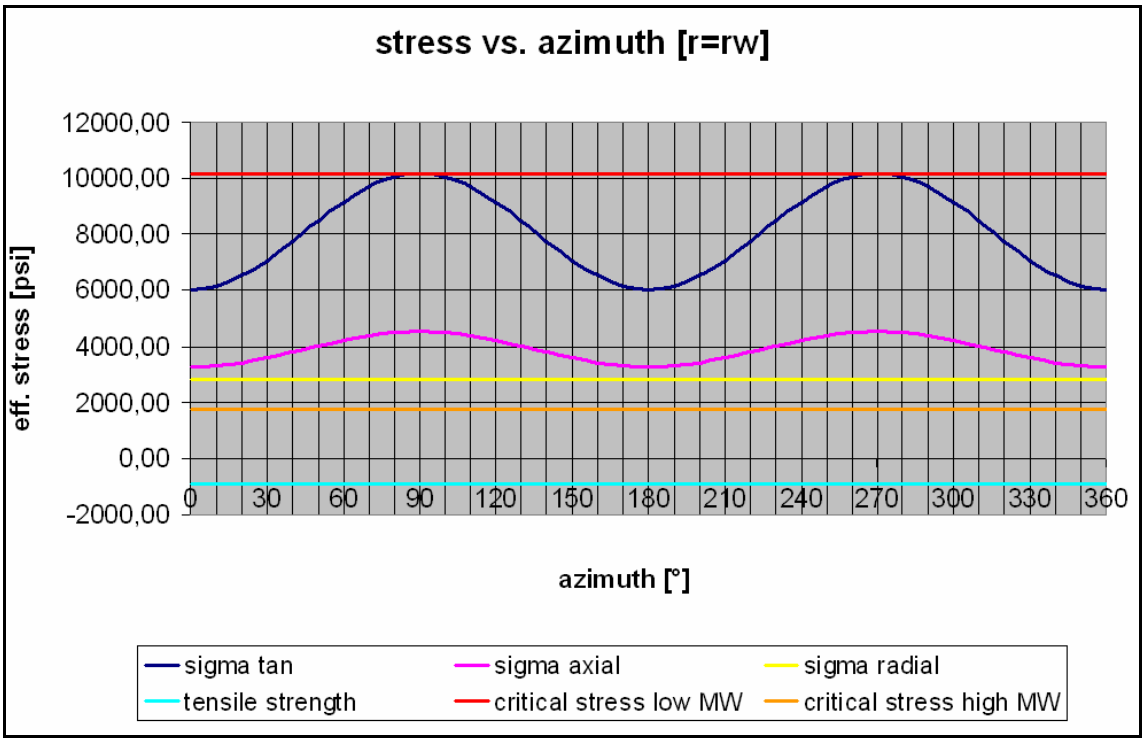

Figure 80, azimuthal stress diagram for S_{hmin} drilling direction and 0° BOW

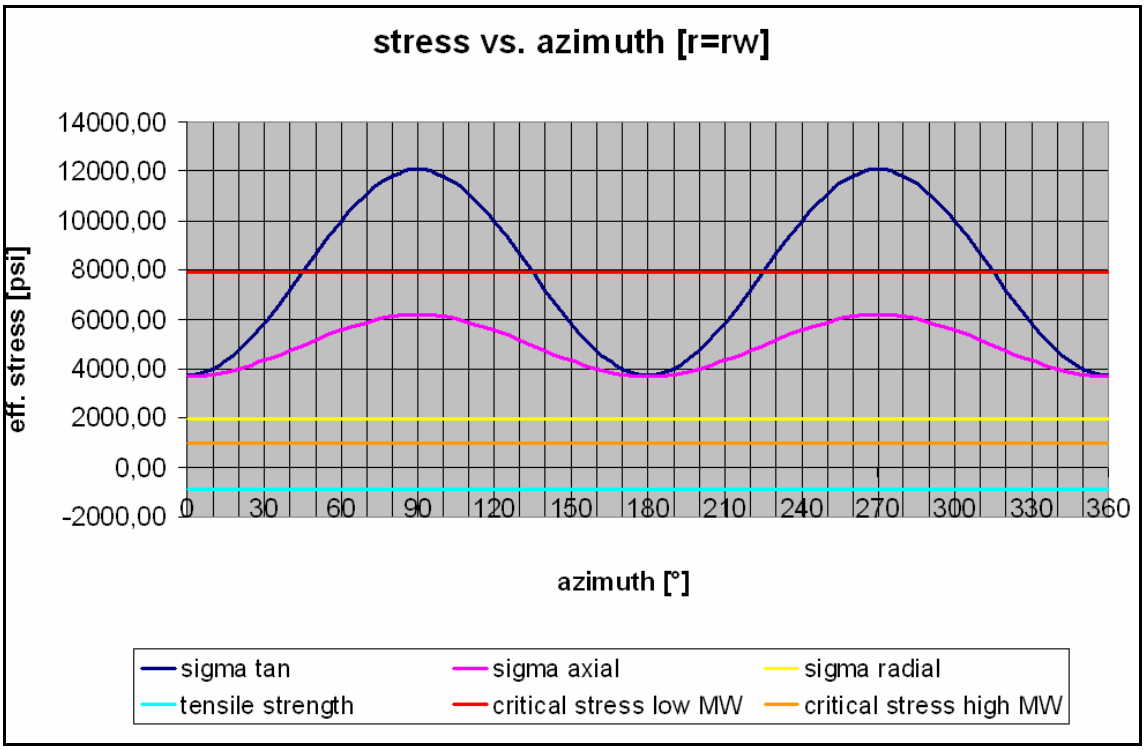

Figure 81, azimuthal stress diagram for S_{Hmax} drilling direction and 90° BOW

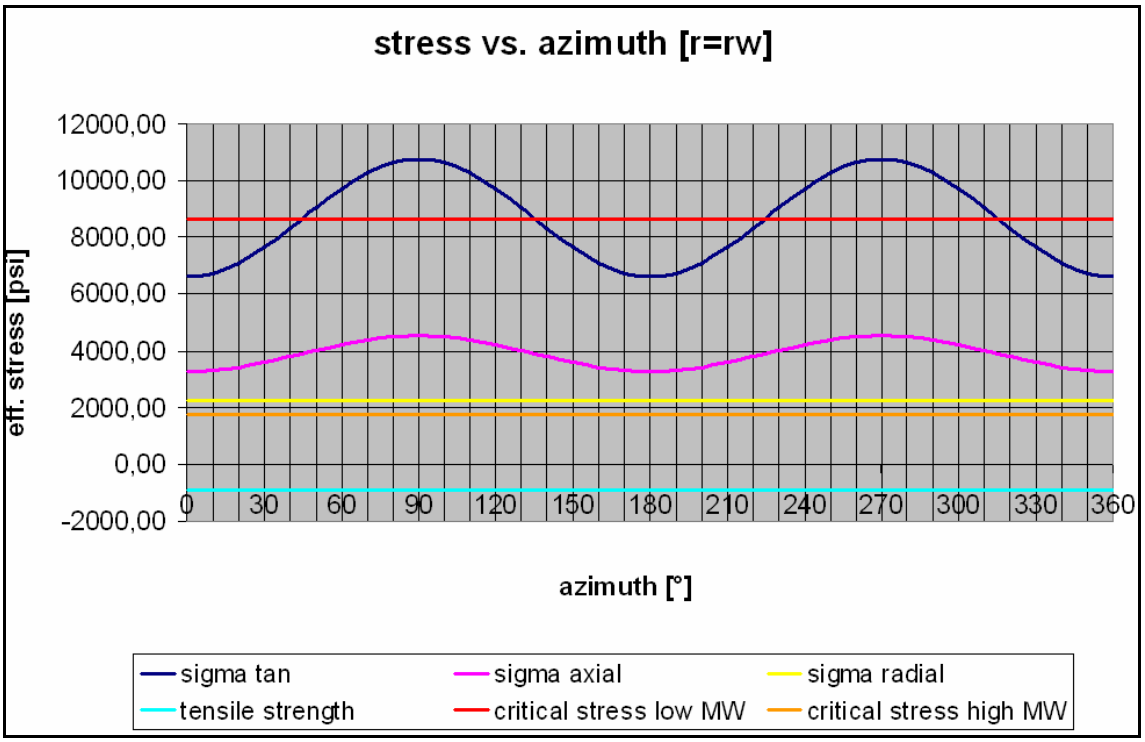

Figure 82, azimuthal stress diagram for S_{hmin} drilling direction and 90° BOW

5.3. S_{hmin} is the most preferable horizontal drilling direction in a normal faulting stress regime from a wellbore stability standpoint

This statement will be proven and explained by the example already presented in the previous chapter for 0 degree break out width. The case of a vertical well is included again for reason of completeness.

Figure 83 and 84 show the Mohr Coulomb stress diagram of the vertical well for the mentioned input parameters as well as the according stress values for a MW of 14.4 ppg.

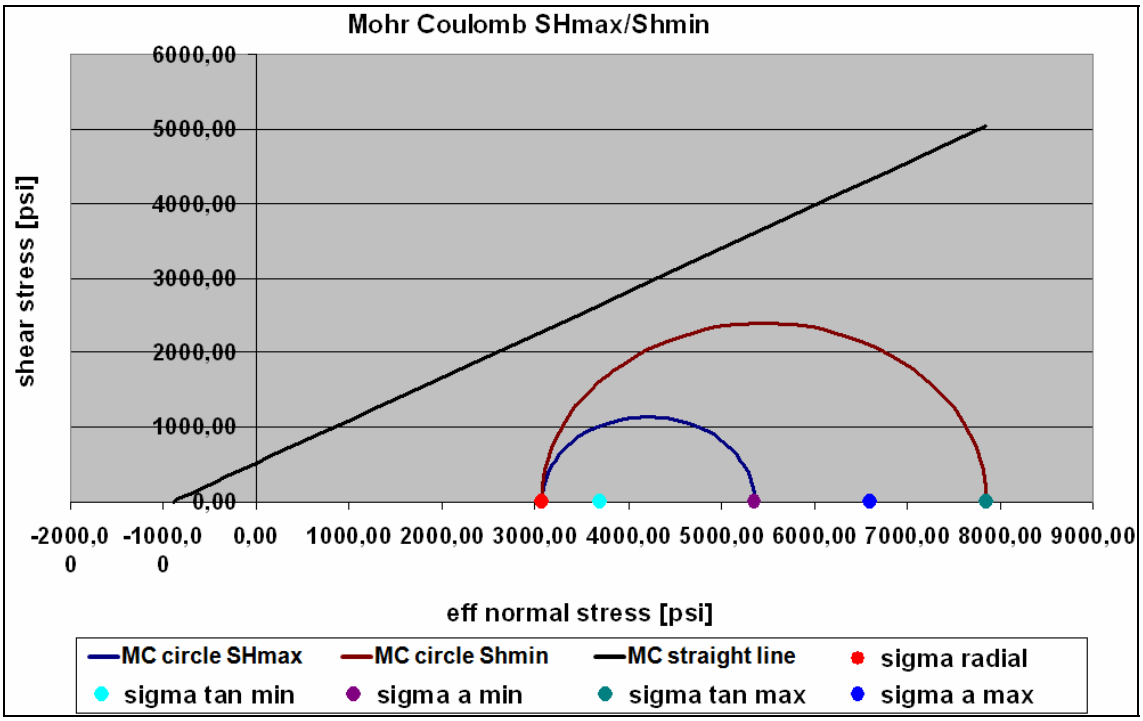

Figure 83, MC stress diagram for the vertical well with 14.4 ppg MW

sigma radial [psi]	3068,00
sigma tan max [psi]	7852,00
sigma tan min [psi]	3692,00
sigma axial max [psi]	6604,00
sigma axial min [psi]	5356,00

Figure 84, stress values for the vertical well and 12.9 ppg MW

For a vertical well a minimum required mud weight of 12.9 ppg was computed whereas for a horizontal well in S_{Hmax} direction 14.4 ppg and for the minimum

horizontal stress direction 13.9 ppg are required. 14.4 ppg MW was chosen for all situations to be able to compare the calculated stress values.

The reason for the vertical well to allow the lowest MW is the maximum tangential stress which is with a value of 7852 psi for a MW of 14.4 ppg the lowest of all three cases compared to 10972 psi for S_{Hmax} and 9932 psi for S_{hmin} (Figure 84, 86, and 88). This is also the reason why the MC circle is smallest for the vertical well and largest for drilling in S_{Hmax} direction (Figure 83, 85, and 87). The three situations can be compared as the radial stress is the same for every case due to the fact that all values have been computed for 14.4 ppg MW.

The simple explanation for the two horizontal drilling directions is the fact that it is more beneficial if the two tangential acting stresses are closer together as this will cause a smaller maximum tangential stress.

The vertical stress will act as a tangential stress for both cases. If the maximum horizontal stress is acting as tangential stress (drilling in S_{hmin} direction) it will produce a smaller maximum tangential stress as its value is closer to the vertical stress value compared to the minimum horizontal stress value. The radial stress is the minimum stress for both cases and so a smaller tangential stress will produce a smaller MC circle and so later failure which means a lower allowable mud weight.

A more exact answer can be found in the equation of the maximum tangential stress.

$$\sigma_{tanmax,\,eff} = 3*S_{Hmax} - S_{hmin} - P_{wellbore} - P_P \qquad (2.8^2)$$

For drilling in the maximum horizontal stress direction the equation will result

$$\sigma_{tanmax,\,eff} = 3*\mathbf{S_v} - \mathbf{S_{hmin}} - P_{wellbore} - P_P \qquad (2.27^2)$$

For drilling in the minimum horizontal stress direction the equation will result

$$\sigma_{tanmax,\,eff} = 3*\mathbf{S_v} - \mathbf{S_{Hmax}} - P_{wellbore} - P_P \qquad (2.28^2)$$

This means that for S_{hmin} direction the S_{Hmax} -term in the equation will reduce the maximum tangential stress more than the S_{hmin}-term for the S_{Hmax} direction. Thus drilling in S_{hmin} direction will produce a lower allowable mud weight.

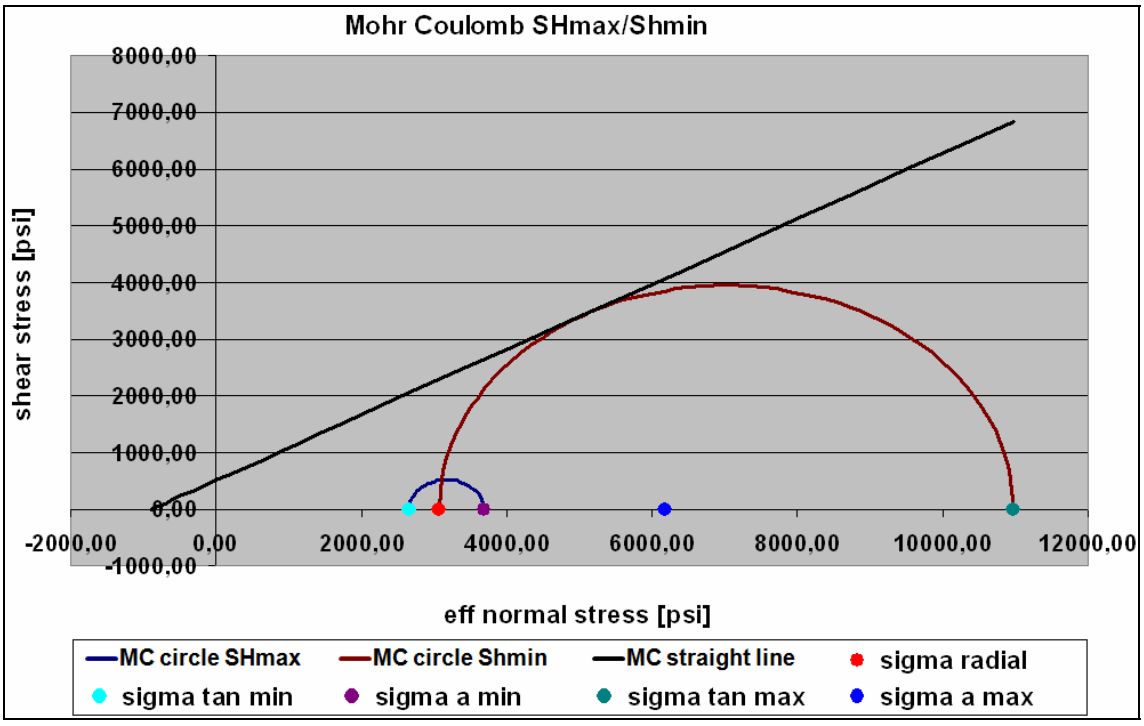

Figure 85, MC stress diagram for the well in S_{Hmax} direction and 14.4 ppg MW

sigma radial [psi]	3068,00
sigma tan max [psi]	10972,00
sigma tan min [psi]	2652,00
sigma axial max [psi]	6188,00
sigma axial min [psi]	3692,00

Figure 86, stress values for the well in S_{Hmax} direction and 14.4 ppg MW

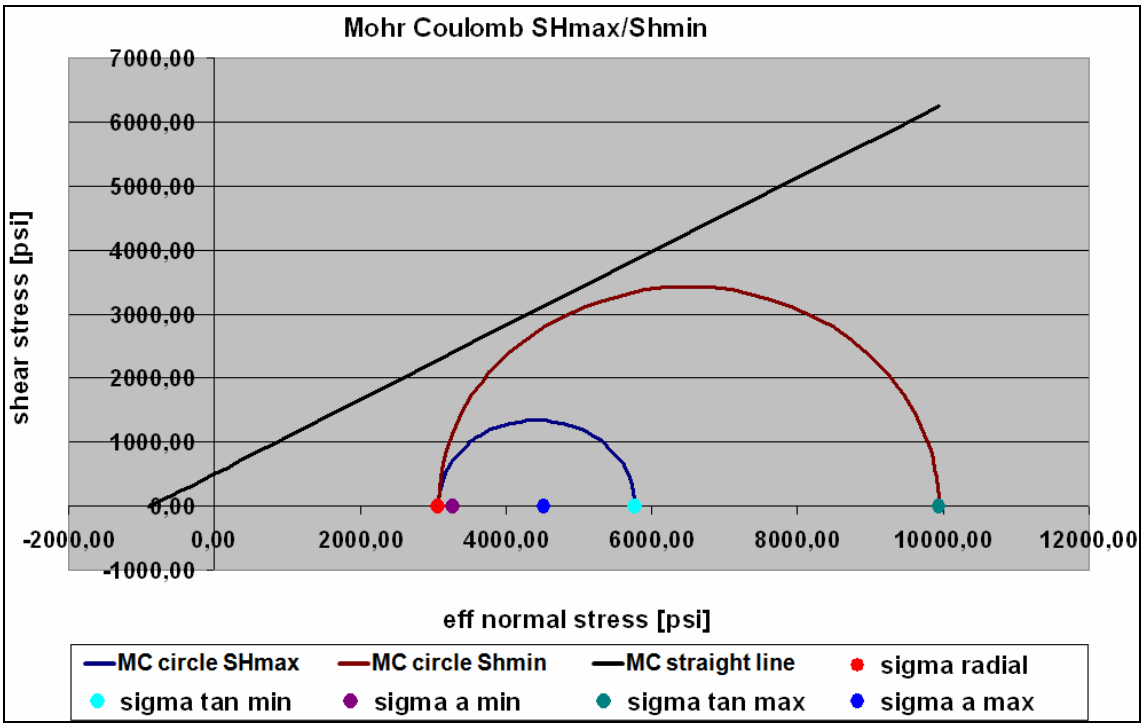

Figure 87, MC stress diagram for the well in S_{hmin} direction and 14.4 ppg MW

sigma radial [psi]	3068,00
sigma tan max [psi]	9932,00
sigma tan min [psi]	5772,00
sigma axial max [psi]	4524,00
sigma axial min [psi]	3276,00

Figure 88, stress values for the well in S_{hmin} direction and 14.4 ppg MW

6. Recommendation

6.1. Geomechanical Study

It is highly recommended to set up a list of requirements before a geomechanical study is performed by a service company. Transparency is the most important issue as a study that can not be followed step by step is not useful even with the availability of "Fastcheck" to challenge the calculation.

The service company has to state the specific logs used for the mud weight window calculation of the different hole sections, the density of available good quality data (confidence level), correlations used for pseudo density and UCS calculation with the according logs as well as the service company´s interpretation of the drilling experience reports.

Further on it has to be explained why specific distributions have been used for the input parameters of Monte Carlo simulation with the according uncertainties and which failure criterion has been utilized. The specific input values for the mud weight window calculation have to be listed for the most critical points in each hole section. According to the results of the Monte Carlo simulation it should be required that the values for P0, P10, P20…P100 have to be mentioned in the study and not just P50 and P90. Lower hemisphere plots have to be explained in great detail which means that the service company has to explain every feature encountered based on general geomechanical principles.

More generally, it has to be stated that from a drilling standpoint the report of a geomechanical study can be significantly shortened compared to the almost 190 pages of Study X. Focus should be on explaining the performed work step by step and sparing of plots where actually no information can be gained from. Each slide in the report should fulfill the requirement of increasing the understanding and/or adding information.

An additional part should be added where the pitfalls of the established geomechanic earth model and the predicted mud weight window might be from the standpoint of the editor.

The results of a geomechanical study can be challenged by the use of Fastcheck from a calculation standpoint. If the results are verified but the predicted mud weight is not meeting the expectations (field experience) the service company has to make the attempt to explain the discrepancy in a reliable, scientific way.

6.2. General

It is highly recommended to critically challenge any outcome of geomechanical studies from a drilling stand point. During this Master thesis it was found out that even the editors of these studies are not always capable of interpreting and explaining the outcome of their own software which generates the risk of loosing information. This makes it even more important to create a fundamental knowledge in geomechanics for drilling personnel within OMV and to have specialists which focus on geomechanics.

The science of geomechanics is the link between all the different disciplines as for drilling engineering the mud weight window prediction, for reservoir engineering critically stressed fractures or poroelasticity, and for production engineering sand production or subsidence effects are of critical importance. As long as we are drilling through a medium which is governed by stresses and pressures geomechanics has to be a key issue.

List of Figures

List of Tables

7. Appendix A, Ballooning Effect

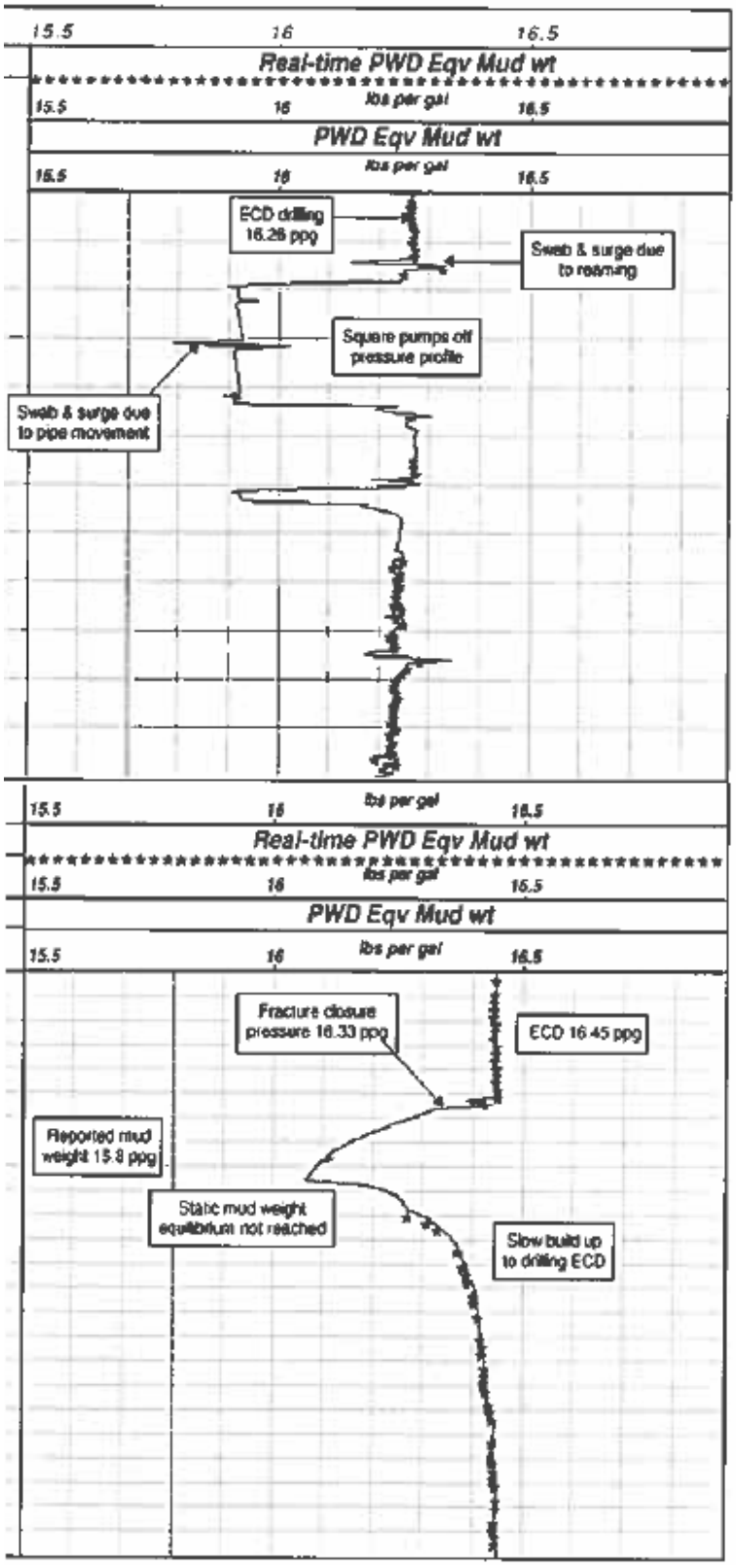

Figure 89 Appendix A, ballooning[2]

8. Appendix B, Correlations for Rock Properties

Equation No.	UCS, MPa	Region where developed	General comments	Reference
1	$0.035\ V_p - 31.5$	Thuringia, Germany	–	(Freyburg 1972)
2	$1200\ \exp(-0.036\Delta t)$	Bowen Basin, Australia	Fine grained, both consolidated and unconsolidated sandstones with wide porosity range	(McNally 1987)
3	$1.4138 \times 10^7\ \Delta t^{-3}$	Gulf Coast	Weak and unconsolidated sandstones	Unpublished
4	$3.3 \times 10^{-20}\ \rho^2 V_p^2\ [(1+\nu)/(1-\nu)]^2(1-2\nu)$ $[1+0.78V_{clay}]$	Gulf Coast	Applicable to sandstones with UCS > 30 MPa	(Fjaer, Holt *et al.* 1992)
5	$1.745\times 10^{-9}\ \rho V_p^2 - 21$	Cook Inlet, Alaska	Coarse grained sands and conglomerates	(Moos, Zoback *et al.* 1999)
6	$42.1\ \exp(1.9 \times 10^{-11}\ \rho V_p^2)$	Australia	Consolidated sandstones with $0.05 < \phi < 0.12$ and UCS > 80MPa	Unpublished
7	$3.87\ \exp(1.14 \times 10^{-10}\ \rho V_p^2)$	Gulf of Mexico	–	Unpublished
8	$46.2\ \exp(0.000027E)$	–	–	Unpublished
9	$A\ (1-B\phi)^2$	Sedimentary basins worldwide	Very clean, well consolidated sandstones with $\phi < 0.30$	(Vernik, Bruno *et al.* 1993)
10	$277\ \exp(-10\phi)$	–	Sandstones with $2 <$ UCS $<$ 360 MPa and $0.002 < \phi < 0.33$	Unpublished

Units used: V_p (m/s), Δt (μs/ft), ρ (kg/m^3), V_{clay} (fraction), E (MPa), ϕ (fraction)

Table 4 Appendix B, correlation for UCS in sandstone[2]

	UCS, MPa	Region where developed	General comments	Reference
11	$0.77\ (304.8/\Delta t)^{2.93}$	North Sea	Mostly high porosity Tertiary shales	(Horsrud 2001)
12	$0.43\ (304.8/\Delta t)^{3.2}$	Gulf of Mexico	Pliocene and younger	Unpublished
13	$1.35\ (304.8/\Delta t)^{2.6}$	Globally	–	Unpublished
14	$0.5\ (304.8/\Delta t)^{3}$	Gulf of Mexico	–	Unpublished
15	$10\ (304.8/\Delta t - 1)$	North Sea	Mostly high porosity Tertiary shales	(Lal 1999)
16	$0.0528E^{0.712}$	–	Strong and compacted shales	Unpublished
17	$1.001\phi^{-1.143}$	–	Low porosity ($\phi < 0.1$), high strength shales	(Lashkaripour and Dusseault 1993)
18	$2.922\phi^{-0.96}$	North Sea	Mostly high porosity Tertiary shales	(Horsrud 2001)
19	$0.286\phi^{-1.762}$	–	High porosity ($\phi > 0.27$) shales	Unpublished

Units used: Δt (μs/ft), E (MPa), ϕ (fraction)

Table 5 Appendix B, correlation for UCS in shale[2]

	UCS, MPa	Region where developed	General comments	Reference
20	$(7682/\Delta t)^{1.82} / 145$	–	–	(Militzer 1973)
21	$10^{(2.44 + 109.14/(t))} / 145$	–	–	(Golubev and Rabinovich 1976)
22	$0.4067\ E^{0.51}$	–	Limestone with $10 < UCS < 300$ MPa	Unpublished
23	$2.4\ E^{0.34}$	–	Dolomite with $60 < UCS < 100$ MPa	Unpublished
24	$C\ (1-D\phi)^2$	Korobcheyev deposit, Russia	C is reference strength for zero porosity ($250 < C < 300$ MPa). D ranges between 2 and 5 depending on pore shape	(Rzhevsky and Novick 1971)
25	$143.8 \exp(-6.95\phi)$	Middle East	Low to moderate porosity ($0.05 < \phi < 0.2$) and high UCS ($30 < UCS < 150$ MPa)	Unpublished
26	$35.9 \exp(-4.8\phi)$	–	Representing low to moderate porosity ($0 < \phi < 0.2$) and high UCS ($10 < UCS < 300$ MPa)	Unpublished

Units used: Δt (μs/ft), E (MPa), ϕ (fraction)

Table 6 Appendix B, correlation for UCS in limestone[2]

K	E	λ	ν	G	M
$\lambda + \frac{2G}{3}$	$G\frac{3\lambda + 2G}{\lambda + G}$	–	$\frac{\lambda}{2(\lambda + G)}$	–	$\lambda + 2G$
–	$9K\frac{K - \lambda}{3K - \lambda}$	–	$\frac{\lambda}{3K - \lambda}$	$3\frac{K - \lambda}{2}$	$3K - 2\lambda$
–	$\frac{9K - G}{3K - G}$	$K - \frac{2G}{3}$	$\frac{3K - 2G}{2(3K + G)}$	–	$K + 4\frac{G}{3}$
$\frac{\varepsilon G}{3(3G - E)}$	–	$G\frac{E - 2G}{3G - E}$	$\frac{E}{2G} - 1$	–	$G\frac{4G - E}{3G - E}$
–	–	$3K\frac{3K - E}{9K - E}$	$\frac{3K - E}{6K}$	$\frac{3KE}{9K - E}$	$3K\frac{3K + E}{9K - E}$
$\lambda\frac{1 + \nu}{3\nu}$	$\lambda\frac{(1 + \nu)(1 - \nu)}{\nu}$	–	–	$\lambda\frac{1 - 2\nu}{2\nu}$	$\lambda\frac{1 - \nu}{\nu}$
$G\frac{2(1 + \nu)}{3(1 - 2\nu)}$	$2G(1 + \nu)$	$G\frac{2\nu}{1 - 2\nu}$	–	–	$G\frac{2 - 2\nu}{1 - 2\nu}$
–	$3K(1 - 2\nu)$	$3K\frac{\nu}{1 + \nu}$	–	$3K\frac{1 - 2\nu}{2 + 2\nu}$	$3K\frac{1 - \nu}{1 + \nu}$
$\frac{E}{3(1 - 2\nu)}$	–	$\frac{E\nu}{(1 + \nu)(1 - 2\nu)}$	–	$\frac{E}{2 + 2\nu}$	$\frac{E(1 - \nu)}{(1 + \nu)(1 - 2\nu)}$

Table 7 Appendix B, relationship of elastic moduli in an isotropic material[2]

9. Appendix C, 3D Stress Diagrams

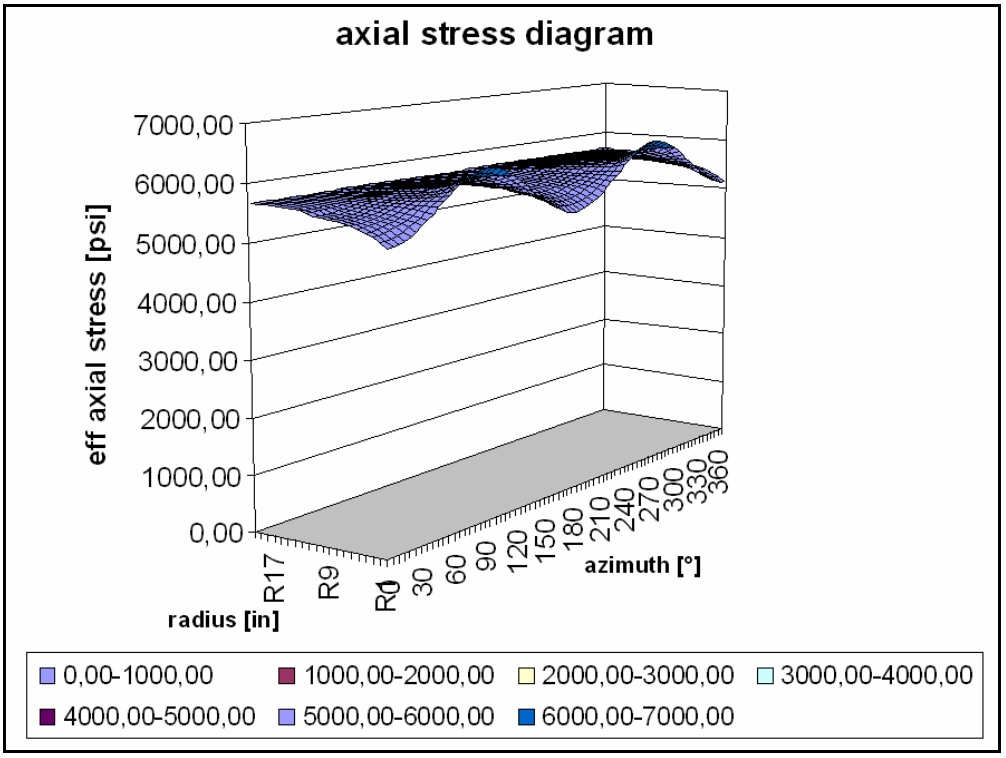

Figure 90 Appendix C, 3D axial stress diagram

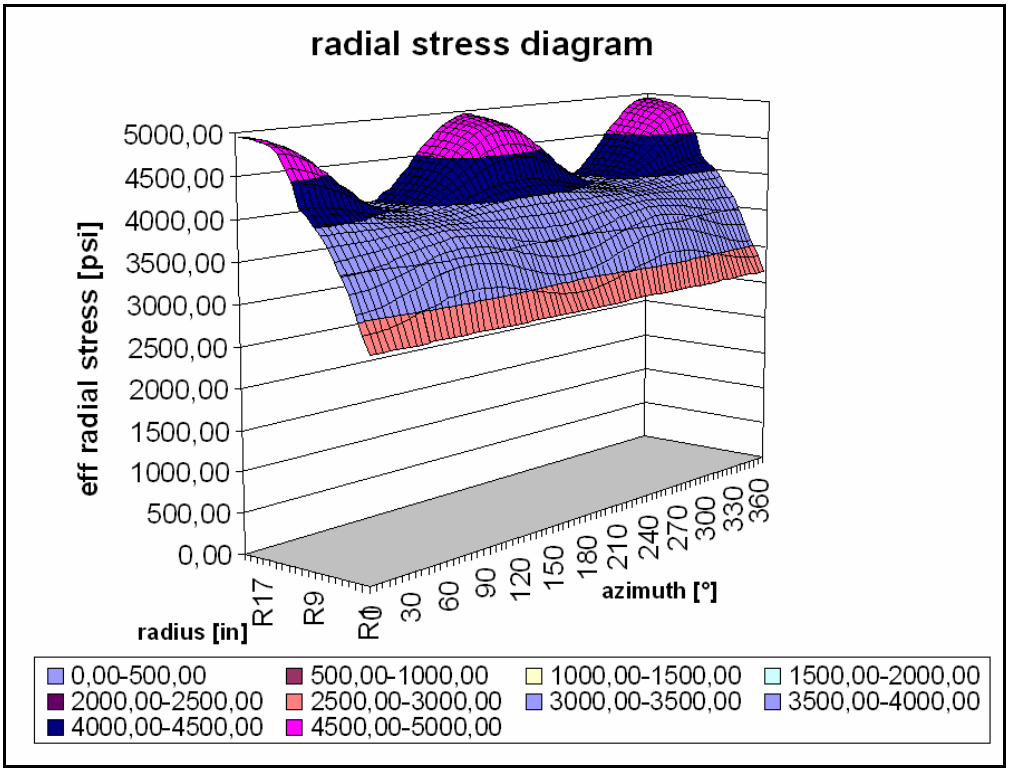

Figure 91 Appendix C, 3D radial stress diagram

10. Appendix D, Tornado Charts

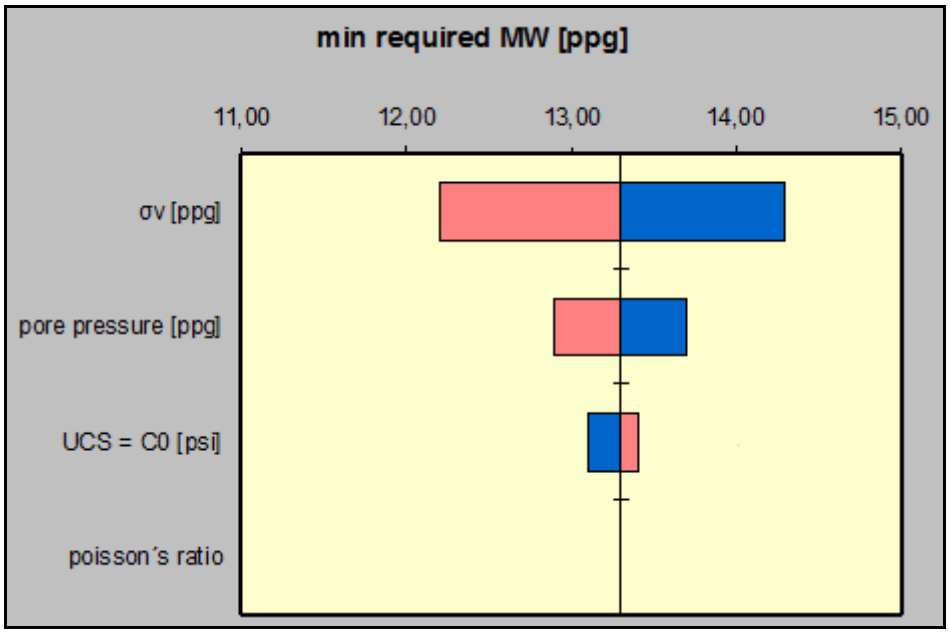

Figure 92 Appendix D, normal faulting 0 degree BOW horizontal stresses dependent on S_v

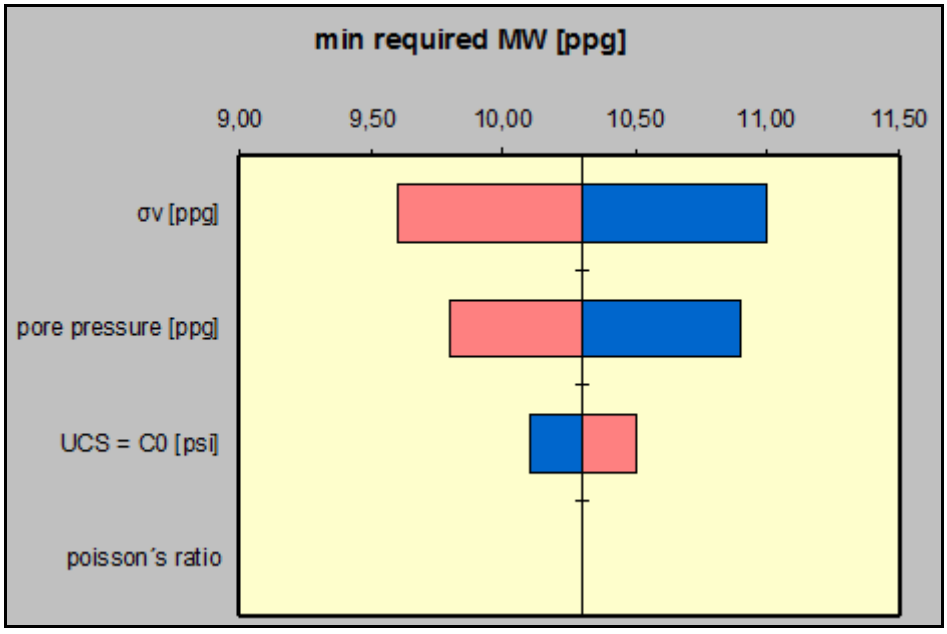

Figure 93 Appendix D, normal faulting 90 degree BOW horizontal stresses dependent on S_v

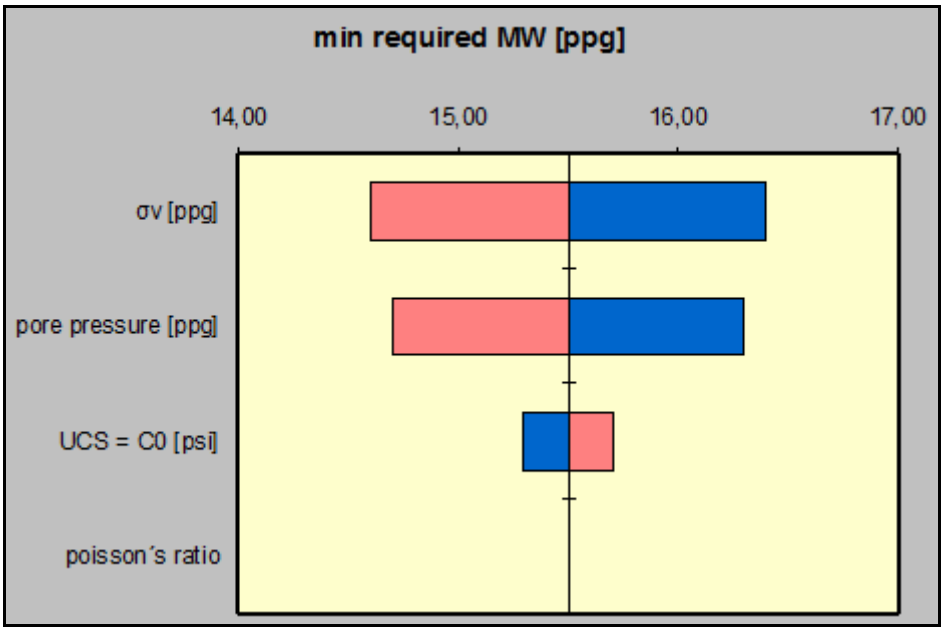

Figure 94 Appendix D, strike-slip faulting 0 degree BOW horizontal stresses dependent on S_v

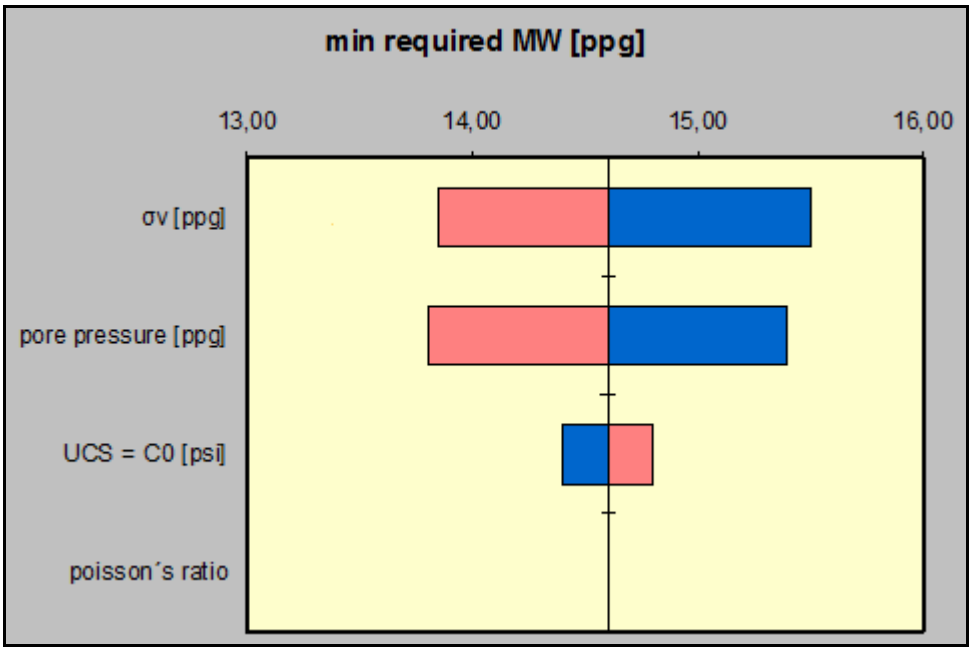

Figure 95 Appendix D, strike-slip faulting 90 degree BOW horizontal stresses dependent on S_v

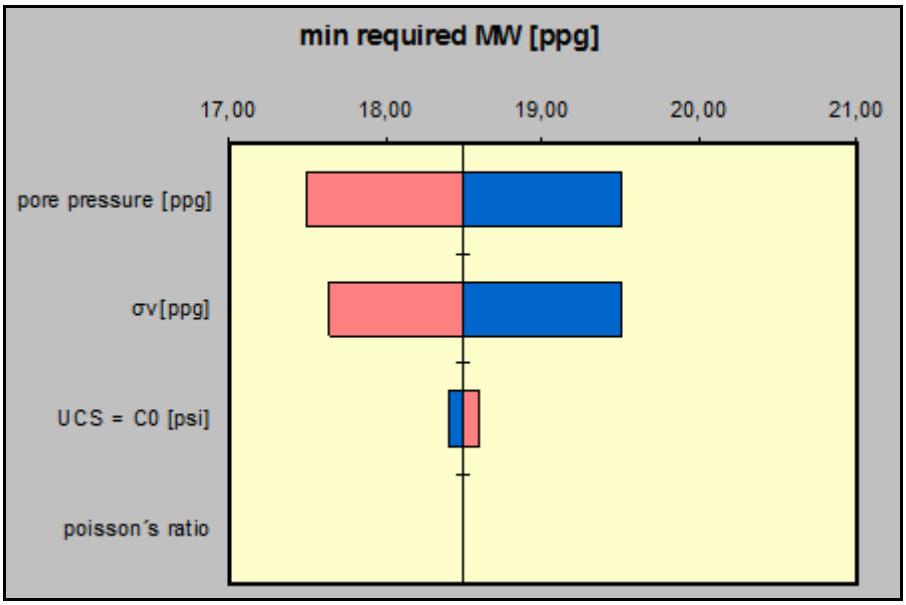

Figure 96 Appendix D, reverse faulting 0 degree BOW horizontal stresses dependent on S_v

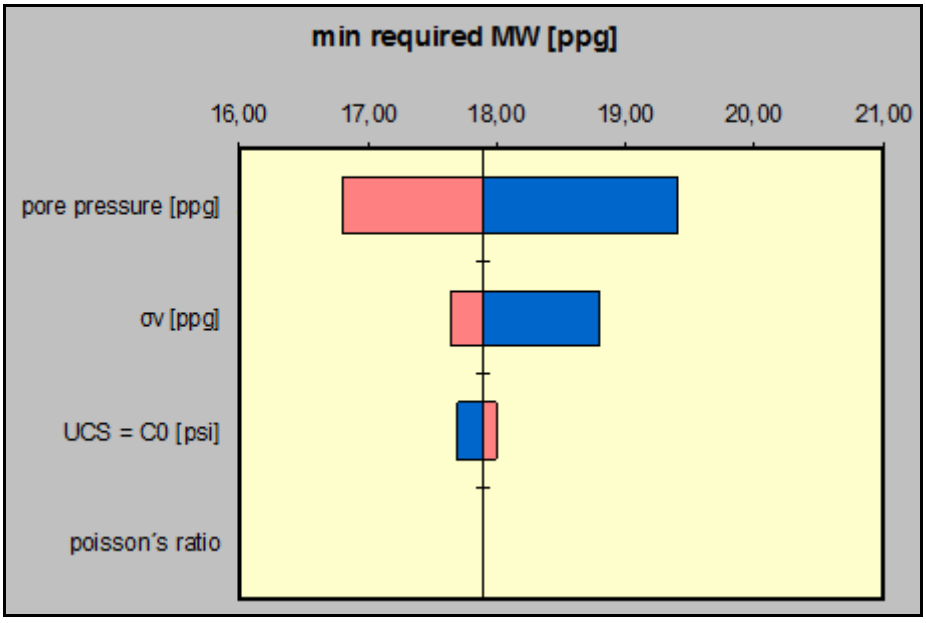

Figure 97 Appendix D, reverse faulting 90 degree BOW horizontal stresses dependent on S_v

Nomenclature

FIT…Formation Integrity Test, Pressure test of the casing shoe to prove the design of the next hole section.

LOT…Leak Off Test, Pressure test of the casing shoe until a fracture at the wellbore wall is initiated which is realized in a non-linear pressure increase in a pressure vs. volume plot. A LOT achieves higher pressures compared to a FIT.

XLOT…Extended Leak Off Test, Pressure test of the casing shoe where a fracture at the wellbore wall is initiated and extended into the far field where the near wellbore effects are no longer present. A XLOT achieves higher pressures compared to a LOT.

PWD…Pressure While Drilling, Means that a tool is installed that measures the pressure downhole.

ECD…Equivalent Circulating Density, A term that describes the dynamic pressure condition (during circulation) in the well in unit of density (equivalent mud weight).

BOW…Break Out Width, Chapter 3.3

NF…Normal Faulting Stress Regime, Chapter2.1.1

SS…Strike-Slip Faulting Stress Regime, Chapter 2.1.2

RF…Reverse Faulting Stress Regime, Chapter 2.1.3

References

1. Robert A. Skopec, “Applied Rock Mechanics”, Petro Skills, November 6, 2006

2. Mark D. Zoback, “Reservoir Geomechanics”, 2008

3. SPE paper 105193, Eric van Oort, Richard Vargo: “Improving Formation-Strength Test and their Interpretation”, 2008

4. Leonhard Ganzer, lecture “Reservoir Engineering” at Montanuniversity, 2007

5. Geomechanical study performed by GMI